Oxidative Medicine and Cellular Longevity

Neuroimaging Molecular Mechanisms of Ocular Chronic Oxidative Stress-related Diseases

Lead Guest Editor: Yi Shao
Guest Editors: Pei-Wen Zhu, Ting Su, Fei Dong, Li-Ying Tang, and Yingying Shi

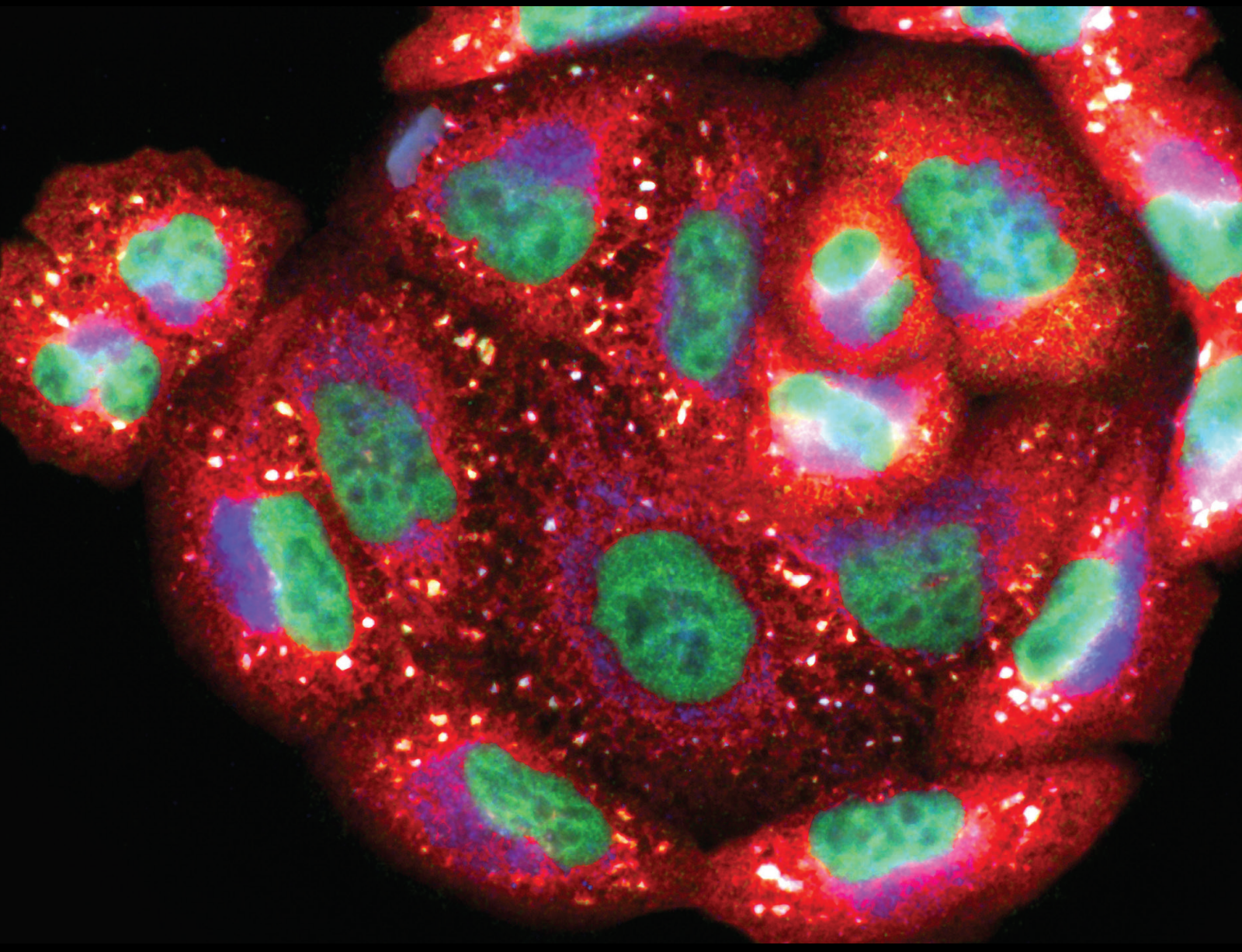

Neuroimaging Molecular Mechanisms of Ocular Chronic Oxidative Stress-related Diseases

Oxidative Medicine and Cellular Longevity

Neuroimaging Molecular Mechanisms of Ocular Chronic Oxidative Stress-related Diseases

Lead Guest Editor: Yi Shao
Guest Editors: Pei-Wen Zhu, Ting Su, Fei Dong, Li-Ying Tang, and Yingying Shi

Contents

Hindawi
Oxidative Medicine and Cellular Longevity
Volume 2024, Article ID 9871986, 1 page
https://doi.org/10.1155/2024/9871986

Retraction

Retracted: Tumor Necrosis Factor-Alpha Disrupts Cx43-Mediated Corneal Endothelial Gap Junction Intercellular Communication

Oxidative Medicine and Cellular Longevity

Received 8 January 2024; Accepted 8 January 2024; Published 9 January 2024

This article has been retracted by Hindawi following an investigation undertaken by the publisher [1]. This investigation has uncovered evidence of one or more of the following indicators of systematic manipulation of the publication process:

(1) Discrepancies in scope
(2) Discrepancies in the description of the research reported
(3) Discrepancies between the availability of data and the research described
(4) Inappropriate citations
(5) Incoherent, meaningless and/or irrelevant content included in the article
(6) Manipulated or compromised peer review

The presence of these indicators undermines our confidence in the integrity of the article's content and we cannot, therefore, vouch for its reliability. Please note that this notice is intended solely to alert readers that the content of this article is unreliable. We have not investigated whether authors were aware of or involved in the systematic manipulation of the publication process.

Wiley and Hindawi regrets that the usual quality checks did not identify these issues before publication and have since put additional measures in place to safeguard research integrity.

We wish to credit our own Research Integrity and Research Publishing teams and anonymous and named external researchers and research integrity experts for contributing to this investigation.

The corresponding author, as the representative of all authors, has been given the opportunity to register their agreement or disagreement to this retraction. We have kept a record of any response received.

References

[1] J. Meng, K. Xu, Y. Qin et al., "Tumor Necrosis Factor-Alpha Disrupts Cx43-Mediated Corneal Endothelial Gap Junction Intercellular Communication," *Oxidative Medicine and Cellular Longevity*, vol. 2022, Article ID 4824699, 9 pages, 2022.

Hindawi
Oxidative Medicine and Cellular Longevity
Volume 2024, Article ID 9871626, 1 page
https://doi.org/10.1155/2024/9871626

Retraction

Retracted: Serum Metabolomics of Benign Essential Blepharospasm Using Liquid Chromatography and Orbitrap Mass Spectrometry

Oxidative Medicine and Cellular Longevity

Received 8 January 2024; Accepted 8 January 2024; Published 9 January 2024

This article has been retracted by Hindawi following an investigation undertaken by the publisher [1]. This investigation has uncovered evidence of one or more of the following indicators of systematic manipulation of the publication process:

(1) Discrepancies in scope
(2) Discrepancies in the description of the research reported
(3) Discrepancies between the availability of data and the research described
(4) Inappropriate citations
(5) Incoherent, meaningless and/or irrelevant content included in the article
(6) Manipulated or compromised peer review

The presence of these indicators undermines our confidence in the integrity of the article's content and we cannot, therefore, vouch for its reliability. Please note that this notice is intended solely to alert readers that the content of this article is unreliable. We have not investigated whether authors were aware of or involved in the systematic manipulation of the publication process.

Wiley and Hindawi regrets that the usual quality checks did not identify these issues before publication and have since put additional measures in place to safeguard research integrity.

We wish to credit our own Research Integrity and Research Publishing teams and anonymous and named external researchers and research integrity experts for contributing to this investigation.

The corresponding author, as the representative of all authors, has been given the opportunity to register their agreement or disagreement to this retraction. We have kept a record of any response received.

References

[1] H. Zhao, W. Wang, T. Lin, and L. Gong, "Serum Metabolomics of Benign Essential Blepharospasm Using Liquid Chromatography and Orbitrap Mass Spectrometry," *Oxidative Medicine and Cellular Longevity*, vol. 2022, Article ID 6876327, 16 pages, 2022.

Hindawi
Oxidative Medicine and Cellular Longevity
Volume 2023, Article ID 9769858, 1 page
https://doi.org/10.1155/2023/9769858

Retraction

Retracted: Fundus-Vascular Responses to Color Deviation Caused by Non-Oxidative Blue Filtering

Oxidative Medicine and Cellular Longevity

Received 26 December 2023; Accepted 26 December 2023; Published 29 December 2023

This article has been retracted by Hindawi, as publisher, following an investigation undertaken by the publisher [1]. This investigation has uncovered evidence of systematic manipulation of the publication and peer-review process. We cannot, therefore, vouch for the reliability or integrity of this article.

Please note that this notice is intended solely to alert readers that the peer-review process of this article has been compromised.

Wiley and Hindawi regret that the usual quality checks did not identify these issues before publication and have since put additional measures in place to safeguard research integrity.

We wish to credit our Research Integrity and Research Publishing teams and anonymous and named external researchers and research integrity experts for contributing to this investigation.

The corresponding author, as the representative of all authors, has been given the opportunity to register their agreement or disagreement to this retraction. We have kept a record of any response received.

References

[1] J. Cai, W. Hao, S. Zeng et al., "Fundus-Vascular Responses to Color Deviation Caused by Non-Oxidative Blue Filtering," *Oxidative Medicine and Cellular Longevity*, vol. 2022, Article ID 9592009, 11 pages, 2022.

Hindawi
Oxidative Medicine and Cellular Longevity
Volume 2023, Article ID 9815835, 1 page
https://doi.org/10.1155/2023/9815835

Retraction

Retracted: The Percutaneous Endoscopic Lumbar Debridement and Irrigation Drainage Technique for the First-Stage Treatment of Spontaneous Lumbar Spondylodiscitis: A Clinical Retrospective Study

Oxidative Medicine and Cellular Longevity

Received 26 September 2023; Accepted 26 September 2023; Published 27 September 2023

This article has been retracted by Hindawi following an investigation undertaken by the publisher [1]. This investigation has uncovered evidence of one or more of the following indicators of systematic manipulation of the publication process:

(1) Discrepancies in scope
(2) Discrepancies in the description of the research reported
(3) Discrepancies between the availability of data and the research described
(4) Inappropriate citations
(5) Incoherent, meaningless and/or irrelevant content included in the article
(6) Peer-review manipulation

The presence of these indicators undermines our confidence in the integrity of the article's content and we cannot, therefore, vouch for its reliability. Please note that this notice is intended solely to alert readers that the content of this article is unreliable. We have not investigated whether authors were aware of or involved in the systematic manipulation of the publication process.

Wiley and Hindawi regrets that the usual quality checks did not identify these issues before publication and have since put additional measures in place to safeguard research integrity.

We wish to credit our own Research Integrity and Research Publishing teams and anonymous and named external researchers and research integrity experts for contributing to this investigation.

The corresponding author, as the representative of all authors, has been given the opportunity to register their agreement or disagreement to this retraction. We have kept a record of any response received.

References

[1] Y. Yang, J. Wang, and Z. Chang, "The Percutaneous Endoscopic Lumbar Debridement and Irrigation Drainage Technique for the First-Stage Treatment of Spontaneous Lumbar Spondylodiscitis: A Clinical Retrospective Study," *Oxidative Medicine and Cellular Longevity*, vol. 2022, Article ID 6241818, 9 pages, 2022.

Hindawi
Oxidative Medicine and Cellular Longevity
Volume 2024, Article ID 9871626, 1 page
https://doi.org/10.1155/2024/9871626

Retraction

Retracted: Serum Metabolomics of Benign Essential Blepharospasm Using Liquid Chromatography and Orbitrap Mass Spectrometry

Oxidative Medicine and Cellular Longevity

Received 8 January 2024; Accepted 8 January 2024; Published 9 January 2024

This article has been retracted by Hindawi following an investigation undertaken by the publisher [1]. This investigation has uncovered evidence of one or more of the following indicators of systematic manipulation of the publication process:

(1) Discrepancies in scope
(2) Discrepancies in the description of the research reported
(3) Discrepancies between the availability of data and the research described
(4) Inappropriate citations
(5) Incoherent, meaningless and/or irrelevant content included in the article
(6) Manipulated or compromised peer review

The presence of these indicators undermines our confidence in the integrity of the article's content and we cannot, therefore, vouch for its reliability. Please note that this notice is intended solely to alert readers that the content of this article is unreliable. We have not investigated whether authors were aware of or involved in the systematic manipulation of the publication process.

Wiley and Hindawi regrets that the usual quality checks did not identify these issues before publication and have since put additional measures in place to safeguard research integrity.

We wish to credit our own Research Integrity and Research Publishing teams and anonymous and named external researchers and research integrity experts for contributing to this investigation.

The corresponding author, as the representative of all authors, has been given the opportunity to register their agreement or disagreement to this retraction. We have kept a record of any response received.

References

[1] H. Zhao, W. Wang, T. Lin, and L. Gong, "Serum Metabolomics of Benign Essential Blepharospasm Using Liquid Chromatography and Orbitrap Mass Spectrometry," *Oxidative Medicine and Cellular Longevity*, vol. 2022, Article ID 6876327, 16 pages, 2022.

Hindawi
Oxidative Medicine and Cellular Longevity
Volume 2022, Article ID 6876327, 16 pages
https://doi.org/10.1155/2022/6876327

Research Article

Serum Metabolomics of Benign Essential Blepharospasm Using Liquid Chromatography and Orbitrap Mass Spectrometry

Han Zhao,[1,2,3] **Wushuang Wang**,[1,2,3] **Tong Lin**,[1,2,3] **and Lan Gong**[1,2,3]

[1]*Department of Ophthalmology, Eye, Ear, Nose, and Throat Hospital of Fudan University, Shanghai 200000, China*
[2]*Laboratory of Myopia, NHC Key Laboratory of Myopia (Fudan University), Chinese Academy of Medical Sciences, Fudan University, Shanghai 200000, China*
[3]*Shanghai Key Laboratory of Visual Impairment and Restoration, Fudan University, Shanghai 200000, China*

Correspondence should be addressed to Lan Gong; 13501798683@139.com

Received 17 July 2022; Revised 4 September 2022; Accepted 24 September 2022; Published 18 November 2022

Academic Editor: Li-Ying Tang

Background. Benign essential blepharospasm (BEB) is a form of focal dystonia that causes excessive involuntary spasms of the eyelids. Currently, the pathogenesis of BEB remains unclear. This study is aimed at investigating the serum metabolites profiles in patients with BEB and healthy control and to identify the mechanism and biomarkers of this disease. *Methods*. 30 patients with BEB and 33 healthy controls were recruited for this study. We conducted the quantitative and nontargeted metabolomics analysis of the serum samples from 63 subjects by using liquid chromatography and Orbitrap mass spectrometry (LC-Orbitrap MS). Multivariate statistical analysis was performed to detect and identify different metabolites between the two groups. The Kyoto Encyclopedia of Genes and Genomes (KEGG) and receiver operating characteristic (ROC) curve analysis of the altered metabolites were performed. *Results*. A total of 134 metabolites were found and identified. The metabolites belonged to several metabolic pathways including phenylalanine metabolism, phenylalanine, tyrosine and tryptophan biosynthesis, arginine biosynthesis, linoleic acid metabolism, tryptophan metabolism, aminoacyl-tRNA biosynthesis, sphingolipid metabolism, glycosphingolipid biosynthesis, leucine and isoleucine biosynthesis, and vitamin B6 metabolism. Eight metabolites were identified as the potential biomarkers. *Conclusions*. These results demonstrated that serum metabolic profiling of BEB patients was significantly different from healthy controls based on LC-Orbitrap MS. Besides, metabolomics might provide useful information for a better understanding of BEB.

1. Introduction

Benign essential blepharospasm (BEB) is an adult-onset focal dystonia marked by excessive involuntary spasms of the orbicularis oculi muscle as well as other motor symptoms such as elevated blink frequency and apraxia of eyelid opening. As the disease progresses, dystonia in about two-thirds of these patients will expand to adjacent muscle sites, including the oromandibular and cervical muscles, within five years of BEB initiation [1]. The mean annual incidence of BEB was reported as 0.10 in a recent population-based retrospective analysis [2]. BEB is more frequent in women, and the peak incidence of them frequently appeared in their fifth and sixth decades [3]. The epidemiological study showed that the majority of BEB cases were considered sporadic, with just 20–30% of cases having a familial history [4]. As the symptoms progress, it may become difficult to open the eyes or even induce functional blindness, resulting in functional impairment at work and in everyday life as well as a reduction in quality of life [5].

Research on BEB has gotten a lot of attention, and there has been a lot of development. While the specific mechanism of BEB remains vague, however anomalies in both the basal ganglia and cortical function have been blamed. Furthermore, both genetic and metabolic variables are implicated in BEB progression [1, 6]. The metabolic alterations were a potential factor involved in the pathogenesis of BEB. Suzuki et al. found that the glucose metabolism level was higher in both sides of the posterior striate cortex and extrastriate cortex of patients with BEB when compared with normal

subjects by using positron emission tomography. During the study, the severity of BEB was also linked to thalamic glucose metabolism [7]. Mostofsky et al. also reported that essential fatty acids administration could alleviate the eye blinking rate in the dopamine depletion-induced blepharospasm rat model [8]. In addition, there was a significant decrease in serum calcium levels in the BEB group compared with the healthy group [9].

Metabolomics is a relatively emerging discipline that analyzes the intermediary and final products of the metabolic pathways within an organism; therefore, it is possible to reflect the alterations in these compounds under any pathological stimulation, genetic effect, or physiological condition. Nontargeted metabolomics analysis, which has been widely utilized in clinical research, may identify metabolites in a variety of materials, including tear fluid, urine, and serum [10]. In addition, metabolomics has a particular advantage over other technologies including genomics, transcriptomics, and proteomics in that it could provide a global phenotype of metabolic changes. This approach is now being utilized to find evidence of major changes in metabolites such as amino acids, lipids, and neurotransmitters in dystonia-related diseases [11–13]. There have been no reports of using metabolomics to uncover pathogenic aspects or diagnostic biomarkers in BEB patients, suggesting that this novel technology must be employed to identify probable biomarkers of BEB as well as explore the disease's pathogenesis and treatment approaches.

In the present study, we have performed a study to determine the metabolic characteristics and networks in the serum of patients with BEB based on liquid chromatography and Orbitrap mass spectrometry (LC-Orbitrap MS). The purpose was to investigate the serological biomarkers for BEB diagnosis and the pathogenesis of the BEB.

2. Materials and Methods

2.1. Standard Protocol Approvals and Patient Consents. The protocols of this study were approved by the Ethics Committee of Eye, Ear, Nose, and Throat Hospital of Fudan University. The informed consent process was adhering to the tenets of the Helsinki Declaration, and all BEB subjects and healthy individuals signed the informed consent forms.

2.2. Study Participants Collection. In total, 30 BEB patients were enrolled from the Department of Ophthalmology of Eye, Ear, Nose, and Throat Hospital of Fudan University from July 2021 to December 2021. To prevent any diagnostic bias, all individuals underwent a routine ophthalmology examination by two ophthalmologists. Inclusion criteria included patients who were 20 years of age or older with the diagnosis of BEB by experienced ophthalmologists or neurologists. The following exclusion criteria were applied to all BEB subjects: (1) any ocular abnormalities such as conjunctivitis, keratitis, glaucoma, or uveitis; (2) any systemic diseases such as hypertension, hyperlipidemia, heart disease, diabetes, metabolic diseases, or hematological diseases; (3) topical or systemic medications. The severity and frequency of blepharospasm were evaluated by using the Jankovic rating scale (JRS) [14]. The functional impairments in daily life activities of BEB in all patients were accessed according to the blepharospasm disability index (BSDI). Disease duration was determined in months from the beginning of symptoms to the date of the examination. In the control group, another 33 healthy individuals without BEB were included, and their serum was taken with normal clinical blood draws.

2.3. Samples Preparation. The 2 mL vacuum blood collection tube was used to collect a whole blood sample from each participant during another normal blood testing. Tubes were then centrifuged for 5 minutes (3000 rpm/min, 4°C) to remove the blood cells, and the supernatant was transformed into 2 mL cryogenic vials (NEST Biotechnology) and promptly stored at -80°C before metabolomic analysis.

For LC-Orbitrap MS analysis, each 100 μL of serum was thawed at 4°C and mixed with a 300 μL solution of cold methanol/phenylalanine. After vortexing for 2 minutes, the samples were then centrifuged for 10 minutes (13000 rpm/min, 4°C) and obtained 200 μL supernatants.

2.4. LC-Orbitrap MS Analysis. The UHPLC system was coupled to an Orbitrap MS (Waters Corp., Milford, MA, USA) equipped with an electrospray ionization source, operating in positive or negative ionization mode, with a mass resolution of 70,000 and m/z of 200. The full scan mass resolution was 17500 at m/z 200 using data correlation (dd-MS2, TopN = 10) MS/MS mode. Scanning range: 100-1500. The chromatographic conditions were as follows: the injection volume was 2 μL, the column temperature was 25°C, the flow rate was 0.35 mL/min, and the mobile phases were 0.1% formic acid aqueous solution (solution A) and 0.1% formic acid acetonitrile solution (solution B). The optimized chromatographic gradient is as follows: 0-2 min, 5% in solution B; 2-10 min, 5%-95% in solution B; 10-15 min, 95% in solution B; 15-18 min, 5% in solution B. The following parameters were used for mass detection in both positive and negative ion modes: scan range, m/z 80-1000; drying gas (N_2) flow rate, 11 L/min; gas temperature, 350°C; pressure of the nebulizer gas, 45 psig; Vcap, 4000 V (-3000 V). Data were acquired in centroid mode using Thermo Excalibur 2.2 software (Thermo Fisher Scientific, MA, USA).

2.5. Statistical Analysis. Data were acquired using Thermo Xcalibur 2.2 software (Thermo Scientific, San Jose, USA). Peak calibration and extraction were performed using composite discovery software (Thermo Fisher Scientific). Data tables were imported into SIMCA-P 13.0 (Umetrics AB, Umea, Sweden) for multivariate statistical analysis. An unsupervised principal component analysis (PCA) was used to assess the overall trend of separation between these samples. Differential metabolites were screened by partial least squares-discriminant analysis (PLS-DA). According to the PLS-DA model, variables with variable importance in the projection (VIP) value greater than 1.0 were selected, SPSS Statistics 18.0.0 was used to perform a two-tailed Student t-test, and $p < 0.05$ was considered statistically significant. Multiple-test adjustment was performed with Bonferroni correction. To identify these potential biomarkers, accurate

ion masses were entered into the Human Metabolome Database (HMDB), Metlin, MoNA, and MassBank databases to match accurate molecular weights and automatically search for MS1/MS2 fragment ions. Finally, to determine the structure of the compound, we used our library of internal standard metabolites, matching accurate masses, fragment ion masses, and retention times. Pathway enrichment analysis was performed using the Kyoto Encyclopedia of Genes and Genomes (KEGG) database and metabolic analysis (https://www.metaboanalyst.ca/). The diagnostic power of the biomarkers was assessed using the area under the (ROC) curve.

3. Results and Discussion

3.1. Baseline Characteristics of the Study Subjects. The workflow of our study is shown in Figure 1. The baseline characteristics of the study subjects are shown in Table 1. Totally 63 participants, including 30 BEB subjects and 33 control subjects were recruited. Differences in age, gender, and BMI were not significant between BEB patients and controls ($p > 0.05$).

3.2. Total Ion Chromatogram and Untargeted Metabolomics Analysis of Serum Samples. Figures 2(a) and 2(b) show a representative total ion chromatogram (TIC) data from the serum of the BEB group and control group. The good overlap of retention time of each main chromatographic peak in both positive and negative ionization modes proved the LC-Orbitrap MS system's exceptional stability and repeatability throughout the procedure. To evaluate the serum level of altered metabolites in BEB, we performed a nontargeted metabolomics analysis of 63 serum samples by LC-Orbitrap MS. Figures 2(c) and 2(d) show PCA score plot for the BEB, control, and quality control (QC) groups. In both positive and negative ionization modes, a high degree of aggregation of the QC groups was identified, indicating the high stability and good repeatability during the whole sequence of the BEB and control groups. The PLS-DA was carried out to determine the metabolites pattern changes in the BEB and control groups. The PLS-DA plot scores (Supplementary Figures 1A and 1B) revealed a strong distinction between the BEB and control groups. The permutation analysis of the PLS-DA plot also indicated a high validity and stability in both the BEB group and control group (Supplementary Figures 1C and 1D).

3.3. Differentiating Metabolite Identification. According to the criteria of VIP > 1 and $p < 0.05$, volcano plot analysis was been applied to determine significant differences of the metabolites between the two groups. The red or green dots depict metabolites that substantially changed between BEB and control groups under positive ionization mode (Figure 3(a)), negative ionization mode (Figure 3(b)), and combination mode (Figure 3(c)). The serum of the BEB group was then compared to that of the control group, yielding 134 differently expressed metabolites, as shown in Supplementary Table 1. To further determine the altered metabolites between the BEB group and the control group, a clustering heatmap showed altered metabolites under the positive ionization mode between these two groups (Figure 4(a)). We also explored the metabolic differences between BEB patients and controls under negative ionization mode of electrospray ionization. Figure 4(b) shows that 41 metabolites were identified between two differentiated clusters. On the other hand, Figure 4(c) shows metabolic differences between BEB patients and controls under combination mode. Pair-wise Spearman analysis was used to analyze the correlation coefficient between serum differential metabolites and clinical parameters (Figure 4(d)). Significant correlations were also observed between the course of disease and penta-L-phenylalanine. However, no significant correlation was observed between serum differential metabolites and JRS or BSDI.

To identify the serum level of nontargeted metabolomics profiles in course of BEB, we performed a nontargeted metabolomics analysis of BEB patients and their control at 0-12 months, 13-24 months, and more than 24 months. At 0-12 months, 57 metabolites were significantly altered, including 36 upregulated metabolites and 21 downregulated metabolites ($p < 0.05$). At 13-24 months, there were 29 metabolites significantly changed ($p < 0.05$). Among them, 22 were increased and 7 were decreased. Moreover, 46 metabolites were significantly changed in the BEB group at more than 24 months. 32 metabolites were significantly increased, whereas 14 metabolites were significantly decreased (Supplementary Table 2).

3.4. KEGG Analysis of Differential Plasma Metabolites. KEGG pathway enrichment studies were done based on the changed metabolites in both positive and negative ionization modes of electrospray ionization to investigate the pathways implicated in these altered serum metabolites. Phenylalanine metabolism, phenylalanine, tyrosine and tryptophan biosynthesis, arginine biosynthesis, linoleic acid metabolism, tryptophan metabolism, aminoacyl-tRNA biosynthesis, sphingolipid metabolism, glycosphingolipid biosynthesis, leucine and isoleucine biosynthesis, and vitamin B6 metabolism were the top 10 enriched pathways, as illustrated in Figure 5.

3.5. Biomarker Identification of Important Metabolites. To further screen the potential metabolic indicators in serum samples of BEB patients, ROC curve analysis was performed to identify the sensitivity and specificity of significantly altered metabolites. ROC curve analysis was considered the candidate diagnostic biomarker for BEB according to an area under the ROC curve (AUC) >0.8. PC (18 : 1(11Z)/24 : 1(15Z)), TG (16 : 0/19 : 0/20 : 0) [iso6], PC (O-22 : 0/22 : 3(10Z,13Z,16Z)), PC (16 : 0/24 : 1(15Z)), PS (16 : 0/22 : 1(11Z)), hexadecyl phosphorodichloridate, methionine sulfoxide, and icotidine all had AUC values of 1.000, 0.991, 0.981, 0.978, 0.915, 0.835, 0.824, and 0.801, respectively (Figure 6, Table 2).

4. Discussion

BEB is regarded as a common movement disorder worldwide characterized by increased activity of the orbicularis oculi muscle and other muscles around the eyelid. Although

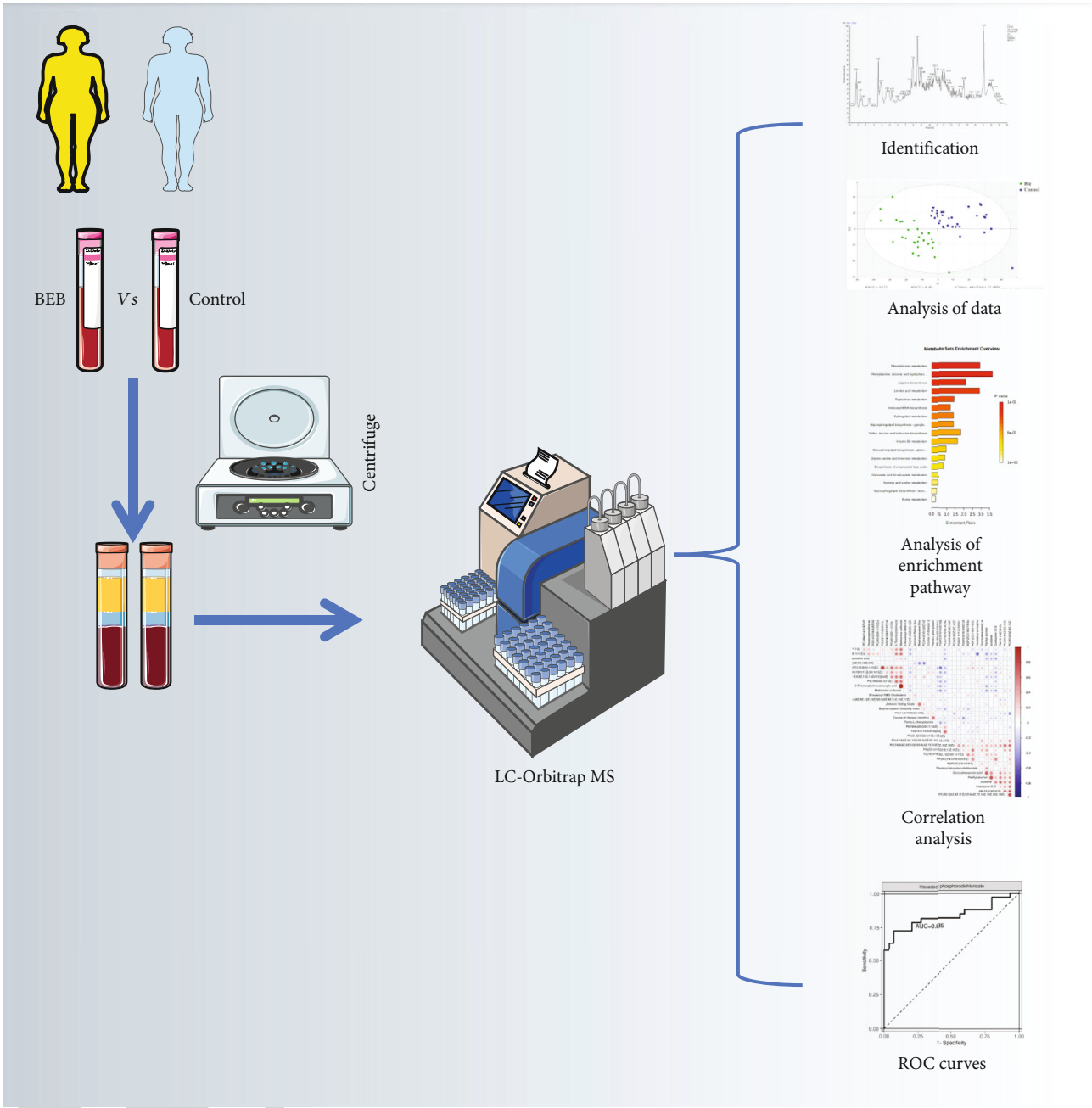

Figure 1: The workflow of our study.

Table 1: Basic characteristics of BEB patients and healthy controls.

Parameter	Control	BEB	p value
Number (n)	33	30	—
Age (year)	50.06	51.43	0.620
Gender (female/male)	25/8	24/6	0.767
BMI (kg/m^2)	22.45	22.62	0.872
Course of disease (months)	—	21.03 ± 12.51	—
Jankovic rating scale	—	5 ± 2	—
Blepharospasm disability index	—	2.32 ± 0.97	—

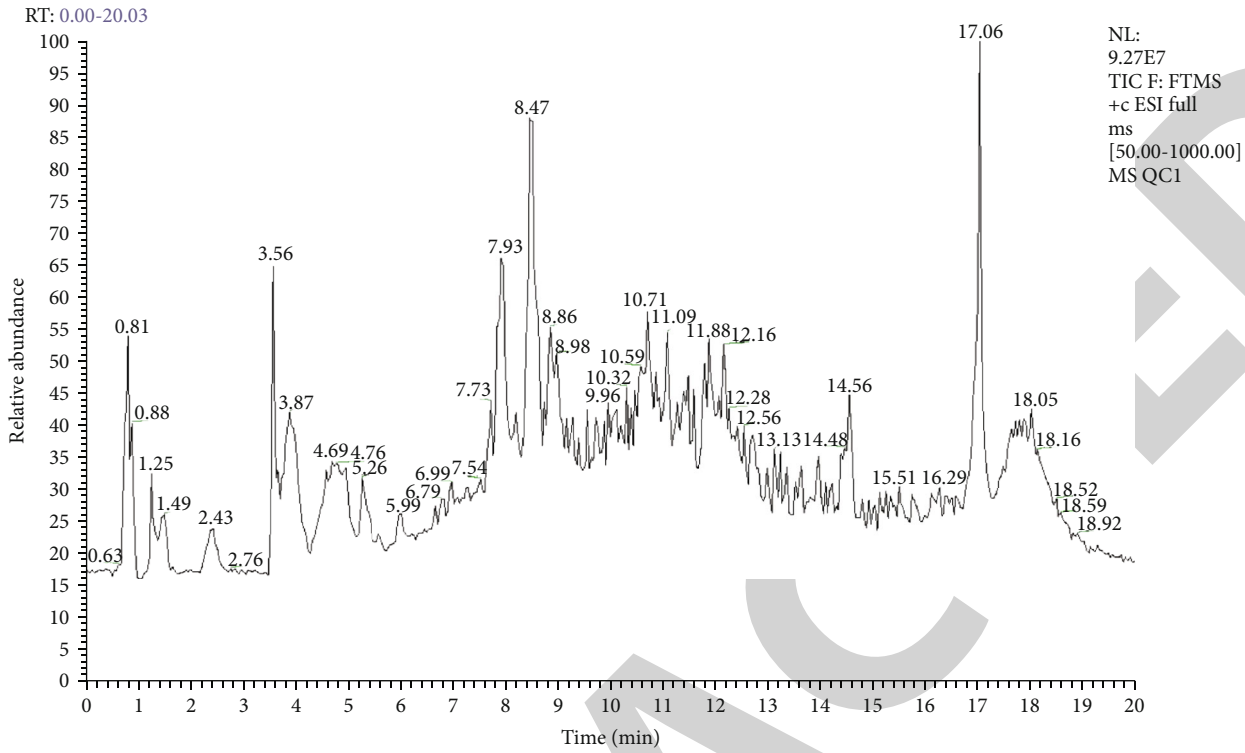

Positive ionization mode

(a)

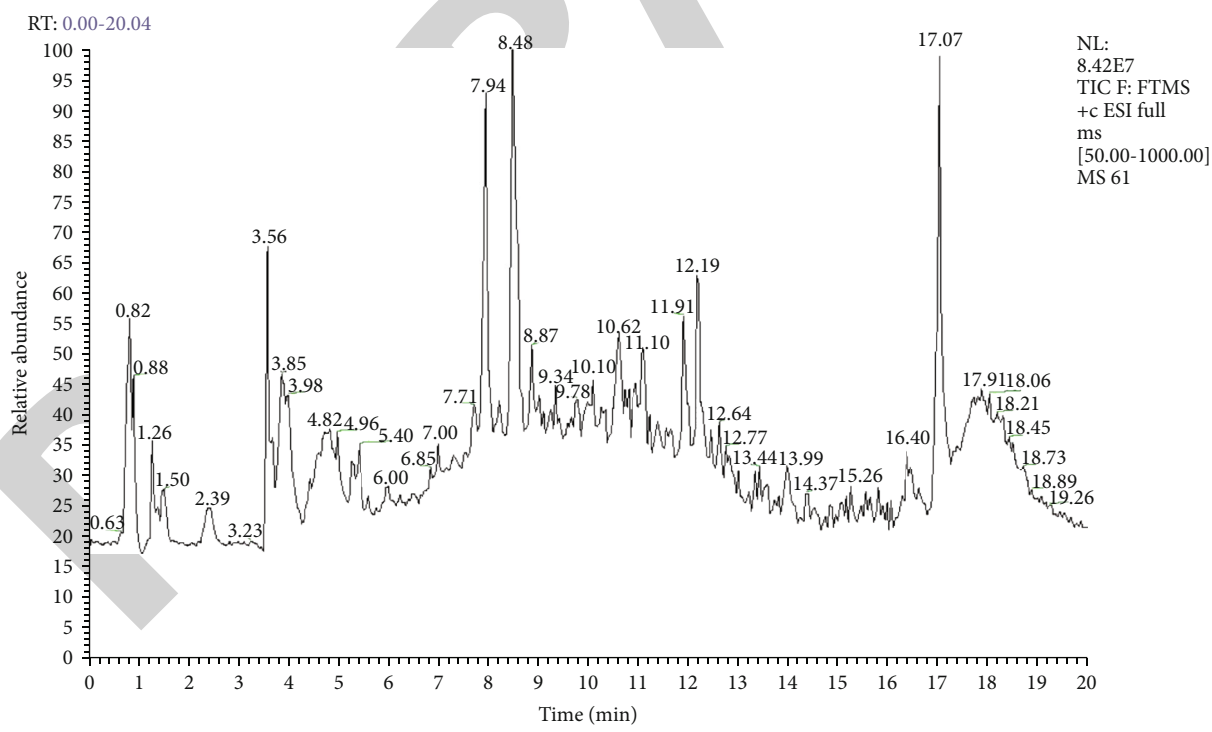

Negative ionization mode

(b)

Figure 2: Continued.

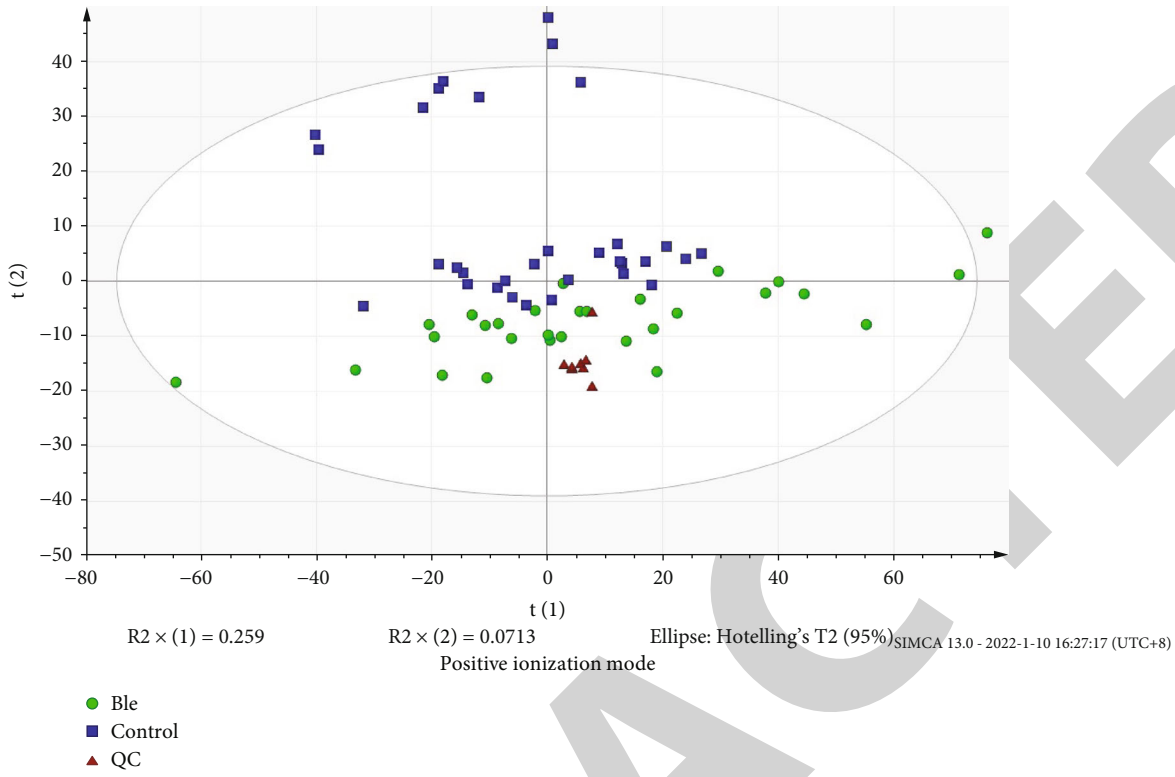

(c)

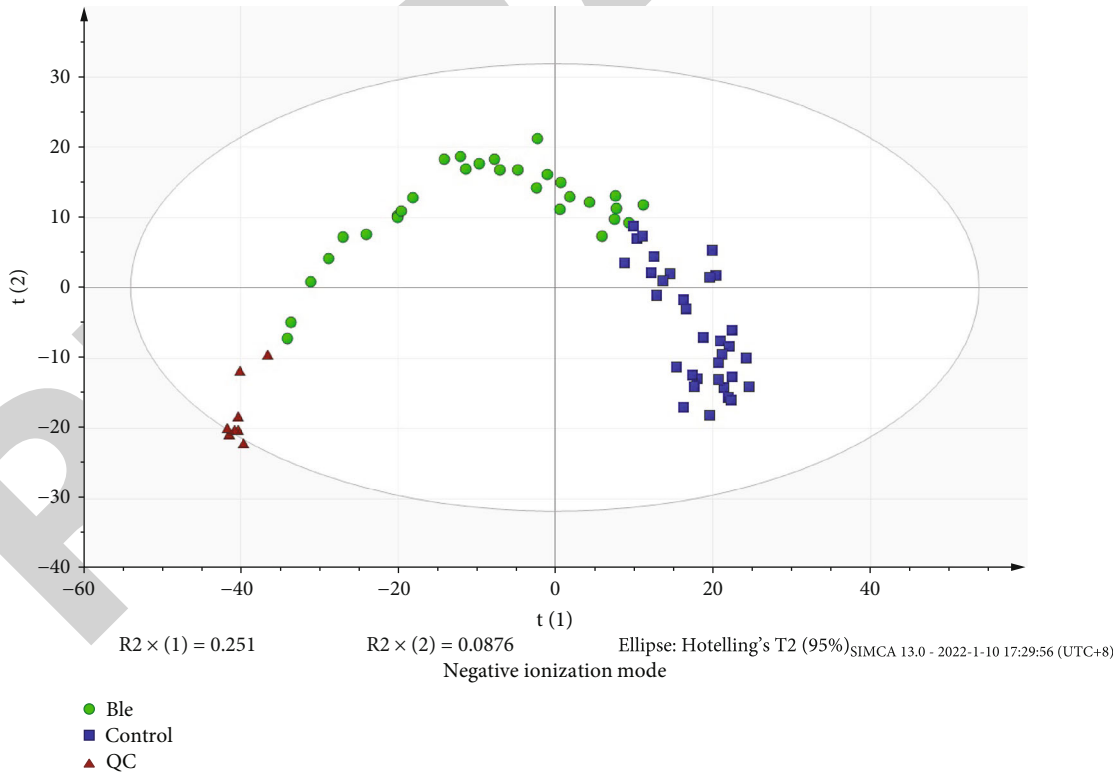

(d)

Figure 2: The total ion chromatogram and unsupervised principal component analyses (PCA) scores plot made from the serum samples from BEB patients, healthy controls, and QC groups. The total ion chromatogram of the BEB and healthy controls in the (a) positive and (b) negative ionization modes. (c) PCA scores plot generated from all serum samples in positive ionization mode. (d) PCA scores plot generated from all serum samples in negative ionization mode. BEB: benign essential blepharospasm; QC: quality control.

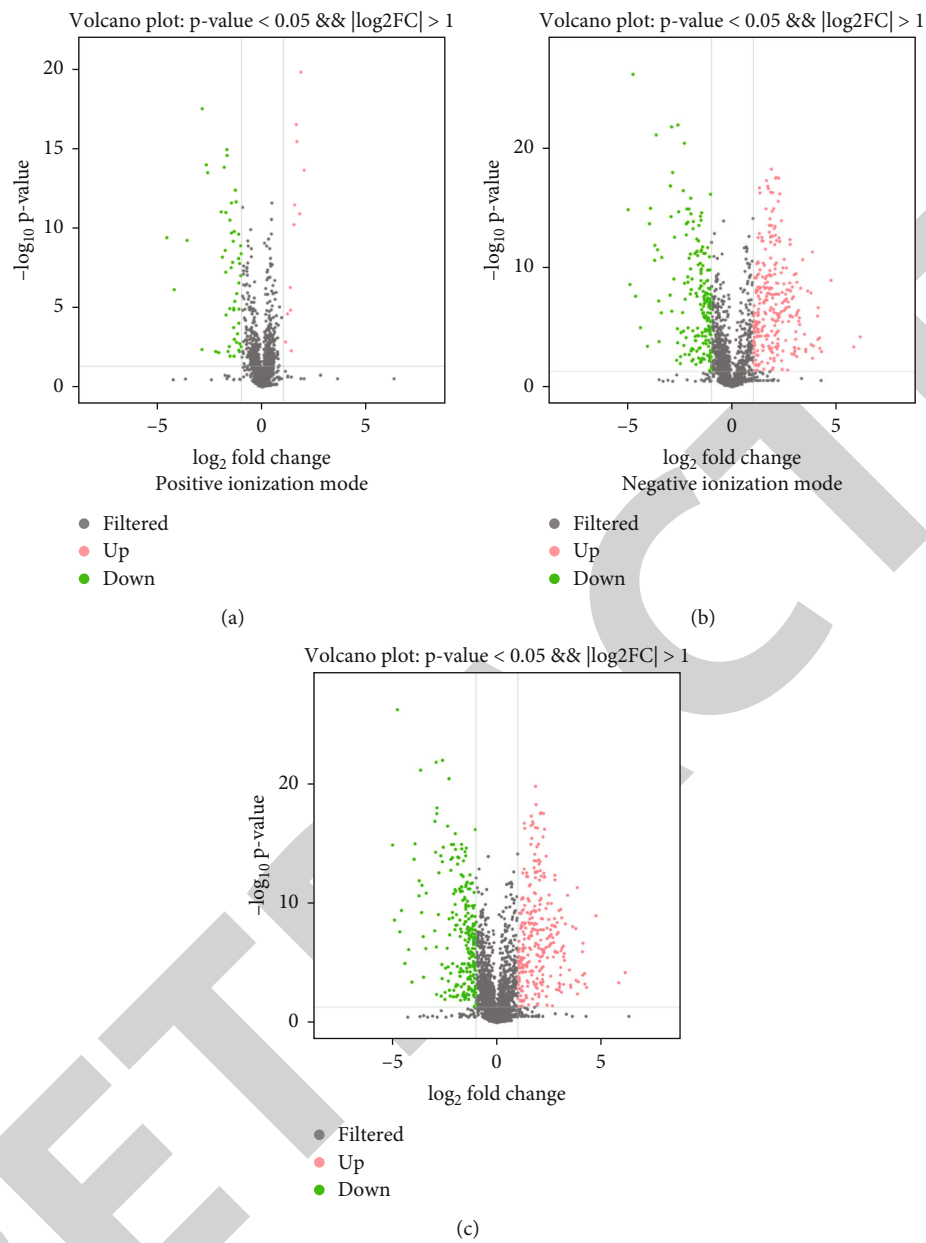

Figure 3: Volcano plot of altered metabolites between the BEB and control groups under positive ionization mode (a), negative ionization mode (b), and combination mode (c). Upregulated metabolites are shown in red, whereas downregulated metabolites are shown in green. BEB: benign essential blepharospasm.

blepharospasm was first reported 80 years ago, the etiological mechanisms remain not clear. There is an urgent need to investigate the etiological mechanisms or find a potential diagnostic biomarker in BEB patients.

The primary aim of this study was to systematically analyze the serum metabolites of BEB. Therefore, we examined altered serum metabolites profiles in 30 subjects with BEB and 33 age-matched healthy controls based on LC-Orbitrap MS. A significant distinction between the BEB patients and healthy individuals was accomplished using multivariate statistical analysis. The potential metabolic indicators responsible for the separation of BEB and the control groups were revealed by the loading plots from the PCA in positive and negative ionization modes. 134 metabolites exhibited significant differences between the two groups, according to the p values of the independent test. Moreover, these altered metabolites with linked to the metabolic pathways of phenylalanine metabolism, phenylalanine, tyrosine and tryptophan biosynthesis, arginine biosynthesis, linoleic acid metabolism, tryptophan metabolism, aminoacyl-tRNA biosynthesis, sphingolipid metabolism, glycosphingolipid biosynthesis, leucine and isoleucine biosynthesis, and vitamin B6 metabolism were identified as preliminary. In addition, we compared metabolite expression levels between patients with different disease courses. Some lipid subclass and amino acids and

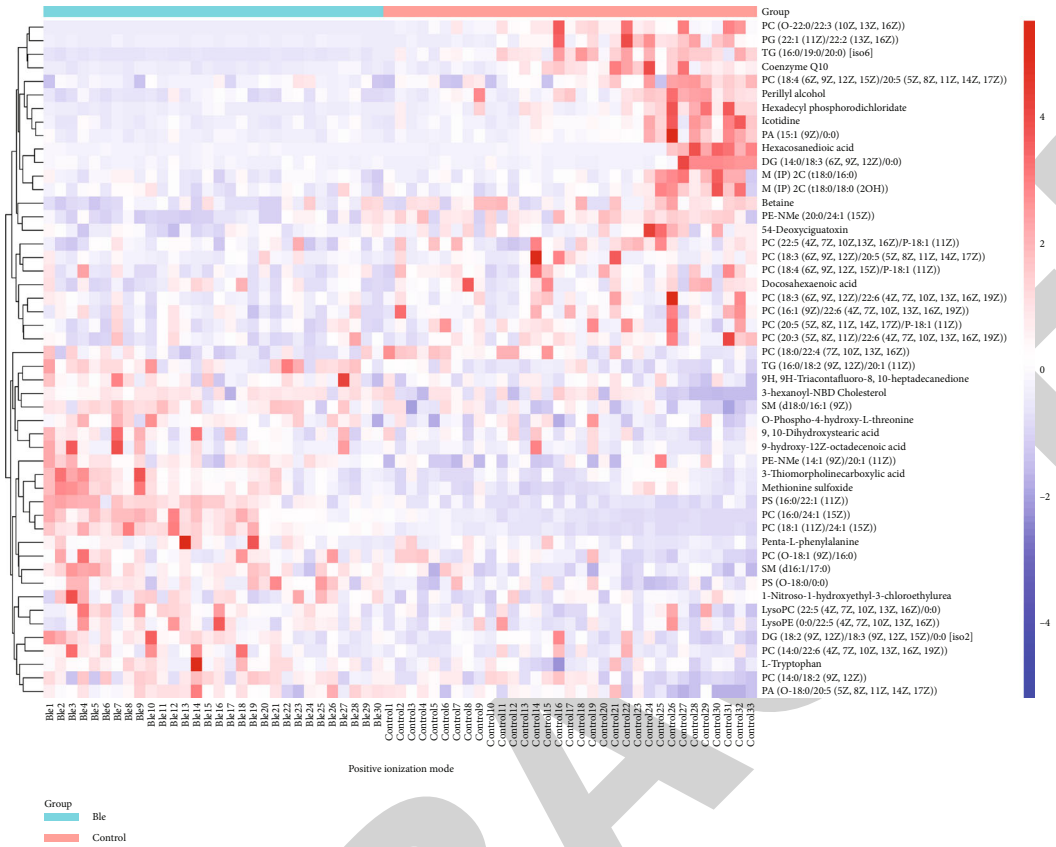

(a)

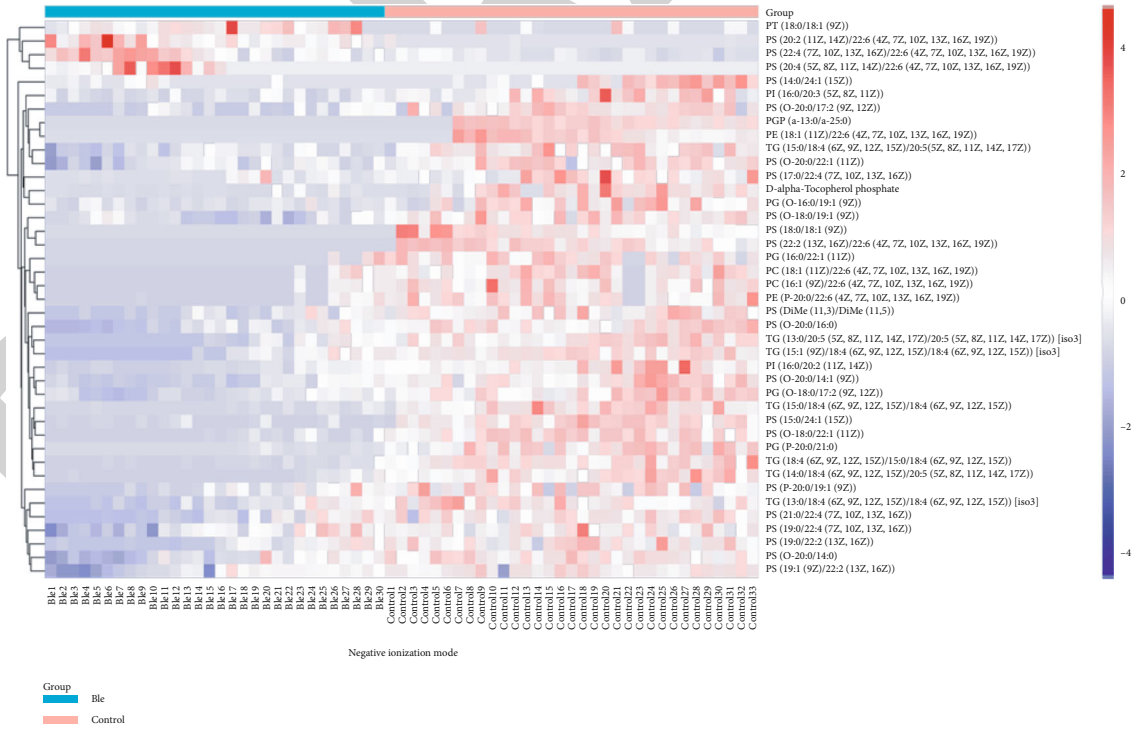

(b)

Figure 4: Continued.

(c)

Figure 4: Continued.

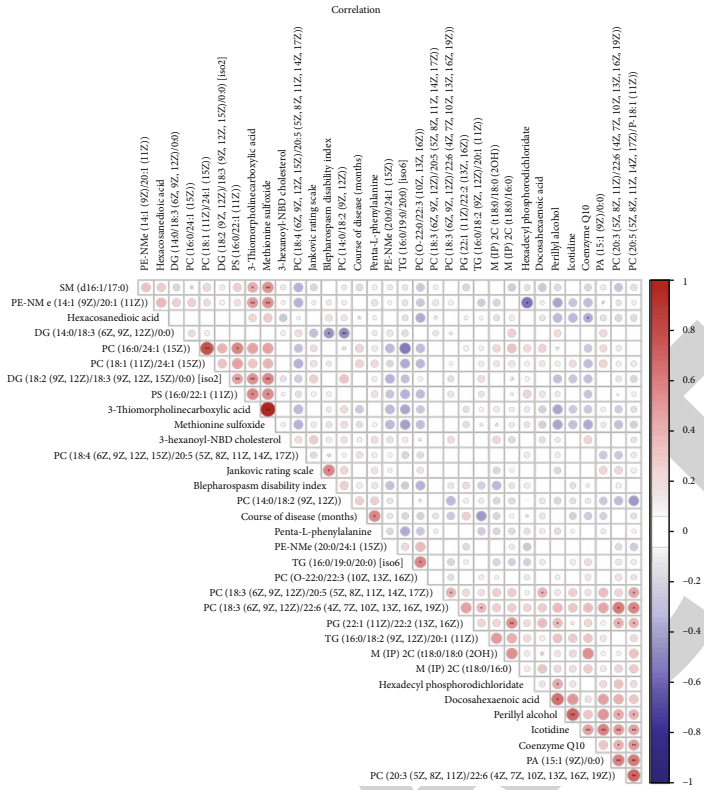

(d)

Figure 4: Hierarchical clustering heatmap of significantly altered metabolites and the Pair-wise correlation (Spearman) analysis. Hierarchical clustering heatmap of the altered metabolites between the BEB and control groups under positive ionization mode (a), negative ionization mode (b), and combination mode(c). (d) Pair-wise correlation (Spearman) among between serum differential metabolites and clinical parameters. BEB: benign essential blepharospasm.

their derivatives were found to be significantly changed at 13-24 months and more than 24 months, respectively. These results suggest that BEB development is accompanied by a metabolomic change of amino acids from the lipid subclass and their derivatives. It is also interesting to observe that the metabolomic change in patients with BBE more than 24 months indicated that BEB may have a long-term effect on the metabolite profile. These metabolites can serve as potential biomarkers or monitoring indicators for different disease processes.

Extensive studies have indicated that movement disorders such as focal dystonia and Parkinson's disease linked to oxidative stress [15]. However, the mechanisms responsible for oxidative stress in BEB are not fully understood. In our study, tryptophan, the antioxidants amino acid, and the production of tyrosine and dihydroxyindole, were markedly decreased in BEB group. Tryptophan can modulate the function of antioxidant enzymes, such as glutathione s-transferase, and tyrosine, an important antioxidant, may reduce oxidative damage by lowering ferryl hemoglobin levels [16]. In addition, previous study suggested the reduced tryptophan levels may be linked to chronic inflammation in white matter [17]. The higher L-kynurenine/tryptophan ratio found in this study suggests that the activation of oxidative stress or inflammation is considerably boosted in BEB (Supplementary Figure 2). These findings suggest that in BEB, downregulation of the tyrosine and tryptophan biosynthesis-related pathway may disturb the antioxidative system.

Phosphatidylcholine (PC) is an important metabolite in the nervous system. PC synthesis was increased in neuronal differentiation [18]. PC's involvement in membrane fluidity is especially critical for neuronal homeostasis by preventing the protein from aggregating [19]. The balance of lipid content as well as lipid-to-protein proportions can be disrupted and therefore a disease risk factor for Parkinson's disease [20]. PC also affects the characteristics of peripheral neurotoxicity. PC may promote the development of neurons and decrease oxidative stress by increasing antioxidant levels [21]. PC is mainly synthesized and abundant in the endoplasmic reticulum, and it synthesize might occur in endoplasmic reticulum stress [22]. However, as shown in the context of obesity and a mouse model of muscular dystrophy, an increase in PC can also activate endoplasmic reticulum stress responses, implying that PC plays a key role in endoplasmic reticulum stress [23, 24]. Moreover, endoplasmic reticulum stress may contribute to the deficits in neuroplasticity and motor function in dystonia [25]. In our study, serum level of PC (16 : 0/24 : 1(15Z)) and PC (18 : 1(11Z)/24 : 1(15Z)) were

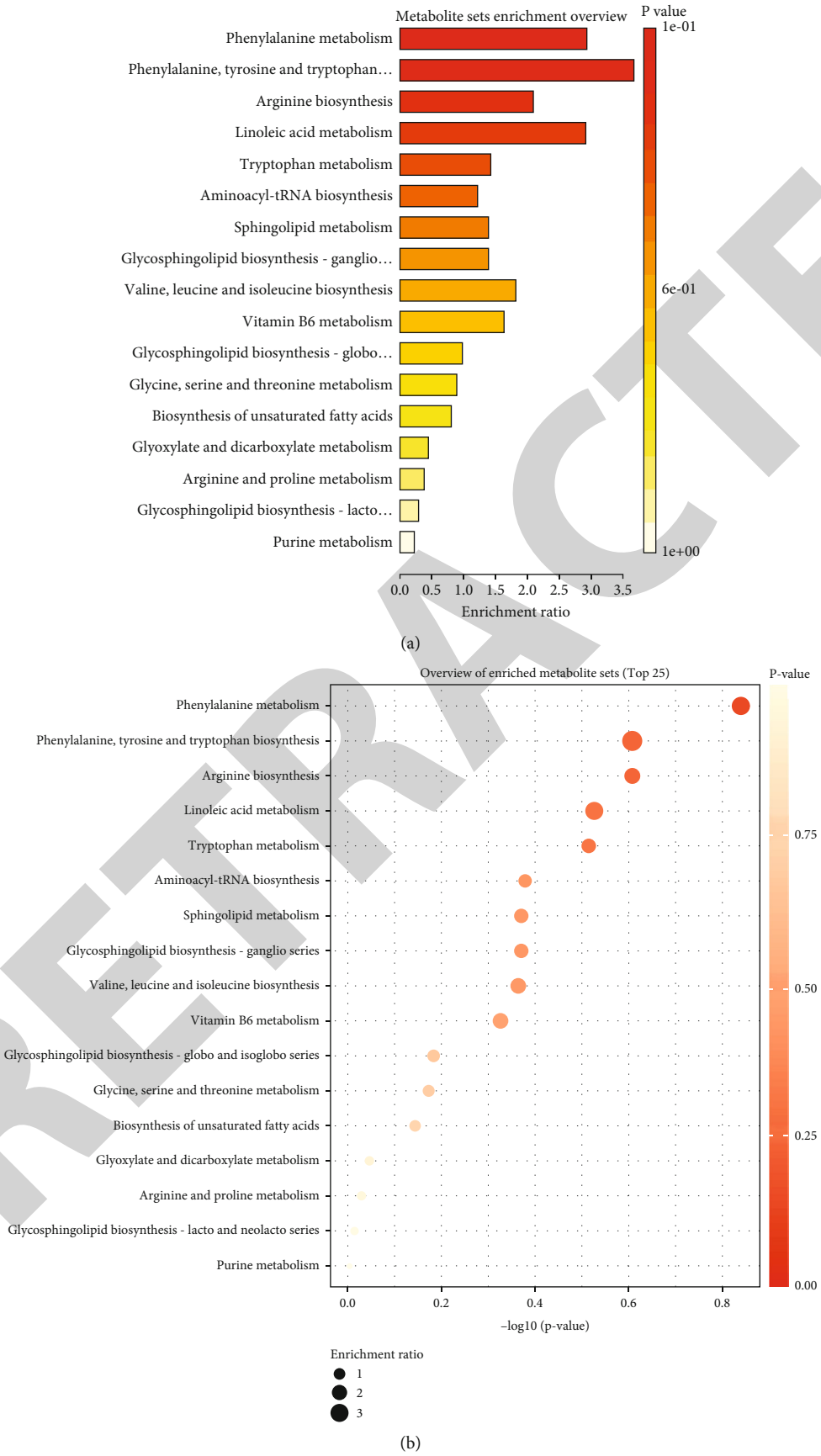

Figure 5: KEGG pathway enrichment analysis of the altered metabolites. KEGG: Kyoto Encyclopedia of Genes and Genomes.

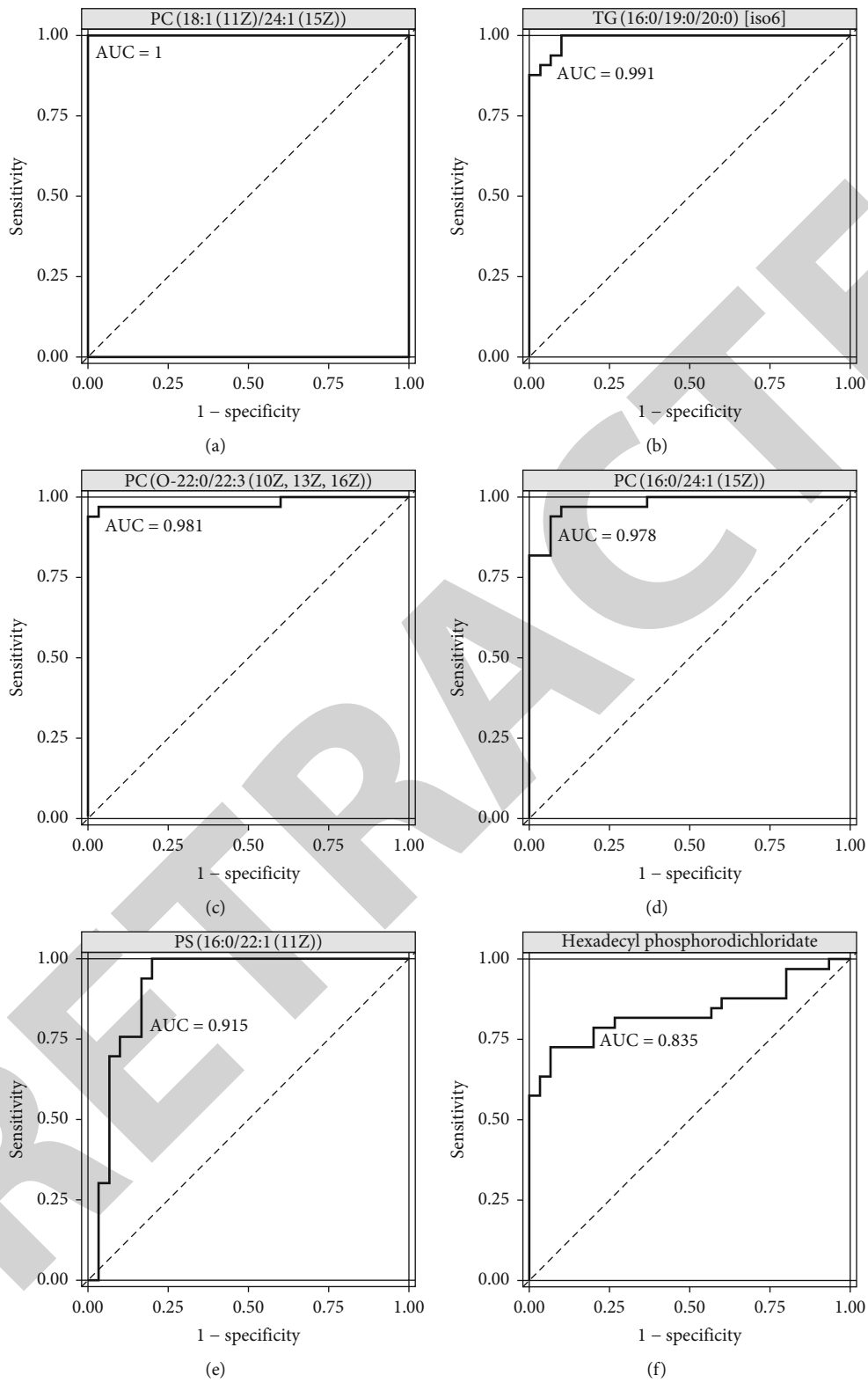

Figure 6: Continued.

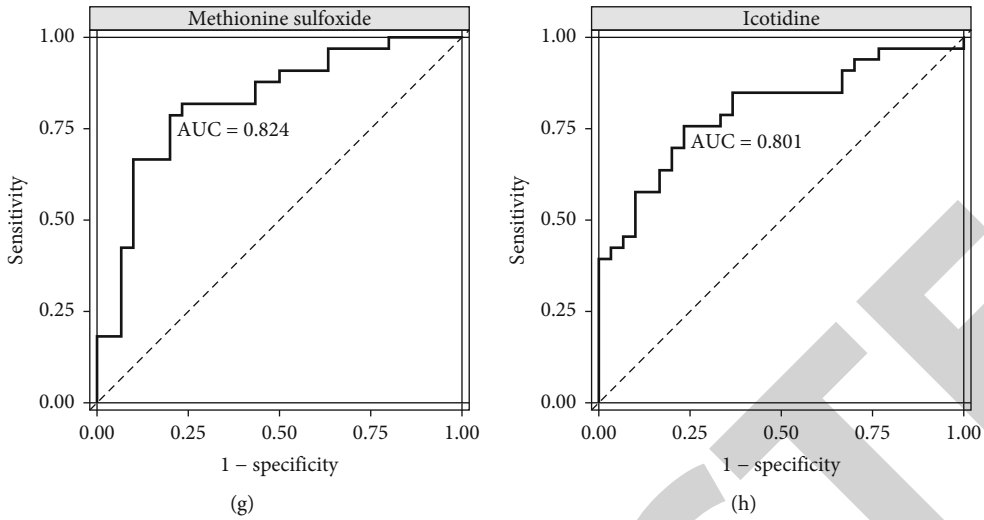

Figure 6: ROC curve of the untargeted altered metabolomics according to the criteria (AUC > 0.8). ROC: receiver operating characteristic; AUC: area under the curve.

Table 2: Diagnostic value of the potential metabolic biomarkers with AUC over 0.8.

Metabolites	AUC	Specificity	Sensitivity	Expression
PC (18 : 1(11Z)/24 : 1(15Z))	1	1	1	-184964
TG (16 : 0/19 : 0/20 : 0) [iso6]	0.99091	0.9	1	63204.1
PC (O-22 : 0/22 : 3(10Z,13Z,16Z))	0.98081	1	0.93939	248438
PC (16 : 0/24 : 1(15Z))	0.97778	0.93333	0.93939	-299051
PS (16 : 0/22 : 1(11Z))	0.91515	0.8	1	-238778
Hexadecyl phosphorodichloridate	0.83535	0.93333	0.72727	51572.7
Methionine sulfoxide	0.82424	0.8	0.78788	-2218584.9
Icotidine	0.80101	0.76667	0.75758	213107

significantly increased in the BEB group, while PC (14 : 0/18 : 2(9Z,12Z)), PC (14 : 0/22 : 6(4Z,7Z,10Z,13Z,16Z,19Z)), PC (O-18 : 1(9Z)/16 : 0), and PC (14 : 1(9Z)/24 : 1(15Z)) were decreased in BEB patients, which indicates dysfunction of PC subclasses. In this study, LysoPC (16 : 0/0 : 0) was decreased in BEB patients, while LysoPC (22 : 5(4Z,7Z,10Z,13Z,16Z)/0 : 0), LysoPC (0 : 0/16 : 0), and LysoPC (22 : 4(7Z,10Z,13Z,16Z)/0 : 0) were increased in BEB. Due to disruption of the cell membrane and the presence of inflammation with BEB, the dysfunction of LysoPCs caused changes in energy metabolism. This might be a possible mechanism of BEB and remains further studied.

Phosphatidylethanolamine (PE) is the main part of phospholipid in human plasma. Phospholipids are the important components of the cell membrane surfactants and affect various membrane functions, including cell membrane formation, activation of several membrane-bound enzymes, cell membrane recognition, and signal transduction [26]. Moreover, studies have confirmed that loss of PE asymmetry in the cell membrane can activate a multitude of pathophysiological processes, such as apoptosis and necrosis [27]. In addition, one of the most important consequences of PE abnormalities is the change in energy metabolism in the endoplasmic reticulum leading to endoplasmic reticulum stress in Parkinson's disease [28]. Wortmann et al. also found a PE remodeling-related gene and gene mutation could impair mitochondrial function and cause dystonia [29]. Our results indicated PE metabolism disorder in patients with BEB as compared to the control group, which was evidenced by altered levels of PE-NMe (14 : 1(9Z)/20 : 1(11Z)), LysoPE (0 : 0/22 : 5(4Z,7Z,10Z,13Z,16Z)), PE (18 : 0/20 : 4(5Z,8Z,11Z,14Z)), and PE (18 : 1(9Z)/0 : 0). However, PE is not only affected by daily diet but also by systemic metabolism, so it is difficult to standardize the diet of all participants at the time of enrollment, so the role of PE in BEB is still not known and remains further study.

Phosphatidylserine (PS) plays a key role in the function and structure of the human nervous system. PS accounts for 13%-15% of the total phospholipids in the adult cerebral cortex [30]. PS is a key compound required for activating several critical signaling pathways in the membrane of plasma, such as the Akt and Raf-1 signaling pathways, which are involved in neuronal survival, process development, and synaptogenesis [31]. PS also plays a role in modulating AMPA glutamate receptors [32]. In the synapses, PS mediates calcium-dependent membrane fusion among synaptic vesicles and

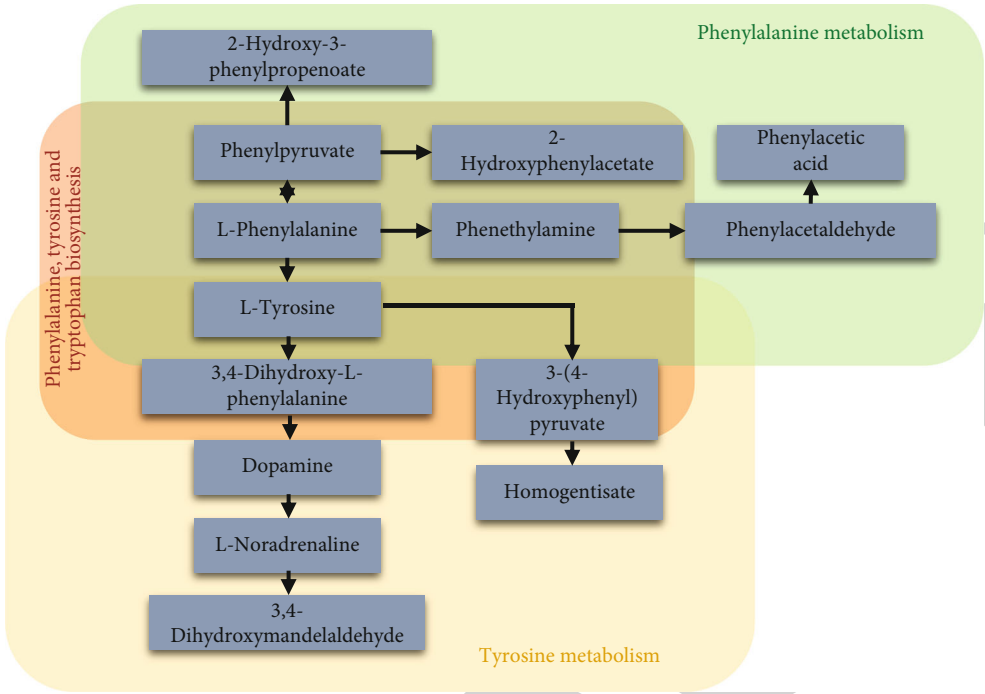

Figure 7: Schematic diagram of the phenylalanine, tyrosine and tryptophan production, phenylalanine metabolism, and tyrosine metabolism pathway. There are still some limitations existed in this study. First of all, we only included 30 BEB patients in our study, and the limited number of BEB patients might not be sufficient to identify the altered metabolic status of BEB patients. So, a larger sample size of BEB patients and cohort are needed to validate our results. Moreover, there is currently a lack of animal and cell models for blepharospasm, so animal and cell-level validation cannot be performed. We have found 134 differential nontargeted metabolites and predicted the possible involvement of signaling pathways of the changed nontargeted metabolites. However, the relationship between these metabolites and BEB is required to be further investigated.

the target membrane, which is regulated by synaptotagmin and the soluble N-ethylmaleimide-sensitive factor attachment protein receptor complex, which is necessary for exocytosis [33]. A recent study showed significantly decreased levels of serum calcium in the BEB group compared with the healthy group [9]. PS synthase in the neurons was also shown to be aberrant in Parkinson's disease [34]. Blepharospasm is common in Parkinson's disease [35]. In this study, PS (16 : 0/22 : 1(11Z)) was increased in the BEB group compared with the control group, while PS (O-16 : 0/13 : 0) and PS (O-18 : 0/0 : 0) were decreased in the BEB groups. The roles of serum PS subclasses in BEB patients have not been fully elucidated. The possible mechanism of PS subclasses in the impairment of the synapses is based on the inhibition of neuronal development and differentiation and regulation of calcium-dependent signal pathways.

The pathway analysis showed that the revealed signaling pathways of BEB were selected by the KEGG. Amino acid pathways have been found to play a key role in central nervous system, functioning as neurotransmitters, neurochemicals, and energy metabolism regulators. These pathways are believed to be linked to the onset and progression of neurodegenerative disorders [36]. It was discovered that BEB has altered important intermediate metabolites in the pathways associated to aromatic amino acids (phenylalanine, tyrosine, and tryptophan) (Figure 7). The vitamin B6 metabolism pathway observed to be dysregulated in BEB. Studies have reported that dysregulation of vitamin B6 in gut microbiome and serum metabolome are evident among dystonia patients than among controls [12].

5. Conclusions

In summary, we generated a nontargeted metabolomic profile in serum between BEB patients and healthy subjects, and we identified 134 differential metabolites for the first time. Then we performed ROC curve analysis and identified several potential biomarkers, including PC (18 : 1(11Z)/24 : 1(15Z)), TG (16 : 0/19 : 0/20 : 0) [iso6], PC (O-22 : 0/22 : 3(10Z,13Z,16Z)), PC (16 : 0/24 : 1(15Z)), PS (16 : 0/22 : 1(11Z)), hexadecyl phosphorodichloridate, methionine sulfoxide, and icotidine. The KEGG pathway enrichment analysis of these differently expressed metabolites in BEB was established. The results suggested that phenylalanine metabolism, phenylalanine, tyrosine and tryptophan biosynthesis, arginine biosynthesis, linoleic acid metabolism, tryptophan metabolism, aminoacyl-tRNA biosynthesis, sphingolipid metabolism, glycosphingolipid biosynthesis, leucine and isoleucine biosynthesis, and vitamin B6 metabolism were responsible for the pathogenesis of BEB. Moreover, antioxidants may become therapeutic targets for BEB due to the role of oxidative stress in the etiology of the disease. The available results are encouraging, considering that the reported biological metabolites will provide novel scientific insights into the pathology and treatment decision of BEB.

Data Availability

The data used to support the findings of this study are available from the corresponding authors upon request.

Ethical Approval

The protocols of this study were approved by the Ethics Committee of Eye, Ear, Nose, and Throat Hospital of Fudan University.

Consent

The informed consent process was adhering to the tenets of the Helsinki Declaration, and all BEB subjects and healthy individuals signed the informed consent forms.

Conflicts of Interest

All authors declare that they have no conflict of interest.

Acknowledgments

This work was supported by the National Natural Science Foundation of China (Grant No.82070924).

Supplementary Materials

Supplementary 1. Supplementary Figure 1: PLS-DA and permutation test plots made from the serum samples from BEB patients and healthy controls. (A) PLS-DA scores plot generated from all serum samples in positive ionization mode. (B) PLS-DA scores plot generated from all serum samples in negative ionization mode. (C) Permutation test plot generated from all serum samples in positive ionization mode. (D) Permutation test plot generated from all serum samples in negative ionization mode. PLS-DA: partial least squares-discriminant analysis; BEB: benign essential blepharospasm.

Supplementary 2. Supplementary Figure 2: the ratios of L-kynurenine/tryptophan and tyrosine/phenylalanine in BEB patients and healthy controls. Boxplots are used to display the median and quartiles for the ratios of L-kynurenine to tryptophan (A) and o-tyrosine to phenylalanine (B). p values below or below 0.05 are indicated by the symbols * and ns.

Supplementary 3. Supplementary Table 1: significantly different metabolites between BEB patients and healthy controls.

Supplementary 4. Supplementary Table 2: significantly altered metabolites at different course of disease.

References

[1] G. Defazio, M. Hallett, H. A. Jinnah, A. Conte, and A. Berardelli, "Blepharospasm 40 years later," *Movement Disorders*, vol. 32, no. 4, pp. 498–509, 2017.

[2] J. Valls-Sole and G. Defazio, "Blepharospasm: update on epidemiology, clinical aspects, and pathophysiology," *Frontiers in neurology*, vol. 7, no. 7, p. 45, 2016.

[3] Y. Sun, P. J. Tsai, C. L. Chu, W. C. Huang, and Y. S. Bee, "Epidemiology of benign essential blepharospasm: a nationwide population-based retrospective study in Taiwan," *PLoS One*, vol. 13, no. 12, article e0209558, 2018.

[4] H. Dong, S. Fan, Y. Luo, and B. Peng, "Botulinum toxin relieves anxiety and depression in patients with hemifacial spasm and blepharospasm," *Neuropsychiatric Disease and Treatment*, vol. 15, pp. 33–36, 2019.

[5] H. A. Jinnah, A. Berardelli, C. Comella et al., "The focal dystonias: current views and challenges for future research," *Movement Disorders*, vol. 28, no. 7, pp. 926–943, 2013.

[6] H. Dong, Y. Luo, S. Fan, B. Yin, C. Weng, and B. Peng, "Screening gene mutations in Chinese patients with benign essential blepharospasm," *Frontiers in Neurology*, vol. 10, p. 1387, 2019.

[7] Y. Suzuki, M. Kiyosawa, M. Wakakura, and K. Ishii, "Glucose hypometabolism in the visual cortex proportional to disease severity in patients with essential blepharospasm," *NeuroImage: Clinical*, vol. 24, article 101995, 2019.

[8] D. I. Mostofsky, S. Yehuda, S. Rabinovitz, and R. Carasso, "The control of blepharospasm by essential fatty acids," *Neuropsychobiology*, vol. 41, no. 3, pp. 154–157, 2000.

[9] K. Serefoglu Cabuk, U. Tunc, G. Ozturk Karabulut et al., "Serum calcium, magnesium, phosphorus, and vitamin D in benign essential blepharospasm," *Graefe's Archive for Clinical and Experimental Ophthalmology*, vol. 258, no. 6, pp. 1293–1297, 2020.

[10] M. Deidda, C. Piras, P. P. Bassareo, C. Cadeddu Dessalvi, and G. Mercuro, "Metabolomics, a promising approach to translational research in cardiology," *IJC Metabolic & Endocrine*, vol. 9, pp. 31–38, 2015.

[11] C. Liu, L. Scorr, G. Kilic-Berkmen et al., "A metabolomic study of cervical dystonia," *Parkinsonism & Related Disorders*, vol. 82, pp. 98–103, 2021.

[12] L. Ma, J. Keng, M. Cheng et al., "Gut Microbiome and Serum Metabolome Alterations Associated with Isolated Dystonia," *Msphere*, vol. 6, no. 4, article e00283, 2021.

[13] S. F. Graham, X. Pan, A. Yilmaz et al., "Targeted biochemical profiling of brain from Huntington's disease patients reveals novel metabolic pathways of interest," *Biochimica et Biophysica Acta - Molecular Basis of Disease*, vol. 1864, no. 7, pp. 2430–2437, 2018.

[14] J. Jankovic and J. Orman, "Botulinum a toxin for cranial-cervical dystonia: a double-blind, placebo-controlled study," *Neurology*, vol. 37, no. 4, pp. 616–623, 1987.

[15] F. F. Peres, A. C. Lima, J. E. C. Hallak, J. A. Crippa, R. H. Silva, and V. C. Abílio, "Cannabidiol as a promising strategy to treat and prevent movement disorders?," *Frontiers in Pharmacology*, vol. 9, p. 482, 2018.

[16] N. Lu, Y. He, C. Chen, R. Tian, Q. Xiao, and Y. Y. Peng, "Tyrosine can protect against oxidative stress through ferryl hemoglobin reduction," *Toxicology In Vitro*, vol. 28, no. 5, pp. 847–855, 2014.

[17] G. Cui, Y. Qing, X. Hu et al., "Serum metabolomic profiling based on Fourier transform-ion cyclotron resonance-mass spectrometry: do the dysfunctions of metabolic pathways reveal a universal risk of oxidative stress in schizophrenia?," *Antioxidants & Redox Signaling*, vol. 33, no. 10, pp. 679–688, 2020.

[18] L. Paoletti, C. Elena, P. Domizi, and C. Banchio, "Role of phosphatidylcholine during neuronal differentiation," *IUBMB Life*, vol. 63, no. 9, pp. 714–720, 2011.

Hindawi
Oxidative Medicine and Cellular Longevity
Volume 2022, Article ID 8296043, 12 pages
https://doi.org/10.1155/2022/8296043

Research Article

Mechanisms of NO-Mediated Protein S-Nitrosylation in the Lens-Induced Myopia

Ying Lu,[1,2,3] **Weitao Song**,[1,2,3] **Yuanjun Li**,[1,2,3] **Jingge Xiao**,[4] **Kaixuan Du**,[1,2,3] **Qiuman Fu**,[1,2,3] **Yanni Zhang**,[1,2,3] **Liting Zhao**,[1,2,3] **Yewei Yin**,[1,2,3] **Tu Hu**,[1,2,3] **and Dan Wen**[1,2,3]

[1]*Eye Center of Xiangya Hospital, Central South University, Changsha, Hunan 410008, China*
[2]*Hunan Key Laboratory of Ophthalmology, Changsha, Hunan 410008, China*
[3]*National Clinical Research Center for Geriatric Diseases, Xiangya Hospital of Central South University, Changsha, Hunan 410008, China*
[4]*Xiangya School of Medicine, Central South University, Changsha, Hunan 410013, China*

Correspondence should be addressed to Dan Wen; wendan@csu.edu.cn

Received 16 August 2022; Accepted 1 October 2022; Published 16 November 2022

Academic Editor: Li-Ying Tang

Background. Myopia is a chronic ocular disease, emerging as the most common type of refractive error. This study intends to preliminarily explore the roles of protein S-nitrosylation of nitric oxide (NO) in the regulation of myopia by detecting the expression of neuronal nitric oxide synthase (nNOS) and downstream S-nitrosylation, using the animal model of lens-induced myopia (LIM) in mice. *Methods*. The 3-week-old C57BL/6 J mice were divided into three groups: group I, lens-induced 0-week group (take eyeballs at the age of 3 weeks); group II, self-control eyes of experimental group (take eyeballs at the age of 7 weeks); and group III, lens-induced 4-week group (take eyeballs at the age of 7 weeks). The diopter and axial length of each group were measured by streak retinoscopes and optical coherence tomography (OCT) before and after model establishment. The protein expressions and locations of nNOS and S-nitrosylated proteins (PSNOs) were measured by western blot and immunofluorescence staining. Site-specific proteomic for protein S-nitrolysation was used to detect the existence and location of S-nitrosylation proteins in the retina of myopic and nonmyopic mice. The Gene Ontology (GO), Kyoto Encyclopedia of Genes and Genomes (KEGG), and motif enrichment analyses were performed. The differential sites were analyzed by GO, KEGG, and motif. Irreversible biotinylation procedure combined with protein purification and western blot was used to detect the protein expression of α-enolase (ENO1), a key player in the hypoxia-related signal pathway. *Results*. The expressions of nNOS and PSNOs were significantly lower in the retina of experimental eyes than that in self-control eyes and 3-week-old baseline group. A total of 595 S-nitrosylated proteins, 709 S-nitrosylated peptides, and 708 S-nitrosylated sites were identified by site-specific S-nitrolysation proteomics in the retina of myopic and control eyes. A total of 19 differentiation loci were screened, of which 13 sites were downregulated and 6 sites were upregulated in experimental eyes compared with the self-control group. Specifically, the expression of SNO-ENO1 was significantly lower in the retina of experimental eyes than that in self-control eyes and 3-week-old baseline group. *Conclusion*. LIM induces the decrease of nNOS and PSNO protein levels in the retina of myopic mice. NO-mediated nonclassical protein S-nitrosylation modification may play an important role in the regulation of lens-induced myopia. ENO1 may be a key factor in the regulation of S-nitrosylation modification of myopia.

1. Introduction

Myopia is a chronic ocular disease, as the most common type of refractive error, and the prevalence of myopia is increasing rapidly in recent years [1]. High myopia can cause a variety of serious complications, including higher risk of posterior vitreous detachment, choroidal atrophy, retinal degeneration, retinal detachment, macular hole, and

macular hemorrhage [2, 3]. However, the occurrence of myopia is affected by many factors, such as genetic susceptibility and environmental factors. The pathogenesis of myopia is complex, and the mechanism of myopia onset remains unclear. The exploration of the pathological process and pathogenesis is an urgent problem to be solved in the study of myopia.

Nitric oxide, produced by NO synthase (NOS), widely participates in the regulation of nervous system, cardiovascular system, and immune system. NO signaling could be classified into classical and nonclassical schemes. In the classical scheme, normal physiological concentrations of NO acts through activation of its specific receptor soluble guanylyl cyclase (sGC), elevating intracellular $3',5'$-cyclic guanosine monophosphate (cGMP) [4], which serves as a second messenger and activates cGMP-dependent protein kinase (PKG) [5]. Recently, there have been several reports of the participation of non-cGMP-dependent way in cell function regulation. S-nitrosylation, the NO mediated redox-type reversible modification of cysteine thiols, affects the modulation of conformation, stability, and activity of protein and protein-protein interactions [6]. Previous studies have indicated that NO exerted its function via the cGMP dependent pathway and dysregulated NO overproduction caused by inducible nitric oxide synthase (iNOS), enduothelial nitric oxide synthase (eNOS), and nNOS and is critically involved in myopia development [7–9]. However, the mechanism underlying the effect of protein S-nitrosylation in myopia has not been understood.

S-Nitrosocysteine residues often affect protein activity, protein-protein interaction, and protein localization [10, 11]. Numerous studies have shown that dysregulation of NO and S-nitrosothiol (SNO) signaling is involved in progression of many neurodevelopmental, neurobehavioral, and neurodegenerative disorders [12–15]. Under physiologic conditions, protein S-nitrosylation provides protection against further cellular oxidative and nitrosative stress [16]. Nevertheless, the role of protein S-nitrosylation in the development of myopia has not been directly investigated. S-Nitrosoproteomics greatly facilitated the elucidation of multiple underlying processes of protein S-nitrosylation in various species, including mitochondrial fatty acid metabolism, neural signaling, and neurodegeneration [11, 17–19].

In this study, site-specific proteomic profiling of endogenously S-nitrosylated proteins in myopia tissues was performed to provide a new perspective for nitric oxide and protein S-nitrosylation during myopia pathogenesis. The goals of this study were to provide mechanistic insight into the contribution of NO in various ophthalmic diseases, especially in myopia, and suggest potential and promising therapeutic protein targets and sites for treatment.

2. Materials and Methods

2.1. Experimental Animal. Sixty-five SPF-grade healthy 3-week-old male C57BL/6 J mice weighed 10-15 g were used in this study obtained from the laboratory Animals Department of Central South University. Tropicamide phenylephrine (0.5%) eye drops were utilized to examine the condition of mice eyes, in order to exclude mice with ophthalmic diseases such as keratitis, corneal leukoplakia, pupil atresia, cataract, and vitreous hemorrhage. Mice were given ad libitum access to food and water and reared in a 12 : 12 hr light:dark cycle at approximately 350-500 lux with good ventilation at the temperature of 20°C-25°C, and the cage box and cushion were changed every 3 days to keep the feeding environment clean. All procedures were approved by the Animal Ethics Committee of Central South University (ethical clearance and approval No. 202103175) and adhered to the ARVO Statement for the Use of Animals in Ophthalmic and Vision Research.

C57BL/6 J mice (3-week-old male, $n = 65$) were randomly divided in 3 groups, viz., group I: 15 mice (30 eyes), lens-induced 0-week group (take eyeballs at the age of 3 weeks); group II: 50 mice (50 left eyes), self-control eyes of the experimental group (take eyeballs at the age of 7 weeks); and group III: 50 mice (50 right eyes), -10D lens-induced 4-week group (take eyeballs at the age of 7 weeks).

2.2. Establishment of a Model of Optical Defocus Myopia. Use the cyanoacrylate adhesive to adhere the rubber ring and the clear -10D lens periphery (about 8 mm diameter) provided by Kang Ming Company to make an optical defocus lens with a diameter of about 10 mm. Mice were anesthetized with 1% pentobarbital sodium (0.01 ml/g), and the lens was sutured on the skin around the right eye with 4-0 braided polyester sutures thread through interrupted sutures. Hand-made plastic collar with an outer diameter of about 50 mm and an inner diameter of 10 mm was glued to the neck to prevent mice from grabbing off the lens. The periocular skin was disinfected with povidone iodine (0.5 g/L, Annjet) before the operation, and the conjunctival sac was washed with levofloxacin eye drops (3 mg/ml, Baush) to prevent infection. Defocus lenses were checked daily for fit and compliance to keep the optical defocus state. And ocular health was also monitored daily; animals with keratitis, corneal leukoplakia, pupil atresia, cataract, and vitreous hemorrhage were excluded from further analysis. After 4 weeks of induction, the lens was removed, the diopter and the axial length were measured, and the retinal tissue was detected. The left eye served as a paired control and received no treatment.

2.3. Diopter and Axial Length Measurement. Refraction and axial length were measured twice for each eye: before and after induction. 1% pentobarbital sodium and 0.5% tropicamide phenylephrine eye drops were applied to the mice eyes to ensure anesthesia and mydriasis, respectively. 10 minutes later, the diopter of the mice was measured using retinal band optometry, and the eye axial length was measured using the Visante OCT (Carl Zeiss Meditec, Germany) by the same experienced optometrist. Each eye was measured three times and averaged.

2.4. Determination of Protein S-Nitrosylation. After the measurement of the diopter and axial length, mice were sacrificed via cervical vertebra dislocation, and eyes were subsequently removed. The muscle and fascia tissue was

Table 1: The refraction and the axial length in 4 weeks after modeling ($\bar{x} \pm s$).

	Group I	Group II	Group III	P_{I-II}	P_{I-III}	P_{II-III}
Diopter/D	11.633 ± 2.385	9.520 ± 3.351	−0.080 ± 1.998	0.003	<0.001	<0.001
Axial length/mm	3.397 ± 0.034	3.415 ± 0.052	3.490 ± 0.048	0.345	<0.001	<0.001

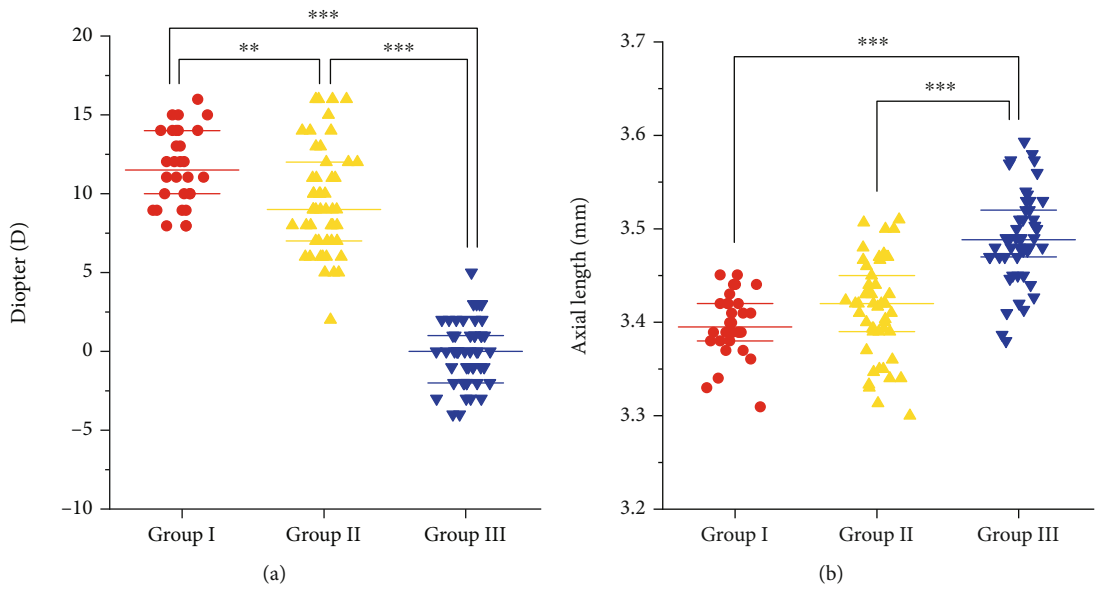

Figure 1: Comparison of refraction and axial length after 4 weeks of LIM. (a) Comparison of refraction. (b) Comparison of axial length ($^{***}P < 0.001$, $^{**}P < 0.01$, $^{*}P < 0.05$).

firstly separated, followed by the eyeball being incised along the limbus under the microscope, then the lens and vitreous tissue in the eye were removed, the sclera was separated, and the retina was stored finally at-80°C. The measurement of S-nitrosylated protein of the retina was performed by immunoprecipitation or the biotin switch assay with anti-biotin antibody (Cayman 1 : 1000). The biotin switch assay was performed as described previously by Jaffrey and Snyder [20]. Briefly, the retina tissues were homogenized in the HEN buffer (250 mM HEPES-NaOH, pH 7.7, 1 mM EDTA, 0.1 mM neocuprione) without sodium dodecyl sulfate (SDS), and the MMTS was added to block free thiol groups. Secondly, S-nitrosothiols were reduced by ascorbate, and then the new free thiol groups were biotinylated by biotin-HPDP. The protein with biotin tag was purified by streptavidin. Finally, the biotinylated protein was analyzed by immunoblotting with biotin antibody.

2.5. Western Blot. Western blot was performed as described previously [21]. Electrophoresis transferred and blocked was performed in sequence with the protein extracted from the retinal homogenate according to the standard protocol. The primary antibodies, nNOS (Abcam, ab229785, 1 : 1000) and ENO1 (Zen-Bio, R23329, 1 : 1000), were incubated overnight, and the secondary antibody was incubated for 2 hours. The densities of light bands were analyzed quantitatively by ImageJ software.

2.6. Immunofluorescence. Another 6 mice in each group were randomly selected, and the eyeballs were fixed in the eyeball fixation at 4°C for 24 hours, followed by the dehydration with graded alcohol. With absorbing water, the eyeballs were transferred to OCT embedding. After frozen in the cryogenic table, retinal tissue was sectioned along the optical axis to a thickness of 15 μm. The section with optic nerve passing through the posterior pole was selected, pasted on the adhesive slides, and stored in the refrigerator at-20°C. Cryosections of each eyeball were frozen in 4% paraformaldehyde for 30 minutes and blocked with 5% normal bovine serum for 1 hour at room temperature. Sections were incubated overnight with primary antibodies specific for nNOS (Affinity, 1 : 100) and washed thoroughly with phosphate-buffered saline. After further incubation with species-appropriate secondary antibodies conjugated to anti-rat 594 (Jackson ImmunoResearch, 1 : 200), sections were counterstained with DAPI (Sigma, Fluoroshield with DAPI), mounted, and photographed using a fluorescence microscope (DM4B, Lecia, Germany).

2.7. Site-Specific Identification of S-Nitrosylated Proteins in Retinal Tissue of Myopic Mice. Retinal tissues from experimental eyes and control eyes were collected, and 10 of them were taken as one sample and two biological replicates. A total of 20 mice, 40 eyes, were separately analyzed by site-specific proteomics for discovery of S-nitrosylated proteins. Negative

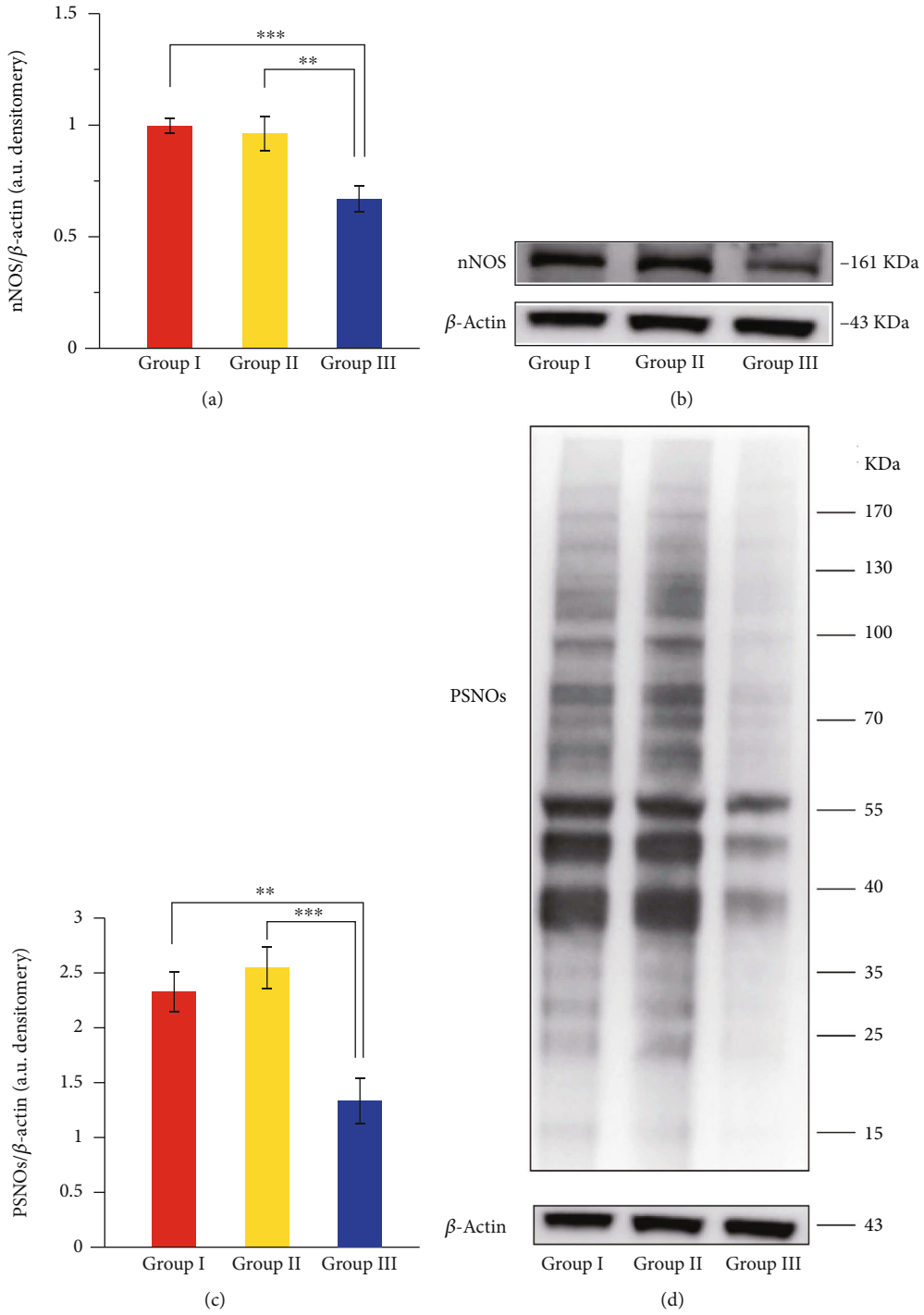

Figure 2: Continued.

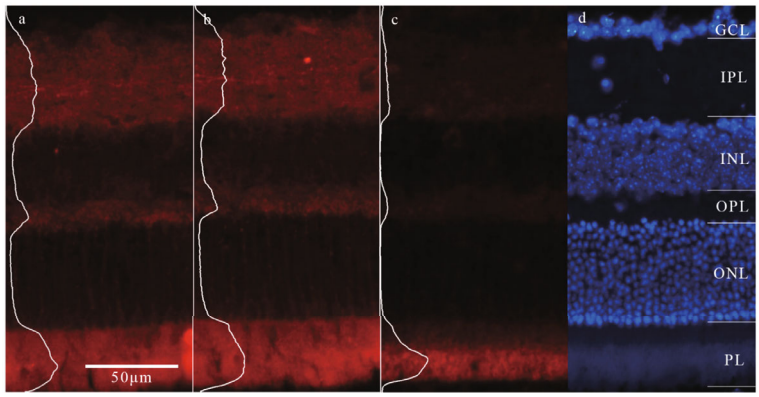

(e)

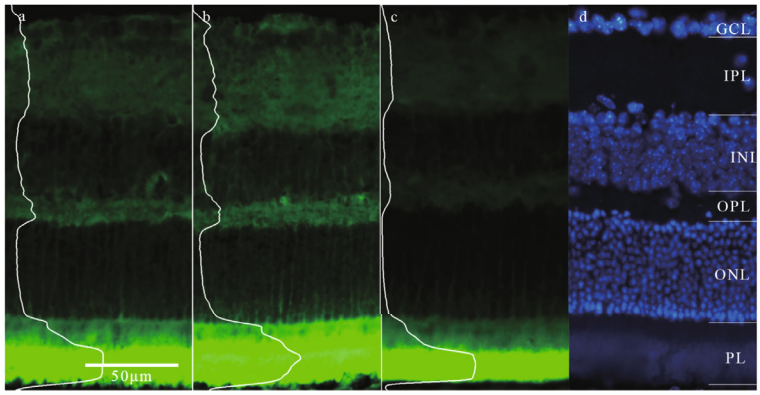

(f)

Figure 2: Expression of nNOS and PSNOs in the retina of groups I, II, and III. (a, b) Expression of nNOS in the retina of groups I, II, and III. (c, d) Expression of PSNOs in the retina of groups I, II, and III. (e) The expression of nNOS in the retina of group I, group II, and group III (nNOS: red fluorescence; DAPI: blue fluorescence). (f) The expression of PSNOs in the retina of group I, group II, and group III (PSNOs, green fluorescence; DAPI, blue fluorescence): (a) retina of group I, (b) retina of group II, (c) retina of group III, and (d) DAPI staining nucleus. GCL: ganglion cell layer; IPL: inner plexiform layer; INL: inner nuclear layer; OPL: outer plexiform layer; ONL: outer nuclear layer; PL: photoreceptor layer ($^{***}P < 0.001$, $^{**}P < 0.01$, $^{*}P < 0.05$).

control without sodium ascorbate treatment during biotinylation of S-nitrosylated proteins was included in each experimental and control tissue, which were also analyzed by mass spectrometry to exclude false positive identification due to incomplete blocking. Reliable identifications of S-nitrosylated peptides were finally obtained by searching with MaxQuant (version 2.0.1.0) using a FDR of <1% at both the peptide and protein group levels for control of false identification.

2.8. Statistical Analysis. Data were analyzed using SPSS software (version no. 24.0; IBM Corp.). Multiple comparisons were analyzed using ANOVA, followed by Tukey's post hoc test. An independent samples t-test was used to analyze independent samples. A paired t-test was used to analyze differences between paired experimental specimens. Data were presented as the mean ± SEM. $P < 0.05$ was considered to indicate a statistically significant difference.

3. Results

3.1. Confirmation of Lens-Induced Myopia. There were no significant differences in refraction or axial length among all groups before the experiment at baseline ($P > 0.05$). Additionally, there were no significant differences in refraction or axial length between the two eyes of the same animal ($P > 0.05$). After 28 days of defocus, refraction for group I, group II, and group III was +11.633 ± 2.385 D, 9.520 ± 3.351 D, and −0.080 ± 1.998 D, respectively (Table 1, Figure 1(a)). After 28 days of defocus, axial length of group I, group II, and group III was 3.397 ± 0.034 mm, 3.415 ± 0.052 mm, and 3.490 ± 0.048 mm, respectively (Table 1, Figure 1(b)).

3.2. The Expression of nNOS and PSNO Protein in Retina Decreased in LIM Group. The expressions of nNOS in retinal tissues of groups I, II, and III were tested. Abundances of nNOS in group III showed an obvious decrease compared with groups I and II (Figures 2(a) and 2(b)). We further found that the total expression level of PSNOs in group III was also significantly lower than groups I and II (Figures 2(c) and 2(d)). Immunofluorescence showed that the expression of nNOS and PSNOs was high in ganglion cell layer (GCL), inner plexiform layer (IPL), and outer plexiform layer (OPL) but low in inner nuclear layer (INL) and outer nuclear layer (ONL). The expression levels of nNOS

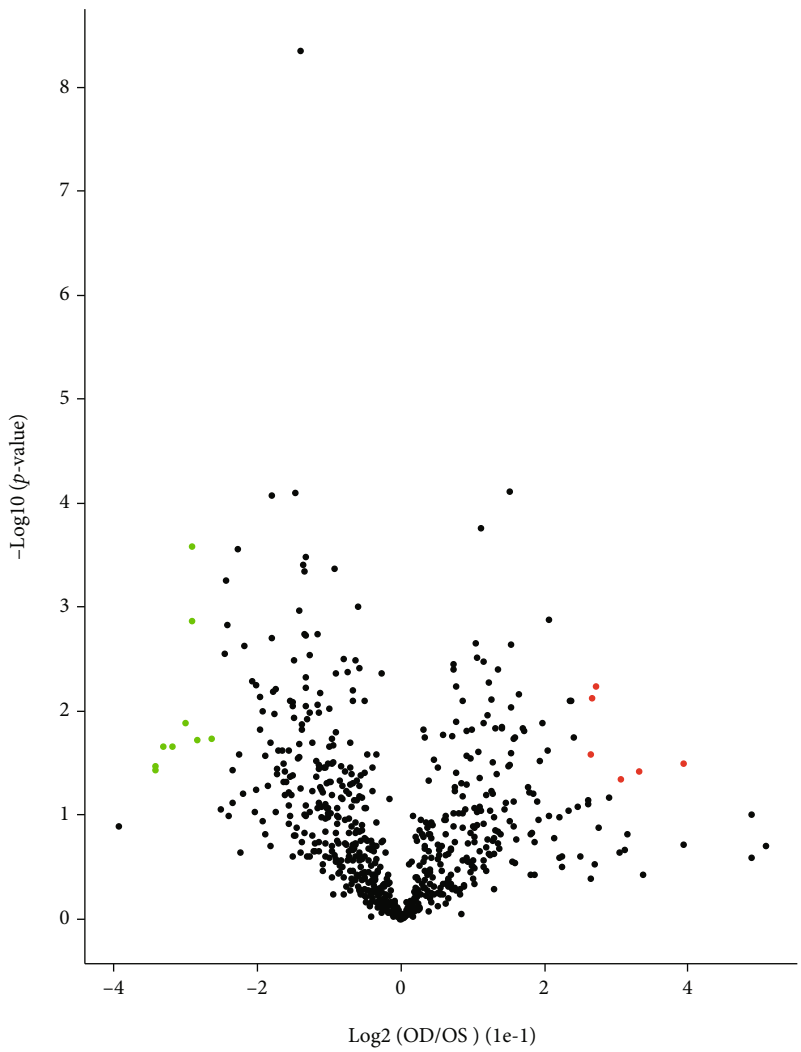

Figure 3: The volcanic map was expressed at the differential site. The green expression is downregulated, the red expression is upregulated, and the black is the differential modification site. The protein S-nitrosytation modification site is derived through LIM versus self-control group.

and PSNOs in retina in group III were significantly lower than those in groups I and group II (Figures 2(e) and 2(f)). Remarkable downregulation of nNOS expression and protein S-nitrosylation suggested that this NO-mediated protein modification might play a role in myopic pathogenesis.

3.3. Site-Specific Identification of S-Nitrosylated Proteins in Retinal Tissue of Myopic Mice. For a comprehensive view of protein S-nitrosylation, we used a site-specific proteomic approach to characterize S-nitrosylated proteins and modified Cys residues in myopic (group III) and control (group II) retina tissues. In this method, endogenously S-nitrosylated proteins in myopic and control retina were first irreversibly biotinylated via biotin-switch, followed by tryptic digestion, biotin-affinity purification, and final identification of protein identity and modification sites using Orbitrap Exploris TM 480 mass spectrometer. LC-MS/MS analysis was performed on each experimental and control tissues. Biotinylated peptides identified in negative controls were excluded from the corresponding S-nitrosylation dataset. In retinas from four groups, a total of 709 S-nitrosylated peptides and 595 S-nitrosylated proteins were identified. 19 differentially modified modification sites were identified between the myopic and control eyes (fold change < 0.83, $P < 0.05$), of which 13 were downregulated and 6 were upregulated in the myopic eyes compared with the control eyes (fold change > 1.2, $P < 0.05$, Figure 3).

3.3.1. GO Classification and GO Enrichment Analysis. A total of 19 differentially modified modification sites were analyzed by GO classification and GO enrichment analysis (Figures 4 and 5). The results showed that the differential S-nitrosytation modified proteins in the LIM myopia model were mainly related to the following biological processes (BP): cell metabolism (GO: 0044237), cell growth (GO: 0048896, GO: 0016049), signal transduction (GO: 0007165), positive and negative feedback regulation (GO: 0048523, GO: 0051094), response to stress and stimulation

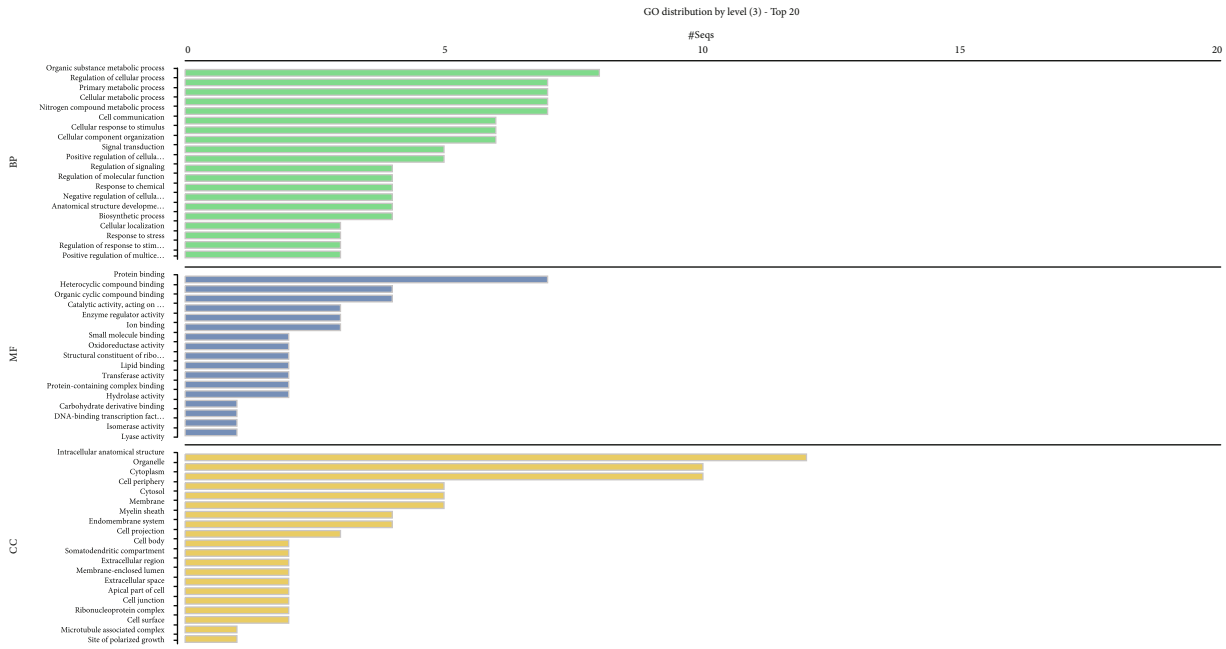

Figure 4: GO classification of differential S-nitrosytation sites in the retina between LIM and self-control group.

(GO: 0050896, GO: 0051716), etc. In myopic eyes, S-nitrosytation protein occurs in different cellular components (CC): cytoplasm (GO: 0016020), nucleus (GO: 0005634), cell membrane (GO: 0016020), ribosome (GO: 0005840), etc. The proteins with differential S-nitrosytation modification in myopic eyes were proved to be mainly related to the following molecular functions (MF): GDP/GTP enzyme activity (GO: 005096, GO: 0005093, GO: 0051020, GO: 0005096), rhodopsin kinase activity (GO: 0050254), etc.

3.3.2. KEGG Pathway Analysis. In order to better understand the biological role of protein S-nitrosytation modification in the pathogenesis of myopia, the KEGG pathways of identified 19 differentiated sites were further analyzed (Figure 6). Analysis showed that S-nitrosytation sites were enriched in signal pathways related to protein processing (mmu04141), glycolysis/gluconeogenesis (mmu00010), photoconduction (mmu04744), and HIF-1 (mmu04066).

3.3.3. Motif Enrichment Analysis. Previous studies have shown that the amino acid compositions on both sides of the cysteine residue have a great influence on the sensitivity and specificity of the redox-mediated posttranslational modification of cysteine [3]. In order to further understand the environmental driving factors of protein, the amino acid composition characteristics near the S-nitrosytation residues of 19 differential sites in the retina of groups II and III were analyzed by using the Motif-X algorithm (Figure 7). The result revealed that the amino acid residues containing basic and acidic side chains near the S-nitrosytation cysteine residues were highly expressed, such as basic amino acid lysine (K) and acidic amino acid glutamic acid (E). It is suggested that the acid-base sequence may play a potential role in promoting the pathological process of myopia mediated by redox modification.

3.4. The Expression of ENO1 and SNO-ENO1 in Retina of LIM Group Showed Differential Changes. Hypoxia has been shown to be an important mechanism of myopic pathological injury in recent years. ENO1 is the key enzyme in the last step of glycolysis pathway, which is closely related to tissue ischemia and hypoxia. The analysis of differential sites found that the expression of SNO-ENO1 was downregulated in the retina of myopia. In order to explore the role of ENO1 in the pathogenesis of myopia, the expressions of ENO1 in the retina of groups I, II, and III were detected by immunoblotting. After 4 weeks of modeling, there was no significant difference in the expression of ENO1 protein among the three groups ($P > 0.05$, Figure 8(a)). Lens induced did not change the protein expression level of ENO1.

In order to explore whether ENO1 participates in the regulation of myopia by S-nitrosytation, the expression levels of SNO-ENO1 in the retina of groups I, II, and III were further detected, and the expression level of ENO1 in the same sample was used as a reference. It was found that the expression level of SNO-ENO1 in group III was significantly lower than that in group I ($P = 0.006$, Figure 8(b)) and the left eye in group II ($P = 0.036$, Figure 8(b)). There was no significant difference in the expression of nNOS between group I and group II ($P = 0.378$, Figure 8(b)). Lens induced decreased the expression of SNO-ENO1.

4. Discussion

Myopia, especially high myopia, as a chronic ophthalmopathy with high incidence, has caused a huge social and economic burden. Complications such as posterior vitreous detachment, choroidal atrophy, retinal degeneration, retinal detachment, macular hole, and macular hemorrhage caused by high myopia are the main causes of blindness [2, 3]. At present, it is believed that the changes of signal pathway

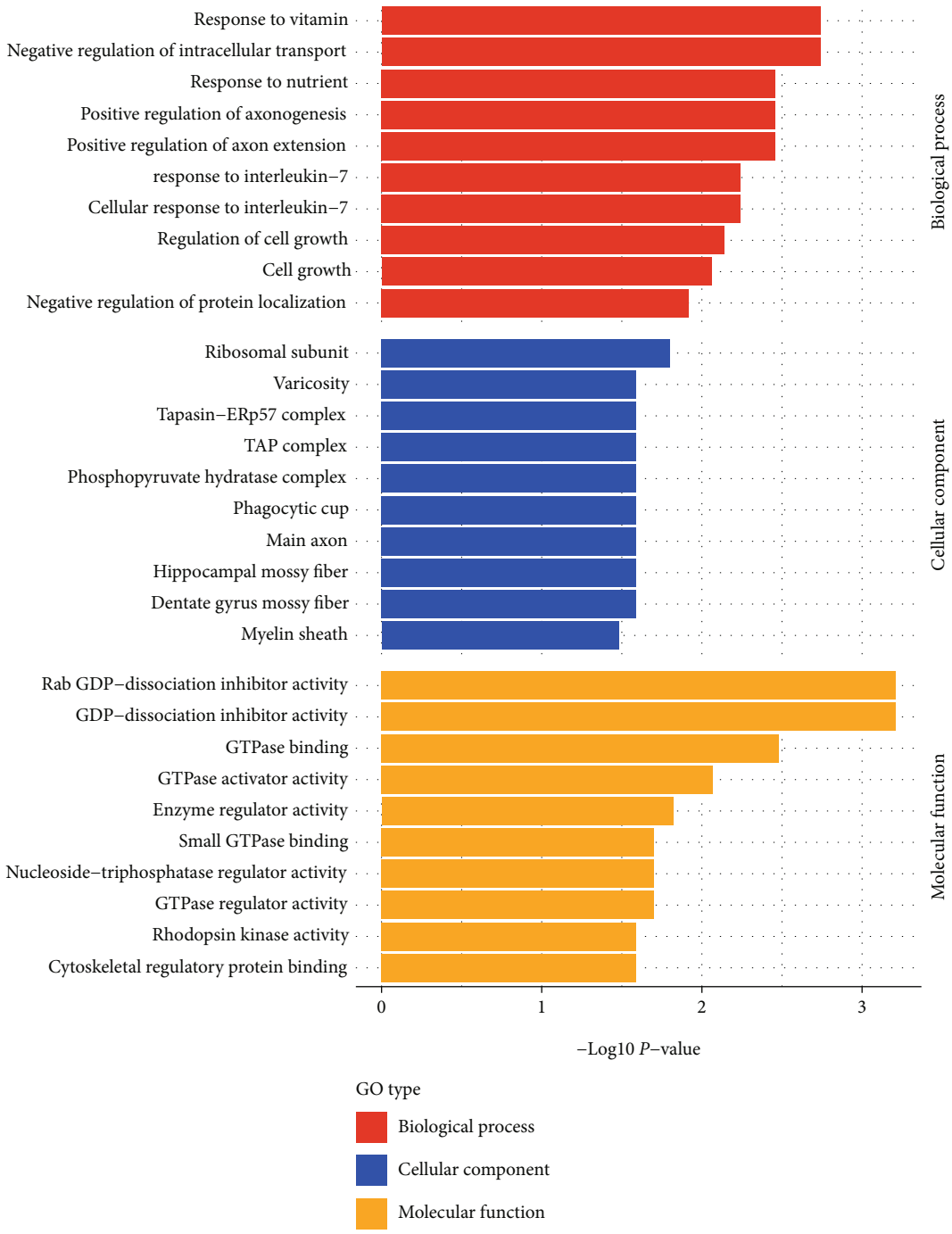

Figure 5: GO enrichment of differential S-nitrosytation site in the retina between LIM and self-control group.

caused by abnormal visual stimulation play an important role in the occurrence and development of myopia. There are many studies focusing on signal pathways related to the myopia. NO is known to participate in the regulation of myopia through the classical cGMP signal pathway [7, 22–24]. Fujii et al. found that form deprivation reduced the iNOS mRNA expression in chick retina-RPE-choroid [22]. Another study showed that after form deprivation 7 days, the activity of NOS in the deprivation group was lower than in the control group, but after form deprivation 14 days and 21 days, the activity of NOS in the deprivation group increased rapidly and significantly higher than in the control group. This trend of decreasing first and then increasing may be a way of regulating myopia through inducing different responses of eNOS and nNOS by acute and chronic hypoxia [7]. Additionally, the results of our previous studies on form deprivation in guinea pigs for 1 week, 2 weeks, and 3 weeks showed that with the extension of form deprivation

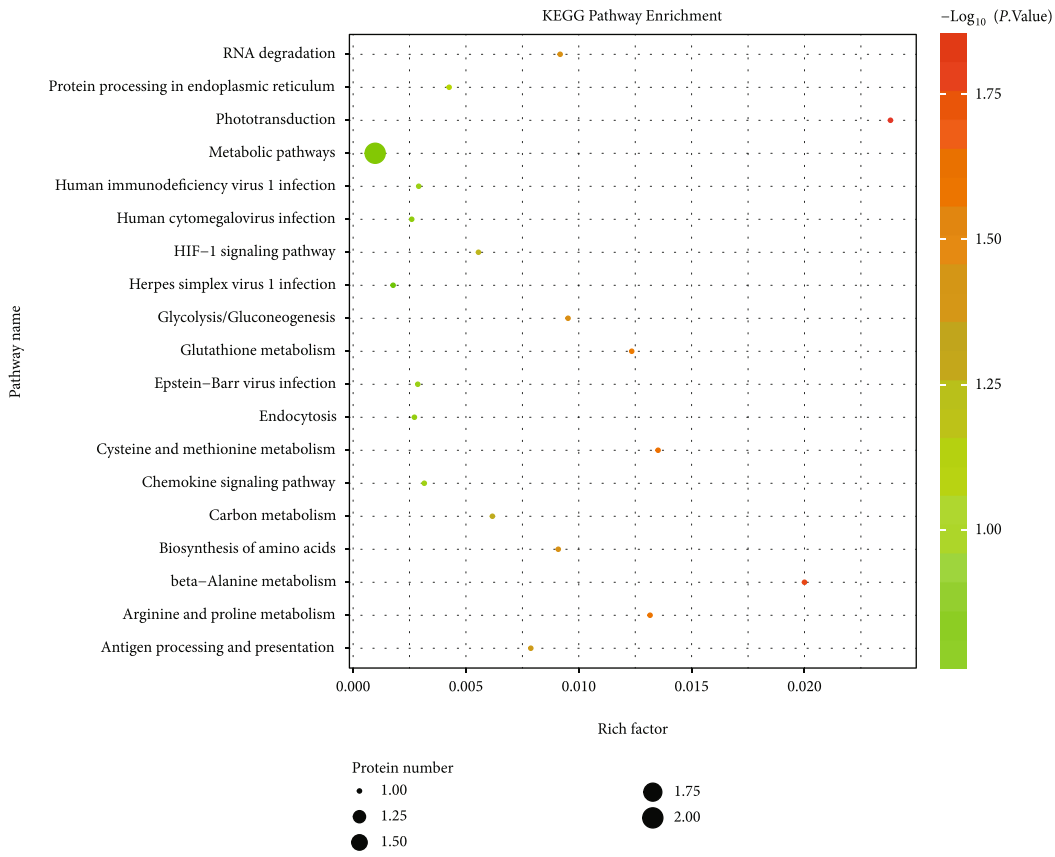

Figure 6: Enrichment analysis of S-nitrosytation KEGG pathway in the retina between LIM and self-control group.

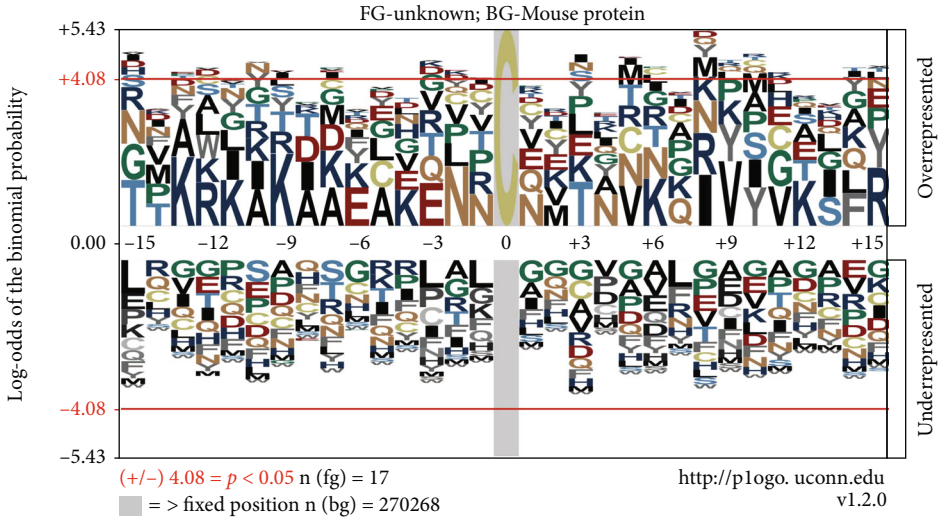

Figure 7: Motif analysis of differential sites of S-nitrosytation in the retina between LIM and self-control group.

time, the expression levels of nNOS and cGMP gradually increased in comparison with the control group, and there was a positive correlation between them [23, 24].

In this study, we showed that after 4 weeks of lens-induced, the expression level of nNOS in the retina of myopic mice was significantly lower than the control group, which was contrary to the previous research results. We speculate that this discrepancy might be due to the differences in animal model, model selection, and modeling time. Since LIM and from deprivation myopia (FDM) belong to two different myopic models in terms of pathogenic mechanism, the expression of NO is likely to be distinct.

We also conjecture that NO may play different roles in different stages of myopia development and may dynamically

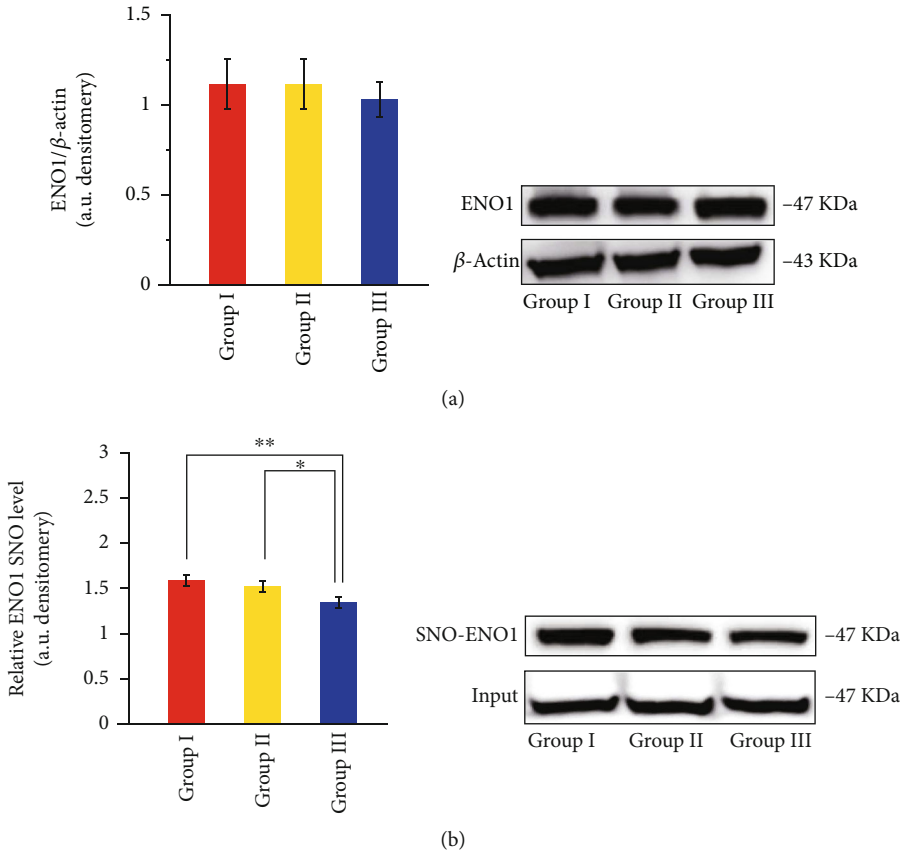

Figure 8: The expression of ENO1 and SNO-ENO1 was detected in the retina of groups I, II, and III. Input was used as the positive control group, and the existence of ENO1 protein in the cell lysate was verified.

regulate the occurrence and development of myopia based on the variance of NOS expression at different time points. In the follow-up research, further investigation like detecting NOS at multiple time points in the LIM model should be done to better clarify the role of NO in the occurrence and development of LIM.

Previous studies of NO mainly focused on the classical cGMP-related signal pathways, especially in the nervous system, and NO is known to activate important physiological cascade responses and participate in the regulation of neuronal differentiation and synaptic plasticity in the central nervous system [4]. Studies have shown that synaptic plasticity of NO and cGMP in various brain regions of hippocampus, cerebellum, cerebellum, and striatum is necessary, and NO-cGMP-related signal pathways have a crucial role in long-term potentiation (LTP), long-term depression (LTD), and learning [25]. Impaired NO and cGMP signaling are closely related to the etiology and progression of neurodegenerative diseases and cognitive impairment [26–28]. In recent years, the role of NO-mediated S-nitrosytation modification in diseases has received more attention. Many diseases such as atherosclerosis, malignant tumor, Alzheimer's disease, Parkinson's syndrome, neuronal degeneration, and Huntington's chorea are characterized by abnormal protein S-nitrosytation products [29]. Some researchers have also studied the regulation of NO-mediated S-nitrosytation on the retina: Vielma et al. found that the amplitude of ERG in rats unrelated to cGMP was increased by vitreous injection of exogenous NO donors, and then NO donors caused the increase of GCL and PL S-nitrosytation protein through S-nitrosytation immunofluorescence experiments. It was suggested that NO may improve retinal function by S-nitrosytation modification [30]. In another study of light and light withdrawal, Bloom found that S-nitrosytation protein signals were strong in the retinas of light-adapted mice, while there was almost no S-nitrosytation signal in dark-adapted retinas, proving that the S-nitrosytation of retinal tissue is light-dependent. Taken together, these studies highlight the wide presence of nitroso-modified proteins in retinal tissue and suggest that myopia is closely related to signals including light intensity and light conduction, which can be influenced by experimental myopia model. However, previous studies have not been able to confirm the role of NO-mediated S-nitrosytation modification in the pathogenesis of myopia. In this study, we found that PSNOs in myopic retina were significantly lower than the control group, and immunofluorescence showed the expression of PSNOs high in GCL, IPL, and OPL layer but low in INL and ONL layer. These findings indicate that the decrease of the PSNO expression in the retina of myopia may be related to the decrease of light stimulation in myopic models.

We identified 19 differential modification sites through site-specific identification of S-nitrosylated proteins. Using bioinformatics analysis, we found that the differentially

modified proteins were enriched in the signal pathways related to the occurrence and development of myopia, such as energy metabolism, photoconduction, and HIF-1. Thus, we hypothesize that NO is involved in the occurrence and development of myopia through S-nitrosytation modification.

Differential site analysis showed that compared with the control group, the expression of SNO-ENO1 in HIF-1 signaling pathway was downregulated. Studies have shown that hypoxia-induced metabolic reprogramming from mitochondrial respiration to glycolysis required the participation of ENO1, which is a key enzyme in glycolysis [31]. ENO1 has also been reported to be associated with hypoxic-ischemic retinal disease. The expression of HIF-1 and ENO1 in human retinal pigment epithelial cells significantly upregulated under hypoxia and anoxia. In subsequent experiments, it was found that silencing ENO1 did not affect the content of hypoxia-induced vascular endothelial growth factor (VEGF), suggesting that ENO1 may be involved in the regulation of hypoxia pathways other than VEGF [32]. Hypoxia injury is an important mechanism of myopia pathological injury proposed in recent years. Previous studies related to myopia hypoxia were mainly concentrated in the sclera, considering that sclera hypoxia was the trigger factor of myopia [33, 34]. The results of mass spectrometry and immunoblotting showed that there was no significant difference in the expression of ENO1 between myopic and nonmyopic mice, but SNO-ENO1 was downregulated in myopic retina. Recent studies have shown that hypoxia is the key mechanism of myopia, and ENO1 is closely related to hypoxic ischemic retinal disease. We speculate that ENO1 may mediate the occurrence and development of myopia through the dynamic regulation of S-nitrosytation modification and denitrification modification in the hypoxia signal pathway. We further suggest that SNO-ENO1 may be an inactivated form of ENO1. When the tissue is in S-nitrosytation state, ENO1 exists in the state of S-nitrosytation modification, while when the tissue is anoxic, SNO-ENO1 is denitrified to activate ENO1 and participate in the process of glycolysis. However, the research to date has not been able to elucidate of the mechanism of action of the protein around the world, which is worthy of further research and exploration, especially in various ischemic and hypoxic diseases and the occurrence and development of myopia.

5. Conclusion

Considering all of this evidence, it seems that NO participates in the occurrence and development of myopia through S-nitrosytation modification, and ENO1 regulates this process as a target protein of S-nitrosytation modification. A large number of endogenously S-nitrosylated proteins and their modification sites in C57BL/6 J mouse retinal tissue were identified by site-specific proteomics. A total of 19 differentiation loci were screened, of which 13 sites were downregulated and 6 sites were upregulated in experimental eyes compared with the self-control group. These differentiation loci involving multiple processes and signaling pathways such as phototransduction, hypoxia, and energy metabolism are closely associated with myopia. These findings provided novel insights into NO signaling and S-nitrosylation in myopia development and also a basis for the diagnosis and treatment of retinal diseases based on protein modification.

Data Availability

The datasets used or analyzed during the current study are available from the corresponding author on reasonable request.

Ethical Approval

All procedures were approved by the Animal Ethics Committee of Central South University (ethical clearance and approval No. 202103175) and adhered to the ARVO Statement for the Use of Animals in Ophthalmic and Vision Research.

Conflicts of Interest

The authors declare that there is no conflict of interest.

Authors' Contributions

Ying Lu and Weitao Song have contributed equally to this work and should be considered co-first authors.

Acknowledgments

The study was supported by the Hunan Provincial Natural Science Foundation (No. 2021JJ70147 to Dan Wen) (36,000 CNY), National Natural Science Foundation of China (No. 82000937 to Yuanjun Li) (25,000 CNY), Hunan Provincial Natural Science Foundation (No. 2021JJ41003 to Yuanjun Li) (13,000 CNY), and College Students' Innovation and Entrepreneurship Training Program of Grade 19 (Grant No. S2022105330513) (500 CNY).

References

[1] P. G. Hysi, H. Choquet, A. P. Khawaja et al.et al., "Meta-analysis of 542,934 subjects of European ancestry identifies new genes and mechanisms predisposing to refractive error and myopia," *Nature Genetics*, vol. 52, no. 4, pp. 401–407, 2020.

[2] S.-M. Saw, G. Gazzard, E. C. Shih-Yen, and W.-H. Chua, "Myopia and associated pathological complications," *Ophthalmic and Physiological Optics*, vol. 25, no. 5, pp. 381–391, 2005.

[3] C. Mak, J. C. Yam, L. Chen, S. Lee, and A. L. Young, "Epidemiology of myopia and prevention of myopia progression in children in East Asia: a review," *Hong Kong Medical Journal*, vol. 24, no. 6, pp. 602–609, 2018.

[4] J. Garthwaite, "Concepts of neural nitric oxide-mediated transmission," *European Journal of Neuroscience*, vol. 27, no. 11, pp. 2783–2802, 2008.

[5] S. H. Francis, J. L. Busch, J. D. Corbin, and D. Sibley, "CGMP-dependent protein kinases and cgmp phosphodiesterases in nitric oxide and cgmp action," *Pharmacological Reviews*, vol. 62, no. 3, pp. 525–563, 2010.

[6] V. Fernando, X. Zheng, Y. Walia, V. Sharma, J. Letson, and S. Furuta, "S-nitrosylation: an emerging paradigm of redox signaling," *Antioxidants*, vol. 8, no. 9, p. 404, 2019.

[7] J. Wu, Q. Liu, X. Yang, H. Yang, X.-m. Wang, and J.-w. Zeng, "Changes of nitric oxide synthase and cyclic guanosine monophosphate in form deprivation myopia in guinea pigs," *Chinese Medical Journal*, vol. 120, no. 24, pp. 2238–2244, 2007.

[8] H. Sun, J. Zhang, X. Li, X. Ji, and L. Wei, "Expression changes of inos and mmp-2 in form deprivation myopia (in chinese)," *Chinese Journal of Practical Medicine*, no. 8, p. 3, 2009.

[9] T. Fujikado, Y. Kawasaki, J. Fujii et al., "*The Effect of Nitric Oxide Synthase Inhibitor on Formdeprivation Myopia*," *Current Eye Research*, vol. 16, p. 98, 1997.

[10] D. T. Hess, A. Matsumoto, S.-O. Kim, H. E. Marshall, and J. S. Stamler, "Protein _S_ -nitrosylation: purview and parameters," *Nature Reviews Molecular Cell Biology*, vol. 6, no. 2, pp. 150–166, 2005.

[11] U. Seneviratne, A. Nott, V. B. Bhat et al., "S-nitrosation of proteins relevant to Alzheimer's disease during early stages of neurodegeneration," *Proceedings of the National Academy of Sciences*, vol. 113, no. 15, pp. 4152–4157, 2016.

[12] M. K. Tripathi, M. Kartawy, and H. Amal, "The role of nitric oxide in brain disorders: autism spectrum disorder and other psychiatric, neurological, and neurodegenerative disorders," *Redox Biology*, vol. 34, p. 101567, 2020.

[13] T. Nakamura, O. A. Prikhodko, E. Pirie et al., "Aberrant protein _S_ -nitrosylation contributes to the pathophysiology of neurodegenerative diseases," *Neurobiology of Disease*, vol. 84, pp. 99–108, 2015.

[14] T. Nakamura, S. Tu, M. W. Akhtar, C. R. Sunico, S.-I. Okamoto, and S. A. Lipton, "Aberrant protein S-nitrosylation in neurodegenerative diseases," *Neuron*, vol. 78, no. 4, pp. 596–614, 2013.

[15] H. Amal, B. Barak, V. Bhat et al., "_Shank3_ mutation in a mouse model of autism leads to changes in the S-nitrosoproteome and affects key proteins involved in vesicle release and synaptic function," *Molecular Psychiatry*, vol. 25, no. 8, pp. 1835–1848, 2020.

[16] J. Sun, C. Steenbergen, and E. Murphy, "S-nitrosylation: NO-related redox signaling to protect against oxidative stress," *Antioxidants & Redox Signaling*, vol. 8, no. 9-10, pp. 1693–1705, 2006.

[17] P.-T. Doulias, M. Tenopoulou, J. L. Greene, K. Raju, and H. Ischiropoulos, "Nitric oxide regulates mitochondrial fatty acid metabolism through reversible protein s-nitrosylation," *Science Signaling*, vol. 6, no. 256, p. rs1, 2013.

[18] H. S. Chung, G. E. Kim, R. J. Holewinski et al., "Transient receptor potential channel 6 regulates abnormal cardiac S-nitrosylation in duchenne muscular dystrophy," *Proceedings of the National Academy of Sciences*, vol. 114, no. 50, pp. E10 763–E10 771, 2017.

[19] J. G. Smith, S. G. Aldous, C. Andreassi, G. Cuda, M. Gaspari, and A. Riccio, "Proteomic analysis of s-nitrosylated nuclear proteins in rat cortical neurons," *Science Signaling*, vol. 11, no. 537, p. eaar3396, 2018.

[20] S. R. Jaffrey and S. H. Snyder, "The biotin switch method for the detection of s-nitrosylated proteins," *Science's STKE*, vol. 2001, no. 86, p. pl1, 2001.

[21] G.-H. Wang and Y.-Q. Xing, "Evaluation of heat shock protein (hsp-72) expression in retinal ganglion cells of rats with glaucoma," *Experimental and Therapeutic Medicine*, vol. 14, no. 2, pp. 1577–1581, 2017.

[22] S. Fujii, S. Honda, Y. Sekiya, M. Yamasaki, M. Yamamoto, and K. Saijoh, "Differential expression of nitric oxide synthase isoforms in form-deprived chick eyes," *Current Eye Research*, vol. 17, no. 6, pp. 586–593, 1998.

[23] H. Xu, K. Huang, Q. Gao, Z. Gao, and X. Han, "A study on the prevention and treatment of myopia with nacre on chicks," *Pharmacological Research*, vol. 44, no. 1, pp. 1–6, 2001.

[24] P. Liu, P. Smith, I. Appleton, C. Darlington, and D. Bilkey, "Potential involvement of nos and arginase in age-related behavioural impairments," *Experimental gerontology*, vol. 39, no. 8, pp. 1207–1222, 2004.

[25] R. Weitzdoerfer, H. Hoeger, E. Engidawork et al., "Neuronal nitric oxide synthase knock-out mice show impaired cognitive performance," *Nitric Oxide*, vol. 10, no. 3, pp. 130–140, 2004.

[26] A. Ugarte, F. Gil-Bea, C. Garcia-Barroso et al., "Decreased levels of guanosine 3′,5′-monophosphate (cGMP) in cerebrospinal fluid (CSF) are associated with cognitive decline and amyloid pathology in Alzheimer's disease," *Neuropathology and Applied Neurobiology*, vol. 41, no. 4, pp. 471–482, 2015.

[27] A. Saavedra, A. Giralt, H. Arumi, J. Alberch, and E. Perez-Navarro, "Regulation of hippocampal cgmp levels as a candidate to treat cognitive deficits in huntington's disease," *PLoS One*, vol. 8, no. 9, article e73664, 2013.

[28] M. A. Hollas, M. B. Aissa, S. H. Lee, J. M. Gordon-Blake, and G. R. Thatcher, "Pharmacological manipulation of cGMP and NO/cGMP in CNS drug discovery," *Nitric Oxide*, vol. 82, pp. 59–74, 2019.

[29] Y. Zhang, Y. Deng, X. Yang, H. Xue, and Y. Lang, "The relationship between protein S-nitrosylation and human diseases: a review," *Neurochemical Research*, vol. 45, no. 12, pp. 2815–2827, 2020.

[30] A. Vielma, L. Delgado, C. Elgueta, R. Osorio, A. G. Palacios, and O. Schmachtenberg, "Nitric oxide amplifies the rat electroretinogram," *Experimental Eye Research*, vol. 91, no. 5, pp. 700–709, 2010.

[31] C. Wang, X. Li, W. Ning et al., "Multi-omic profiling of plasma reveals molecular alterations in children with covid-19," *Theranostics*, vol. 11, no. 16, pp. 8008–8026, 2021.

[32] F. Zheng, W.-C. Jang, F. K. Fung, A. C. Lo, and I. Y. Wong, "Up-regulation of eno1 by HIF-1α in retinal pigment epithelial cells after hypoxic challenge is not involved in the regulation of vegf secretion," *PLoS One*, vol. 11, no. 2, article e0147961, 2016.

[33] B.-M. Francisco, M. Salvador, and N. Amparo, "Oxidative stress in myopia," *Oxidative Medicine and Cellular Longevity*, vol. 2015, Article ID 750637, 2015.

[34] H. Wu, W. Chen, F. Zhao et al.et al., "Scleral hypoxia is a target for myopia control," *Proceedings of the National Academy of Sciences*, vol. 115, no. 30, pp. E7091–E7100, 2018.

Hindawi
Oxidative Medicine and Cellular Longevity
Volume 2023, Article ID 9815835, 1 page
https://doi.org/10.1155/2023/9815835

Retraction

Retracted: The Percutaneous Endoscopic Lumbar Debridement and Irrigation Drainage Technique for the First-Stage Treatment of Spontaneous Lumbar Spondylodiscitis: A Clinical Retrospective Study

Oxidative Medicine and Cellular Longevity

Received 26 September 2023; Accepted 26 September 2023; Published 27 September 2023

This article has been retracted by Hindawi following an investigation undertaken by the publisher [1]. This investigation has uncovered evidence of one or more of the following indicators of systematic manipulation of the publication process:

(1) Discrepancies in scope
(2) Discrepancies in the description of the research reported
(3) Discrepancies between the availability of data and the research described
(4) Inappropriate citations
(5) Incoherent, meaningless and/or irrelevant content included in the article
(6) Peer-review manipulation

The presence of these indicators undermines our confidence in the integrity of the article's content and we cannot, therefore, vouch for its reliability. Please note that this notice is intended solely to alert readers that the content of this article is unreliable. We have not investigated whether authors were aware of or involved in the systematic manipulation of the publication process.

Wiley and Hindawi regrets that the usual quality checks did not identify these issues before publication and have since put additional measures in place to safeguard research integrity.

We wish to credit our own Research Integrity and Research Publishing teams and anonymous and named external researchers and research integrity experts for contributing to this investigation.

The corresponding author, as the representative of all authors, has been given the opportunity to register their agreement or disagreement to this retraction. We have kept a record of any response received.

References

[1] Y. Yang, J. Wang, and Z. Chang, "The Percutaneous Endoscopic Lumbar Debridement and Irrigation Drainage Technique for the First-Stage Treatment of Spontaneous Lumbar Spondylodiscitis: A Clinical Retrospective Study," *Oxidative Medicine and Cellular Longevity*, vol. 2022, Article ID 6241818, 9 pages, 2022.

Hindawi
Oxidative Medicine and Cellular Longevity
Volume 2022, Article ID 6241818, 9 pages
https://doi.org/10.1155/2022/6241818

Research Article

The Percutaneous Endoscopic Lumbar Debridement and Irrigation Drainage Technique for the First-Stage Treatment of Spontaneous Lumbar Spondylodiscitis: A Clinical Retrospective Study

Yang Yang, Jingming Wang, and Zhengqi Chang

Department of Orthopedics, 960th Hospital of PLA, Jinan, 250031 Shandong, China

Correspondence should be addressed to Zhengqi Chang; 26766771@qq.com

Received 22 August 2022; Accepted 8 October 2022; Published 15 October 2022

Academic Editor: Pei-Wen Zhu

Background. Minimally invasive or open surgery is contentious in the treatment of spondylodiscitis, therefore finding a balance between the two is urgently needed. In this study, we propose a new treatment paradigm for treating spontaneous lumbar spondylodiscitis by percutaneous endoscopic lumbar debridement and irrigation drainage (PELDID). Then, the Pola classification was used to guide subsequent treatment. *Methods.* From November 2017 to April 2019, this study collected data on 16 patients with lumbar spondylodiscitis who were surgically treated utilizing this treatment paradigm in our department. Clinical effectiveness was determined using the visual analogue scale (VAS), the Oswestry Disability Index (ODI), the MOS 36-item short-form health survey (SF-36), and Kirkaldy-Willis criteria. *Results.* All 16 patients completed the treatment using the above paradigm and were followed up for 28.13 ± 10.15 months. The preoperative Pola classification is as follows: 7 cases of type A, 3 cases of type B, and 6 cases of type C. After the first-stage surgery, the evaluation results of Pola classification were as follows: 8 cases of type A, 8 cases of type B, and 0 cases of type C. Four patients received second-stage surgery with internal fixation through the paravertebral multifidus space approach and intervertebral bone graft fusion through the transforaminal approach, and the reoperation rate was 25% (4/16 cases). The Visual analogue scale (VAS), Oswestry Disability Index (ODI), and SF-36 score all improved significantly from 2.43 ± 0.89 to 0.18 ± 0.40, from $77.31\% \pm 11.15\%$to $16.93\% \pm 5.45\%$, and from 18.34 ± 7.47 to 80.3 ± 15.36. The CRP and ESR decreased dramatically from 49.61 ± 48.84 to12.50 ± 12.18 and from 65.56 ± 26.89 to 29.68 ± 20.68. There were no recurrences of infection in our study. *Conclusions.* The paradigm of the first-stage PELDID technique combined with the Pola classification system to guide the second-stage treatment for spontaneous spondylodiscitis is a novel and effective strategy for treating spontaneous spondylodiscitis.

1. Introduction

Spinal infection is a rare but serious disease, which is a pyogenic infection of the intervertebral disc, adjacent vertebral bodies, and surrounding soft tissues caused by pathogenic microorganisms, also known as spondylodiscitis [1, 2]. The disease has the characteristics of difficult early diagnosis, long treatment period, and relatively poor prognosis [3]. Spine infection encompasses a broad range of clinical entities, including spondylodiscitis, septic discitis, vertebral osteomyelitis, and epidural abscess. Spondylodiscitis is the most common, which accounts for about 50%. [4]. It is possible that it occurs as a result of invasive lumbar surgery, long-term hormone therapy, haemodialysis, or intravenous medication injection. It mainly occurs in the elderly, patients with underlying diseases and immune insufficiency, and as usual in males, with a male-to-female ratio of 1.5 to 2 : 1 [5, 6].

The treatment of patients with lumbar spondylodiscitis follows the principle of early diagnosis and early treatment. The two primary modes of therapy available today are conservative and surgical. However, owing to the intricacy of lumbar infection, the best course of therapy remains debatable. Additionally, open surgery is associated with significant

trauma, a high rate of perioperative complication, and a lengthy postoperative recovery. Prolonged operative time, blood loss, instrument type, and number of procedures are important risk factors for open surgery, resulting in a complication rate of 1–4% after spinal surgery [7]. Lumbar and posterior surgery have more complications than open cervical and anterior surgery [8]. With the development of minimally invasive lumbar spine surgery, transforaminal, lateral, and extremely lateral lumbar spine minimally invasive approaches have been introduced to treat lumbar spine infections [9]. These minimally invasive operations decrease surgical trauma but have a number of drawbacks, including limited indications, insufficient intraoperative debridement, and infection recurrence [10, 11]. How to strike an optimal balance between minimally invasive and open surgery is a critical issue that should be addressed immediately [12].

In the present study, the percutaneous endoscopic lumbar debridement and irrigation drainage (PELDID) technique is proposed as a novel and effective surgical paradigm for treating spontaneous lumbar spondylodiscitis. Then, after the first stage of surgery, the follow-up treatment is evaluated utilizing Pola classification. A retrospective analysis of this treatment paradigm was conducted to assess clinical outcomes.

2. Materials and Methods

2.1. Study Population. Patients with neurological deficits, instability, progressive pain, or progression on magnetic resonance imaging (MRI)/computed tomography (CT) despite conservative treatment underwent surgical treatment. The Visual analogue scale (VAS), Oswestry Disability Index (ODI) at the time of initial diagnosis, and the final follow-up were compared. X-rays and CT were used to seek out endplate erosion, cavitation, disc space loss, and instability. Preoperative and postoperative MRIs were routinely performed to assess treatment response. Clinical evaluation was performed using the ASIA score, ODI, SF-36, and VAS scores. The functional outcome of the study was measured by the modified criteria of Kirkaldy-Willis. All patients were treated with empirical antibiotics or antibiotics based on microbial culture and sensitivity results. Patients received intravenous broad-spectrum antibiotics for six to eight weeks, followed by three months of oral antibiotics. Antibiotic administration was discontinued based on clinical improvement and infection-related laboratory test findings, such as average C-reactive protein (CRP) and erythrocyte sedimentation rate (ESR).

2.2. Inclusion Criteria. Patients who had one or more of the following characteristics were included in this study: (1) neurological deficit caused by spinal canal involvement, (2) spinal instability caused by large vertebral body destruction, (3) kyphosis observed on imaging, (4) epidural or paravertebral abscess formation, and (5) aged patients who could not bear long time bed rest.

2.3. Exclusion Criteria. Patients with the following conditions were excluded in this study: (1) combined with truncation, (2) combined with systemic and septic shock, (3) combined with spinal deformity, and (4) with less than one year of follow-up.

2.4. Operative Procedure. The operation was carried out in the level where the infection had been identified on the preoperative MRI. The patient is placed in a prone or lateral position with a pillow on the chest and iliac so that the abdomen is suspended. The puncture point was determined under fluoroscopic guidance and marking of the iliac crest and the midline of the spinous process (8-12 cm next to the spinous process, local infiltration anesthesia with 1% lidocaine). Under fluoroscopic guidance, the puncture needle was punctured into the intervertebral space of the lesion through the Kambin safety triangle, a guidewire was inserted, a step-by-step dilation catheter was placed along the guidewire, and a working channel was established. Under the microscope, the infected nucleus pulposus and endplate tissues were removed entirely with nucleus pulposus forceps until fresh blood oozes. The corresponding segments of nerve roots were separated and exposed, the necrotic tissues were fully removed, and abscess walls around the lesions were removed with plasma electrodes. During the operation, 3000~6000 ml of normal saline was continuously used for flushing the abscess cavity. The tissue obtained during the operation was retained for bacterial culture, drug susceptibility, and pathological biopsy. Radiofrequency electrocoagulation was used to stop bleeding, a three-lumen drainage catheter was indwelled and fixed, and the incision was wrapped with a dressing. The operation was completed.

2.5. Post-Operative Management. After the operation, the patients were treated by continuous lavage with normal saline for 3 days. Bacterial culture and pathological examination were performed on the infected tissue removed during the operation. After bacterial culture and drug susceptibility results, sensitive antibiotics were selected for treatment. Patients with Mycobacterium tuberculosis infection continued to receive intensive treatment with 4 combination antituberculosis drugs for 3 months. Subsequently, consolidation therapy was continued for 9 to 15 months with isoniazid, rifampicin, and pyrazinamide. If the culture result is negative, broad-spectrum and potent antibiotic treatment is performed [13]. The irrigation drainage cycle is 7-14 days. The drainage tube was removed when the following criteria were met: (1) the drainage fluid became clear and the pain symptoms disappeared, (2) the erythrocyte sedimentation rate and C-reactive protein were both significantly decreased and stable, and (3) the bacterial culture of menstrual blood and drainage fluid was negative for 2 consecutive times [14].

2.6. Pola Classification. After the drainage catheter was removed, MRI and CT were performed for Pola classification (Table 1). The Pola classification was performed by evaluating the extent of the abscess and the stability of the lumbar spine. Follow-up treatment was guided according

Table 1: Pola classification criteria.

Type A without biomechanical instability neither acute neurological impairment or epidural abscesses	Type B with radiological evidence of significant bone destruction or biomechanical instability without acute neurological impairment or epidural abscesses	Type C with epidural abscesses or acute neurological impairment
A1: simple discitis without the involvement of vertebral bodies	B1: destructive spondylodiscitis without segmental instability	C1: epidural abscess (+), neurological impairment (-), segmental instability (-)
A2: spondylodiscitis involving the intervertebral disc and adjacent vertebral bodies	B2: destructive spondylodiscitis extended to paravertebral soft tissues without segmental instability	C2: epidural abscess (+), segmental instability (+), neurological impairment (-)
A3: spondylodiscitis with limited involvement of paravertebral soft tissues	B3: destructive spondylodiscitis with biomechanical instability and segmental kyphosis (B3.1 < 25 ∘ ;B3.2 > 25 ∘)	C3: epidural abscess (+), neurological impairment (+), segmental instability (-)
A4: spondylodiscitis with unilateral or bilateral intramuscular abscesses		C4: epidural abscess (+), neurological impairment (+), segmental instability (+)

to the results of Pola classification. The specific treatment flow chart is shown in Figure 1.

2.7. Follow-Up. At the final follow-up, the postoperative clinical outcomes were examined using VAS, ODI, SF-36, and Kirkaldy-Willis modified criteria. Changes in the WBC count, CRP, and ESR were used to measure infection control. After 1, 3, 6, and 12 months, X-rays, CT scans, and MRIs were performed. An MRI was performed to evaluate the local state of the treated vertebral segment and to look for any epidural or paraspinal abscesses.

2.8. Statistical Analysis. This study was a retrospective case series study, and SPSS 22.0 statistical software (SPSS, USA) was used for statistical analysis. Measurement data conforming to the normal distribution (operation time, hospitalzation time, follow-up time, WBC count, CRP, ESR, and VAS score) were expressed in the form of mean ± standard deviation, and a paired *t*-test was used for comparison between preoperative and final follow-up. The test level α value was set to be 0.05 on both sides.

3. Results

From November 2017 to April 2019, there were 16 cases of spontaneous infectious spondylitis in our department, including 10 males and 6 females, with an age of 49.31 ± 17.36 years (range 25-83 years). All patients were diagnosed with spontaneous spondylitis and treated with the proposed paradigm.

3.1. Improvement of Pola Classification. The preoperative Pola classification of the 16 patients in this group is as follows: 7 cases of type A, including 5 cases of type A2 and 2 cases of type A3; 3 cases of type B, including 2 cases of type B2 and 1 case of type B3; and 6 cases of type C, of which there was 1 case of type C1, 4 cases of type C3, and 1 case of type C4. The following is the reevaluation after the first-stage PELDID: 8 cases of type A, all of which were type A2; 8 cases of type B, including 5 cases of type B2, 3 cases of type B3, and 0 cases of type C. The Pola classification is designed to evaluate patients before treatment to differentiate between conservative (A) and surgical (B, C) treatments. PLEDID significantly reduced the probability of instrumental surgery, from 43.75% (7/16) to 25% (4/16).

3.2. Intraoperative and Postoperative Management. Among the 16 patients in this group, a large amount of pus could be extracted during the operation in 2 patients, and the wounds were lavaged with normal saline during the operation in all cases. Inflammatory granulation tissue hyperplasia, brittle, significantly narrowed intervertebral space. Among them, 12 patients had osteophytes at the periphery of the space accompanied by a small amount of small sequestrum. Part of the osteophytes and small sequestrum was cut off with a trephine under the endoscope and then removed. Cage prosthesis was seen in one case of infection after lumbar internal fixation, and its loosening was obvious. In all cases, the granulation tissue and necrotic cartilage endplate within the visual field were completely removed under the endoscope, and the nerve root running segment of the corresponding level was also revealed. There was no rupture of the dural sac and nerve root injury in all 16 cases.

Postoperative management, all 16 cases underwent postoperative flushing for 3 days and continued indwelling drainage. The drainage fluid was red at first, then turned into pale yellow fluid, and finally turned into colorless transparent fluid or clear pale yellow tissue fluid. The drainage tube removal time was 10.18 ± 2.65 days (range: 7-14 days). Four patients underwent second-stage surgical treatment, and the reoperation rate is 25% (4/16 cases); the surgical methods were paravertebral multifidus space approach and internal fixation and transforaminal interbody fusion. All patients were treated with antibiotics under bracing protection.

3.3. Surgical Results. All 16 patients in this group underwent surgery successfully. The operation time was 94.76 ± 31.97 min (range, 60-175 min), the intraoperative blood loss was 23.24 ± 11.31 ml (range, 10-50 ml), and the hospital stay was 46.71 ± 21.54 d (range, 16~93 d). All 16 patients were followed up (Figure 2), and the follow-up time was 28.13 ± 10.15 months (range, 19-36 months).

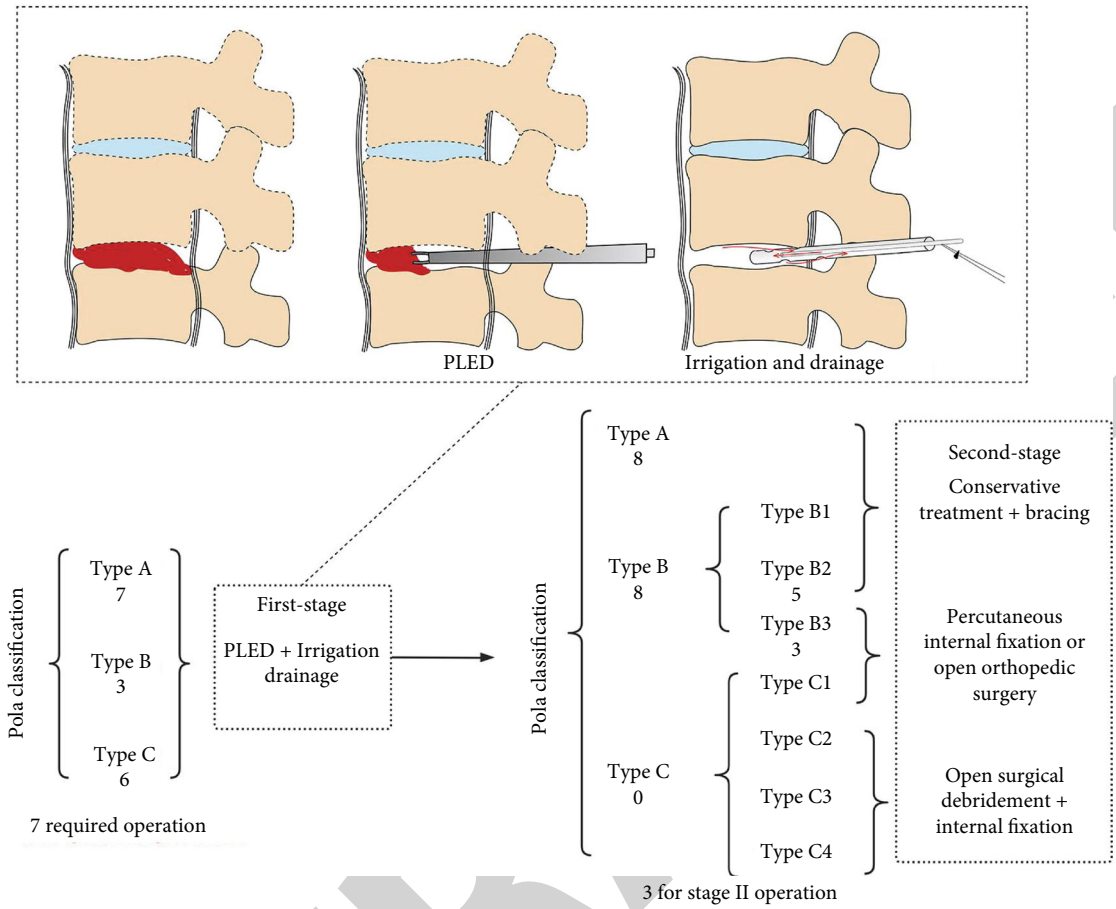

Figure 1: A schematic drawing of the surgical paradigm.

3.4. Complication. The 16 patients in this group had no nerve injury, paravertebral hematoma formation, cerebrospinal fluid leakage, meningitis, and so on. Six patients with lower extremity radiculopathy were recovered at final follow-up. Two patients who received continuous irrigation drainage postoperative developed high fever and chills, and the irrigation treatment was immediately terminated. The antibiotic was upgraded to imipenem and then recovered.

3.5. Infection Control and Clinical Outcomes. Pathological culture results were positive in 6 cases, with a positive rate of 37.5% (6/16), including 2 cases of *Staphylococcus aureus* (including 1 case of methicillin-resistant *Staphylococcus aureus*), 2 cases of *Escherichia coli*, and 2 cases of *Klebsiella pneumonia*. One case of primary bacteria and one case of fungal infection were *Candida tropicalis*. One instance of tuberculosis was identified, and culture findings were negative. However, the gene-sequencing analysis and imaging data validated the diagnosis. The description of pathological results varies, mainly including inflammatory necrotic exudation, caseous necrosis, acute and chronic inflammatory cell infiltration, and mucopurulent foci.

WBC count [$(5.74 \pm 2.24) \times 10^9$/l] decreased compared with preoperative [$(6.46 \pm 1.15) \times 10^9$/l], but there was no significant difference between the two ($P = 0.132$, Table 2); while CRP and ESR [12.50 ± 12.18 mg/l and 29.68 ± 20.68 mm/1 h] were significantly lower than those before surgery [49.61 ± 48.84 mg/l and 65.56 ± 26.89 mm/1 h], the differences were all statistically significant ($P < 0.05$, Table 2). At the last follow-up, except for 1 case with aplastic anaemia and 1 case with rheumatoid arthritis, the CRP and ESR were normal.

3.6. VAS Score. In this group of 16 patients, the postoperative low back pain was significantly relieved compared with the preoperative, and the low back pain VAS score [2.43 ± 0.89 points] when the drainage tube was removed was significantly lower than that before the operation [8 ± 1.21 points], and there were statistical differences ($P < 0.05$, Table 2). At the last follow-up, the symptoms of low back pain basically disappeared [0.18 ± 0.40 points], and the difference was statistically significant ($P < 0.05$, Table 2).

3.7. ODI and SF-36 Scores. The living ability and health status of the 16 patients in this group were significantly improved at the last follow-up, and the ODI ($16.93\% \pm 5.45\%$) at the last follow-up was significantly lower than that before the operation ($77.31\% \pm 11.15\%$), and the difference was statistically significant ($P < 0.05$, Table 2). 1). At the last follow-up, SF-36 [80.3 ± 15.36 points] was significantly higher than preoperative

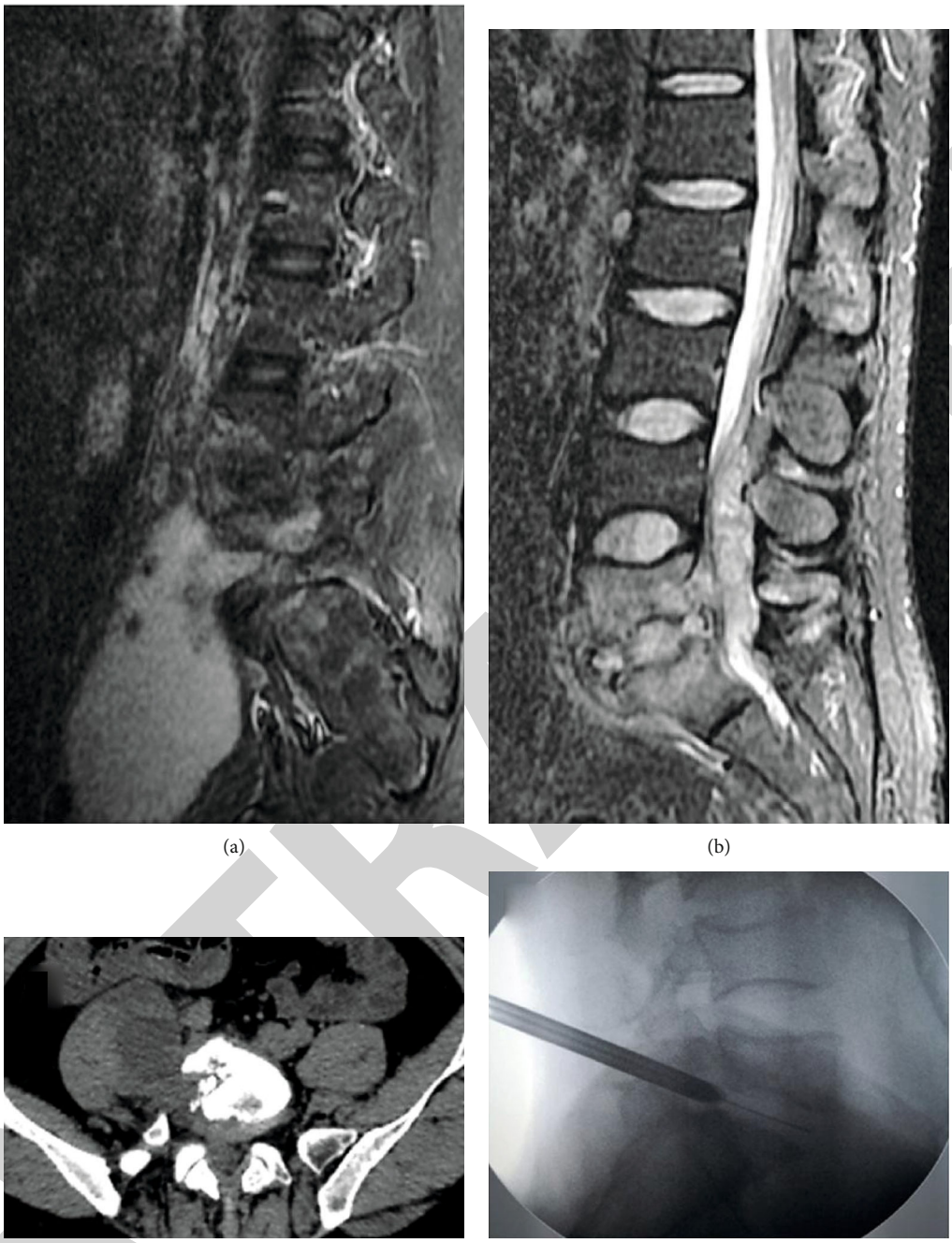

(a) (b) (c) (d)

Figure 2: Continued.

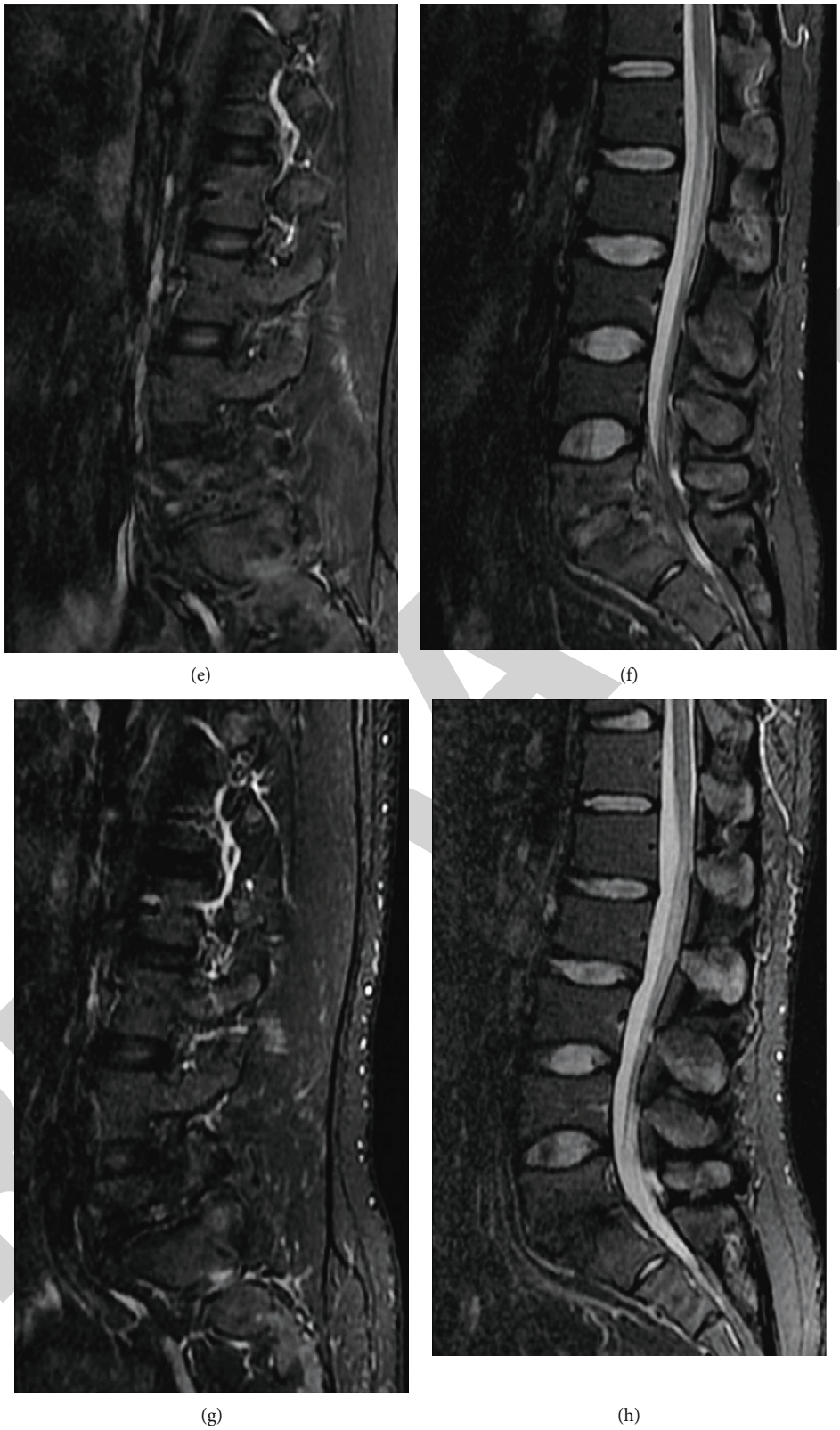

Figure 2: A 30-year-old man suffered from low back pain and right lower extremity numbness with lumbar spondylodiscitis. Preoperative MRI (a, b) and cross-sectional CT (c) showed psoas major abscess, epidural abscess, and vertebral bone destruction with nerve compression. Pola type C3. (d) The first-stage treatment with PELDID was performed, and lumbar tuberculosis was diagnosed by gene chip sequencing technology. (e, f) MRI of the lumbar spine after removal of the drainage tube 2 weeks after surgery showed that the abscess of the psoas major disappeared, and the abscess in the spinal canal improved significantly. Pola type B2 type. Antituberculosis drugs and braces were given. (g, h) MRI of the lumbar spine at the last follow-up showed that the psoas abscess and the intraspinal abscess disappeared.

Table 2: The experimental and clinical evaluations of 16 patients were compared preoperative, postoperative, and at the final follow-up ($\bar{x} \pm s$).

Time point	WBC ($\times 10^9$/l)	ESR (mm/1 h)	CRP (mg/l)	VAS score	Time point	VAS score	ODI score	SF-36 score
Preoperative	6.46 ± 1.15	65.56 ± 26.89	49.61 ± 48.84	8 ± 1.21	Preoperative	8 ± 1.21	77.31 ± 11.15	18.34 ± 7.47
Postoperative	5.74 ± 2.24	29.68 ± 20.68	12.50 ± 12.18	2.43 ± 0.89	Final follow-up	0.18 ± 0.40	16.93 ± 5.45	80.3 ± 15.36
t value	1.592	6.350	3.084	2.920		25.551	29.760	28.341
P value	0.132	0.001	0.008	0.001		0.001	0.001	0.001

[18.34 ± 7.47 points], and the difference was statistically significant ($P < 0.05$, Table 2).

3.8. Kirkaldy-Willis Criteria. Kirkaldy-Willis criteria were used to evaluate the clinical efficacy. At the last follow-up, 14 cases (87.5%) were excellent, 2 cases (12.5%) were good, and the excellent and good rate was 100%.

4. Discussion

Lumbar vertebra infection is a severe infection with insufficient blood supply in the intervertebral region, making antibiotics ineffective. As the condition progresses, it is frequently accompanied with deterioration of the vertebral body and intervertebral space, abscess formation, and nerve compression symptoms. Systemic symptoms such as bacteremia, sepsis, and septic shock may occur if bacteria invade the circulation. The three major aims of lumbar spine infection therapy are to reduce pain, preserve or restore spinal stability, and prevent or cure neurological impairments [15]. One objective of surgical treatment is infection control, destroying the internal microenvironment of the lesion (closed to open), and stabilizing the spine. In recent years, with the development of minimally invasive spine technology, the percutaneous transforaminal technique has become a new choice for the treatment of lumbar spine infection [16]. Through first-stage PELDID technique, we may get etiological and pathological tissue to assist in clinical antibiotic selection. Simultaneously, local lesion elimination by irrigation drainage may remove the microenvironment of infection. However, minimally invasive techniques have a number of limitations, including limited indications, insufficient clearance of infected areas after surgery, and infection recurrence [17]. As a result, clinicians are primarily concerned with how to choose the most suitable surgical strategy.

The paradigm of the first-stage PELDID technique combined with the Pola classification system to guide the second-stage treatment for spontaneous spondylodiscitis has the following advantages. First, according to the Pola classification, stage I PLEDID operation can reduce the probability and difficulty of second stage surgery for patients. Second, pathogenic tissue can be obtained early, which is beneficial to guide antibiotic selection. Third, intraoperative irrigation drainage can convert closed lumbar spine lesions to open lesions with adequate drainage to prevent infection progression. Finally, it is very operable for patients who cannot withstand open surgery due to severe comorbidities.

Spinal infection is complicated, and the treatment methods are various. At present, there is no exact standard for selecting an appropriate treatment method. Pola classification is a new classification method for the treatment of spinal infections [18], and corresponding treatment suggestions can be made according to different classifications. For type A, conservative treatment and bracing or percutaneous screw internal fixation is recommended. Conservative treatment and bracing or percutaneous screw internal fixation is recommended for B1 and B2 types. For type B3, percutaneous internal fixation or open internal fixation is recommended. For type C1, conservative treatment and bracing or percutaneous immobilization are recommended (close monitoring and follow-up are required). Types C2, C3, and C4 are recommended for incision, decompression, debridement and internal fixation. The 16 cases in this group all underwent percutaneous transforaminal debridement and drainage of the lumbar spine in stage I, and the Pola classification was used to evaluate the surgical effect before and after the operation. There were 7 cases of type A before operation, including 5 cases of type A2 and 2 cases of type A3. After reevaluation, all 7 cases were A2 type, and then, conservative treatment with antibiotics was undertaken. There were 3 cases of type B before operation (2 cases of type B2 and 1 case of type B3); 2 cases of type B2 and 1 case of type B3 were re-evaluated after operation, of which 2 cases underwent stage II incision bone graft fusion and internal fixation, 1 case of conservative treatment with antibiotics against infection. There were 6 cases of type C before operation, including 1 case of type C1, 4 cases of type C3, 1 case of type C4, 1 case of type A2, 3 cases of type B2, and 2 cases of type B3 after reevaluation. In stage II, 2 cases were treated with incision, bone grafting, fusion, and internal fixation, and 4 cases were treated conservatively with antibiotics and brace. The lumbar vertebra infection was clinically cured at the last follow-up.

Therefore, the first-stage PELDID can convert lumbar infection type C to type A or type B, effectively reducing the rate of second-stage surgery. Following the first-stage PELDID operation, the second-stage operation adopts minimally invasive techniques, which considerably reduces the difficulties associated with conventional open surgery. As a consequence, intraoperative dural harassment of the spinal canal is minimized, there are no postoperative complications such as nerve root damage, meningitis, or neurological

complaints in the lower extremities, and the clinical impact is spectacular.

As for comorbidities, lumbar spontaneous spondylodiscitis cases are often associated with a variety of severe diseases. In this group, more than half of the cases were associated with chronic diseases. The patients were characterized by low body mass index, anaemia, and low immunity [19]. The traditional open surgery is traumatic, and many patients are unable to tolerate it and lose the opportunity for surgical treatment, resulting in the progressive aggravation of spinal deformity and lower extremity neurological symptoms, which has a serious impact on life and work of patients. Our proposed surgical paradigm is characterized by minimal surgical trauma. Compared with the relevant literature reports, the operation time (94.76 ± 31.97 min) and intraoperative blood loss (23.24 ± 11.31 ml) were significantly reduced in this group of cases [20]. In terms of clinical symptoms, after irrigation and drainage treatment, the inflammatory indexes such as ESR and CRP in this group were significantly decreased compared with those before surgery, and the difference was statistically significant. In addition, with minimally invasive surgery, the postoperative VAS score of the patients was also significantly decreased, and the difference was statistically significant. These results suggest that our proposed surgical paradigm is effective and clinically significant. Through follow-up, the low back pain VAS score and ODI of 16 patients were significantly lower than that preoperation, indicating that low back pain symptoms were significantly relieved. The SF-36 scores at the last follow-up were significantly higher than those before surgery, indicating that the patient's health was significantly improved. In addition, the Kirkaldy-Willis criteria were used to evaluate the clinical efficacy of patients after surgery, and the excellent and good rate was 100%. This result shows that the first-stage percutaneous lumbar lavage and drainage has an obvious effect on the treatment of lumbar infection and is clinically effective.

It is also worth noting that a clear etiology is very important for the selection of antibiotics. The positive rate of pathogens detected in this group of cases was 37.5% (6/16), which was similar to the 10.3%-60.4% reported in the literature [4]. With the development of gene sequencing technology, the etiological detection rate of spinal infection has increased significantly in recent years [21]. Whether it is a specific infection or a non-specific infection, effective and sufficient antibiotics are the basis for the treatment of lumbar spine infections. For nonspecific infections, intravenous antibiotics can be appropriately shortened to 3 weeks after thorough debridement and drainage [22]. For specific infections, including tuberculosis, brucellosis, and fungi, early, combined, regular, and full-course anti-infective treatment should be used. For those with unclear etiological results, potent broad-spectrum antibiotics can be used for treatment. No matter what treatment plan is used, vital signs and laboratory indicators should be regularly monitored during the clinical process, and treatment should be adjusted at any time.

During postoperative irrigation, two patients suffered chills and a high fever, with the maximum recorded at 41.1°C. Body temperature gradually returned to normal when antibiotics were escalated and flushing was discontinued. Investigating the reasons, the lumbar intervertebral space is closed, and the pus often flows along the psoas muscle to form paravertebral and iliac fossa abscesses. Flushing too fast can cause the irrigation fluid to get trapped in the abscess space, causing chills and high fever. Therefore, the irrigation speed should not be too fast after surgery, the flow rate of irrigation should be adjusted at all times, and the irrigation speed should be less than the drainage.

This retrospective analysis included only 16 patients, there was substantial heterogeneity, and the gathered data were biased. This research was limited to the lumbar spine, excluding the thoracic and cervical regions. In the future, we will continue to collect more cases, achieve a longer duration of follow-up, and develop a multicenter, large-sample prospective randomized controlled trial in order to obtain more rigorous, precise, and exhaustive data.

5. Conclusions

In this study, radiculopathy improved in all cases after being treated with the proposed paradigm. Except for two cases of high fever patients, there were no serious complications. Our findings suggest that the paradigm of first-stage PELDID combined with the Pola classification system to guide second-stage treatment is feasible for the treatment of spontaneous spondylodiscitis, effectively reducing the difficulty of the second stage procedure. However, the safety and efficacy need to be further verified by multicenter randomized controlled studies.

Abbreviations

PELDID: Percutaneous endoscopic lumbar debridement and irrigation drainage
CT: Computed tomography
MRI: Magnetic resonance imaging
VAS: Visual analogue scale
ODI: Oswestry Disability Index
ESR: Erythrocyte sedimentation rate
CRP: C-reactive protein.

Data Availability

All data analyzed during this study are included in the manuscript. The datasets used in this article are available from the corresponding author (ZQC) on reasonable request.

Ethical Approval

This study has been approved by the 960th hospital of PLA. Each author certifies that all investigations were conducted in accordance with ethical principles. All protocols involving human subjects were approved by the Ethics Committee of the 960th Hospital of PLA (approval number: KYLL2021133).

Hindawi
Oxidative Medicine and Cellular Longevity
Volume 2023, Article ID 9769858, 1 page
https://doi.org/10.1155/2023/9769858

Retraction

Retracted: Fundus-Vascular Responses to Color Deviation Caused by Non-Oxidative Blue Filtering

Oxidative Medicine and Cellular Longevity

Received 26 December 2023; Accepted 26 December 2023; Published 29 December 2023

This article has been retracted by Hindawi, as publisher, following an investigation undertaken by the publisher [1]. This investigation has uncovered evidence of systematic manipulation of the publication and peer-review process. We cannot, therefore, vouch for the reliability or integrity of this article.

Please note that this notice is intended solely to alert readers that the peer-review process of this article has been compromised.

Wiley and Hindawi regret that the usual quality checks did not identify these issues before publication and have since put additional measures in place to safeguard research integrity.

We wish to credit our Research Integrity and Research Publishing teams and anonymous and named external researchers and research integrity experts for contributing to this investigation.

The corresponding author, as the representative of all authors, has been given the opportunity to register their agreement or disagreement to this retraction. We have kept a record of any response received.

References

[1] J. Cai, W. Hao, S. Zeng et al., "Fundus-Vascular Responses to Color Deviation Caused by Non-Oxidative Blue Filtering," *Oxidative Medicine and Cellular Longevity*, vol. 2022, Article ID 9592009, 11 pages, 2022.

Hindawi
Oxidative Medicine and Cellular Longevity
Volume 2022, Article ID 9592009, 11 pages
https://doi.org/10.1155/2022/9592009

Research Article

Fundus-Vascular Responses to Color Deviation Caused by Non-Oxidative Blue Filtering

Jianqi Cai,[1,2] Wentao Hao,[3] Shanshan Zeng,[2] Junkai Li,[4] Ya Guo,[2] Kai Tan,[5] Yongyin Kang,[6] Yitao Huang,[5] Yue Zhang,[5] Thebano Santos,[7] Cheng Qian,[8] and Aiqin Luo[1]

[1]*School of Life Science, Beijing Institute of Technology, Beijing 100081, China*
[2]*Lab of Visual Health and Safety Protection, China National Institute of Standardization, Beijing 100191, China*
[3]*Beijing Yangming Zhidao Photoelectric Science and Technology Co., Ltd, Beijing 100102, China*
[4]*Hangzhou Innovei Technology Co., Ltd, Hangzhou 311199, China*
[5]*Guangzhou Shirui Electronics Co., Ltd, Guangzhou 510663, China*
[6]*Najing Technology Co., Ltd, Hangzhou 310052, China*
[7]*Center of Information Technology "Renato Archer" (CTI), Ministry of Science Technology Innovations and Communications, Brazil*
[8]*School of Reliability and Systems Engineering, Beihang University, Beijing 100191, China*

Correspondence should be addressed to Jianqi Cai; caijq@cnis.ac.cn, Cheng Qian; cqian@buaa.edu.cn, and Aiqin Luo; bitluo@bit.edu.cn

Received 28 July 2022; Accepted 17 August 2022; Published 12 October 2022

Academic Editor: Ting Su

Aims. Short-wavelength blue light damaged retina by the oxidative stress in the retinal pigment epithelial (RPE) cells. Filtering blue light from screen could reduce blue hazard, whereas it inevitably altered color-gamut coverage and color-deviation level. Although abnormal fundus-vascular density (FVD) sometimes indicated fundus disease, few researchers noticed its responses to the variation of color-gamut coverage and color-deviation level. *Methods*. In this study, we performed cellular experiments and analyzed the RPE cell viabilities (CVs) in spectrums with different blue (455-475 nm) ratios to describe the corresponding oxidative-stress levels. Further, we investigated the effects of color-gamut and deviation on FVD variations during the screen-watching task using human factor experiments with 30 participants (university students, including 17 males and 13 females, 21 to 30 years old). *Results*. RPE CVs were similar in different spectrums, implying that non-oxidative blue filtering hardly contributed to CV improvement. Color-deviation level seems to induce more significant effects on the visual function compared to color-gamut coverage, and MTF and FVD presents similar variation trends during the visual task. *Conclusion*. Oxidative-free blue filtering contributed little to decrease retinal oxidative stress yet caused color-deviation increase, which caused significant FVD reduction.

1. Introduction

Short-wavelength blue light threatens the RPE cells by increasing the risk of fundus diseases, comprising age-related macular degeneration (AMD) [1, 2], diabetic retinopathy (DR) [3, 4], idiopathic parafoveal telangiectasis (IPT) [5, 6], retinal vein occlusion (RVO) [7, 8], retinal artery occlusion (RAO) [9, 10], central serous chorioretinopathy (CSC) [11, 12], and polypoidal choroidal vasculopathy (PCV) [13, 14].

Although in display blue wavelength filtering reduced blue hazard, it caused other issues such as variations in color-deviation level and color-gamut coverage. Whether human eyes benefit from non-oxidative blue filtering remained unclear. Researchers have performed ergonomic studies to clarify the effects of display brightness [15–17] on visual and nonvisual effects [18–20], whereas they focused little on the fundus-vascular responses to different color-gamut coverages and color-deviation levels.

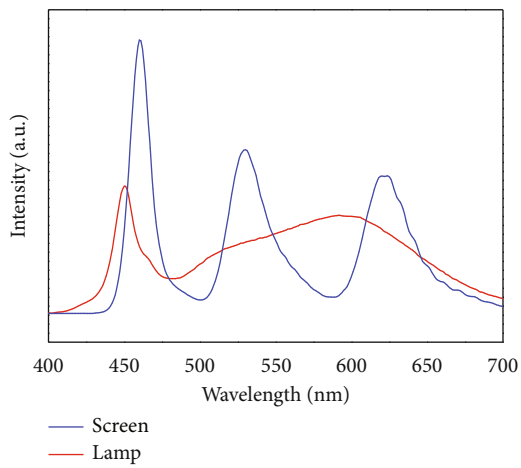

Figure 1: Spectral power distributions (SPDs) of the screen and ceiling lamp.

Table 1: Color features of screens used in the study.

Screen ID	Color-gamut (% NTSC)	Color-deviation (ΔE) level
1	71%	
2	77%	
3	82%	$0.9 < \Delta E < 1.8$
4	89%	
5	95%	
6	71%	
7	77%	
8	82%	$1.8 < \Delta E < 2.7$
9	89%	
10	95%	
11	71%	
12	77%	
13	82%	$2.7 < \Delta E < 3.6$
14	89%	
15	95%	

Generally, non-oxidative blue filtering is inevitably accompanied by several negative consequences, including complicated control circuits and algorithms [21], distorted display-input signals [22], and reduced color-deviation levels [23–25]. In this study, we measured FVD variations in different color-gamut coverages and color-deviation levels, which were caused by the non-oxidative blue filtering, during screen-watching tasks in experiences with human subjects. We also analyzed the correlation between FVD and MTF.

Table 2: Test sample information based on participants visual task experiments.

Participant item	Distribution
Anisometropia	(i) <2.5 D
Intraocular pressure	(i) 14-20
Diopter	(i) − 0.75 D to 0.75 D: 40% (ii) − 1.00 D to − 3.00 D: 60%
Corrected visual acuity	(i) 0.8: 40% (ii) 1.0: 60%
Male-female ratio	(i) Males: 17 (ii) Females: 13

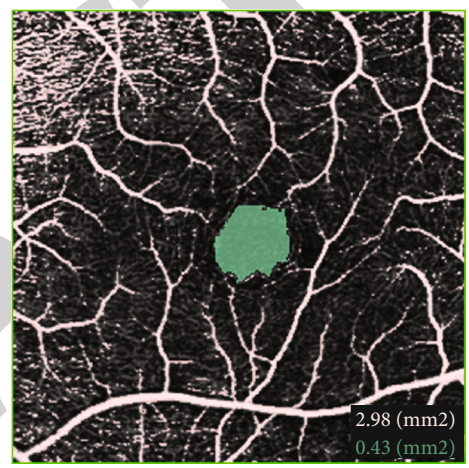

Figure 2: FVD results. The red number represents the vascular area and the green number represents the optic-disk area.

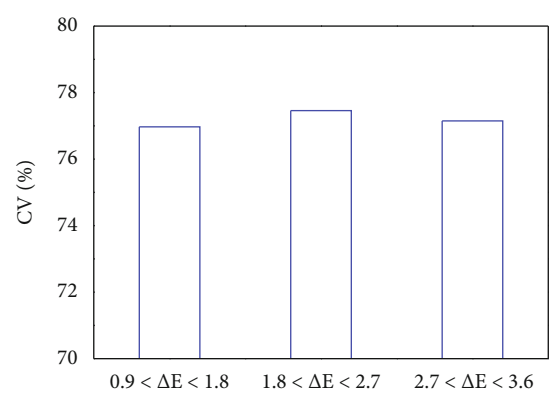

Figure 3: CVs in different spectrums corresponding to the color-deviation level of $0.9 < \Delta E < 1.8$, $1.8 < \Delta E < 2.7$, and $2.7 < \Delta E < 3.6$, respectively.

2. Materials and Methods

2.1. Light Environment. A light-emitting diode (LED) lamp fixed on a 2.1-m ceiling was used for lighting with the following characteristics: size of 90 cm × 90 cm and a correlated color temperature (CCT) of 5250 ± 250 K. The screen brightness was set to a value of 190 ± 10 cd/m^2. Spectral power distributions (SPD) of the screen and the ceiling lamp are shown in Figure 1. To obtain all of the color features in this study, color corrections were performed using Truecolor

Table 3: Comparisons of ΔFVD between the adjacent color-gamut coverage pairs in multiple color-deviation levels; t represents Student's t-test value, and P represents significance probability; $^{*}P < 0.05$ and $^{**}P < 0.01$.

Color-deviation Level	Color-gamut Coverages	t	P
0.9 < ΔE < 1.8	95% vs 89%	− 0.589	0.561
	95% vs 82%	− 1.132	0.267
	95% vs 77%	− 0.659	0.515
	95% vs 71%	− 1.410	0.169
	89% vs 82%	− 0.553	0.585
	89% vs 77%	− 0.181	0.858
	89% vs 71%	− 1.072	0.293
	82% vs 77%	0.451	0.655
	82% vs 71%	− 0.211	0.834
	77% vs 71%	− 0.680	0.502
1.8 < ΔE < 2.7	95% vs 89%	0.172	0.864
	95% vs 82%	− 0.421	0.677
	95% vs 77%	− 0.247	0.807
	95% vs 71%	0.041	0.967
	89% vs 82%	− 0.652	0.520
	89% vs 77%	− 0.403	0.690
	89% vs 71%	− 0.115	0.910
	82% vs 77%	0.230	0.820
	82% vs 71%	0.545	0.590
	77% vs 71%	0.390	0.700
2.7 < ΔE < 3.6	95% vs 89%	0.41	0.685
	95% vs 82%	0.342	0.735
	95% vs 77%	− 0.519	0.608
	95% vs 71%	− 0.724	0.475
	89% vs 82%	0	1
	89% vs 77%	− 0.970	0.340
	89% vs 71%	− 1.292	0.207
	82% vs 77%	− 0.798	0.432
	82% vs 71%	− 1.407	0.171
	77% vs 71%	− 0.224	0.824

Table 4: Comparisons of ΔFVD between the adjacent color-deviation level pairs in multiple color-gamut coverages; t represents Student's t-test value, and P represents significance probability; $^{*}P < 0.05$ and $^{**}P < 0.01$.

Color-gamut Coverage	Color-deviation Levels	t	P
95%	1.5 vs 2.3*	2.503	0.018
	2.3 vs 3.3**	4.343	0.001
89%	1.5 vs 2.3**	3.452	0.002
	2.3 vs 3.3**	4.611	0.001
82%	1.5 vs 2.4**	3.452	0.002
	2.4 vs 3.3**	6.413	0.001
77%	1.6 vs 2.4**	3.417	0.002
	2.4 vs 3.3**	5.541	0.001
71%	1.6 vs 2.4**	4.019	0.001
	2.4 vs 3.4**	3.983	0.001

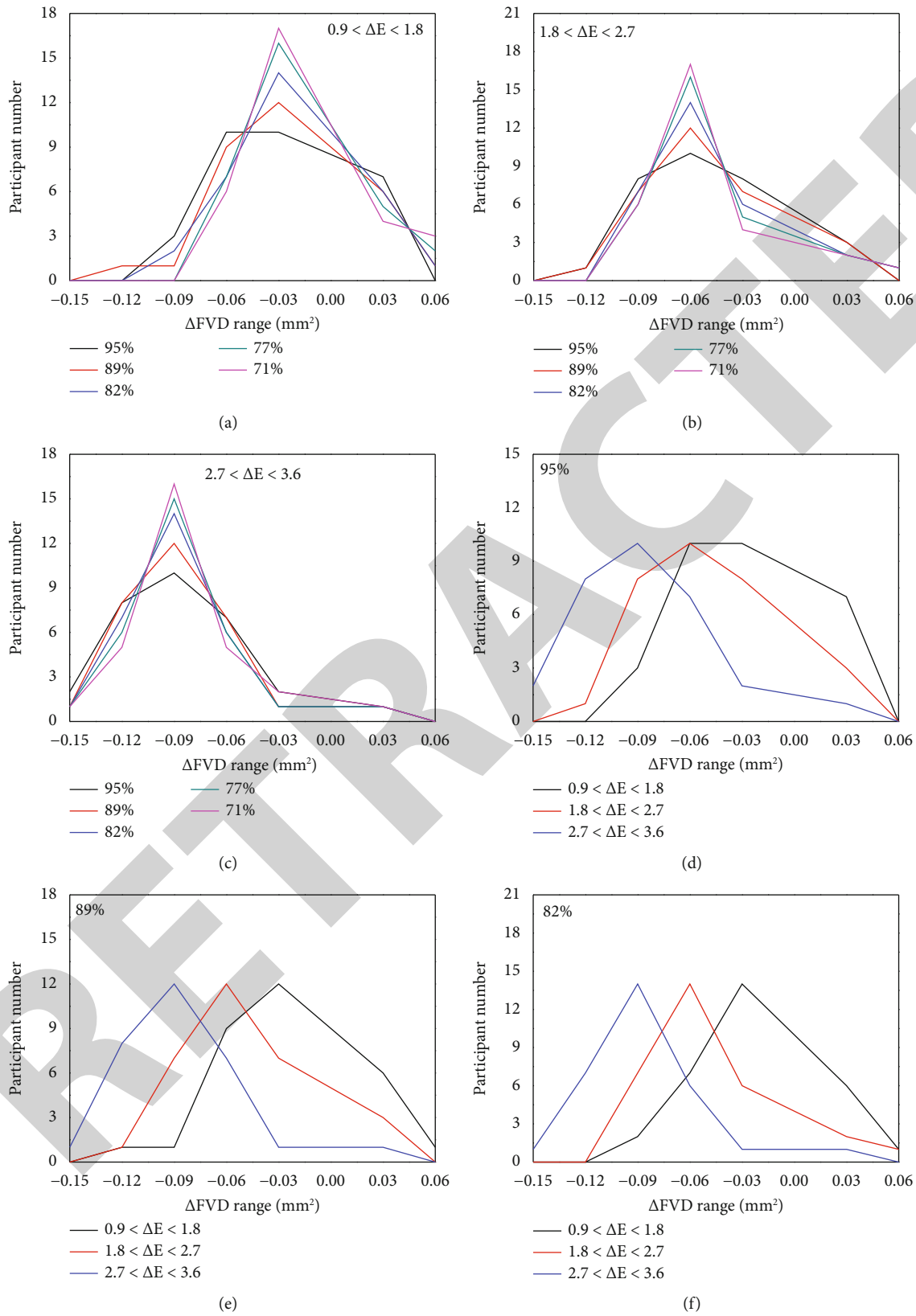

Figure 4: Continued.

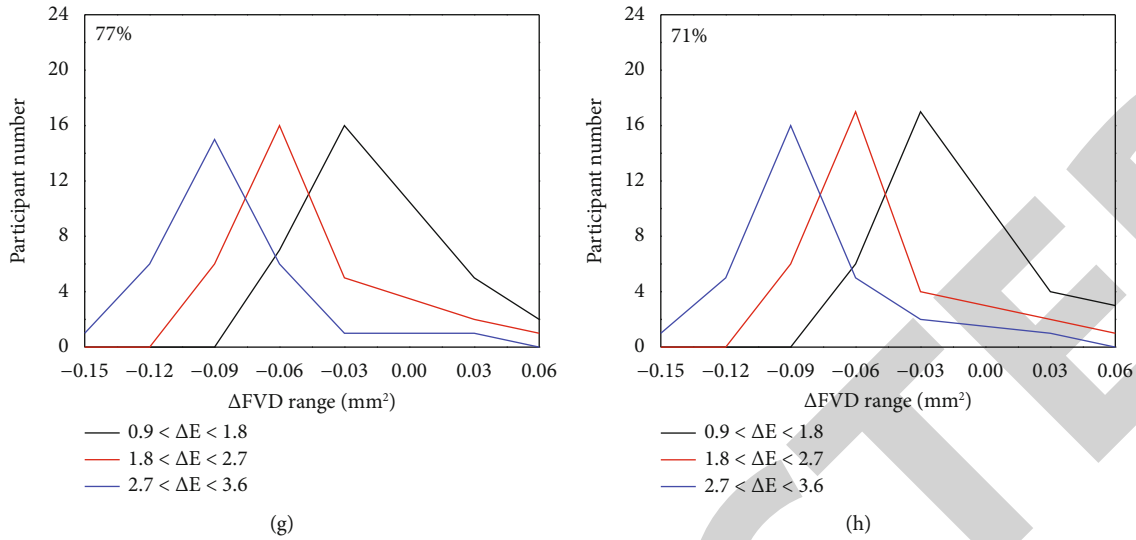

Figure 4: ΔFVD-distribution curves induced by various color-gamut coverages in the range of (a) 0.9 < E < 1.8, (b) 1.8 < E < 2.7, and (c) 2.7 < E < 3.6, and caused by different color-deviation levels in (d) 95%, (e) 89%, (f) 82%, (g) 77%, and (h) 71%.

Analyzer 2.6 software. A total of 15 screens presenting 15 color features (Table 1) were used.

2.2. Cellular Experiments. We carried out cellular experiments to investigate the effects of different spectrums. The retinal cells for this study were human ARPE-19 cells purchased from Procell Co. Ltd. We cultivated the ARPE-19 cells with the DMEM-F12 solution (10% fetal-calf serum) in the cell-culture incubator with 5% CO2. All the ARPE-19 cells were divided into three groups and cultivated in the screen with the three color-deviation levels shown in Table 1. The screens were set to the status of white balance, and the illuminance value was 400 lux.

For CV measurement, we performed cellular staining with the Trypan Blue and then analyzed the CV using the ThermoFisher Scientific Flow Cytometer instrument. CV data were automatically collected.

2.3. Human Factor Experiments. In this study, all 30 participants (university students, including 17 males and 13 females, 21 to 30 years old) provided written informed consent. All of the methods used were performed in accordance with the relevant guidelines and regulations. Participants were assessed to ensure that they had no oculopathies such as cataracts, heterotropia, or amblyopia. Based on the survey data from all participants, anisometropia levels were below 2.5 D, the intraocular pressure distribution ranged from 14 to 20, and the diopter distribution was as follows: 40% in the range −0.75–0.75 D and 60% in the range −1.00 D to −3.00 D. The corrected visual acuities were 0.8 (40%) and 1.0 (60%). All information on participants parameters are listed in Table 2.

We performed two visual tasks: a color-recognition task and a video-watching task. Both tasks were completed on 15 separate days, with a visual task and corresponding color status performed. Before the tasks, participants were asked to relax their eyes by looking into the distance for 20 mins. Next, the color-recognition task was administered. For this task, we used a 100-page document in portable document format (PDF) with 20 color options and a reference color box on each page. Each participant was asked to identify which color option was in the same color as the reference color box on each page. Each participant was given 20 mins to complete the color-recognition task. During this time, participants also performed the video-watching task. For the video-watching task, participants watched the movie "Angry Birds" (produced by Rovio Mobile and released on May 20th, 2016). The duration of the video-watching task was also 20 mins.

2.4. Human Ocular Measurements. We measured the FVD of each screen user prior to and following the screen-watching task. FVD was measured using an Optical Coherence Tomography Angiography (OCTA) instrument with RS-3000 equipment. The areas of the fovea vascular and avascular zones were automatically calculated for each participant and are shown in Figure 2 with the red and green colors representing the vascular area and the optic-disk area, respectively. We calculated FVD variations (ΔFVD) by subtracting the FVD data following the screen-watching task with the data collected prior to the task.

Each participant was asked to attach his or her forehead and chin to the specified location on the instrument and to look at the target on the screen binocularly under natural conditions. FVD data were collected automatically by the instrument. A training trial simulating the complete task content was run for each participant before data collection until the task was well understood.

We also collected the modulation-transfer function (MTF) as a supplementary piece of data. MTF was recorded using the NIDEK OPD Scan III, which collected data automatically. Likewise, all participants were allowed to blink during the measurement to avoid aggravation of ocular fatigue caused by extended interblink intervals. We calculated MTF variations (ΔMTF) by subtracting the final MTF (following the task) with the initial MTF (prior to the task).

Table 5: Comparing ΔMTF between the adjacent color-gamut coverage pairs in multiple color-deviation levels; t represents Student's t-test value, and P represents significance probability; $^{*}P < 0.05$ and $^{**}P < 0.01$.

Color-deviation Level	Color-gamut Coverages	t	P
0.9 < ΔE < 1.8	95% vs 89%	− 0.367	0.717
	95% vs 82%	− 0.711	0.483
	95% vs 77%**	− 3.456	0.002
	95% vs 71%**	− 3.269	0.003
	89% vs 82%	− 0.317	0.754
	89% vs 77%*	− 2.683	0.012
	89% vs 71%*	− 2.247	0.033
	82% vs 77%*	− 2.766	0.01
	82% vs 71%*	− 2.506	0.018
	77% vs 71%	0.268	0.791
1.8 < ΔE < 2.7	95% vs 89%	− 1.204	0.238
	95% vs 82%	0.593	0.558
	95% vs 77%	− 0.258	0.798
	95% vs 71%	0.162	0.873
	89% vs 82%	1.978	0.058
	89% vs 77%	0.772	0.446
	89% vs 71%	1.264	0.217
	82% vs 77%	− 1.431	0.164
	82% vs 71%	− 0.548	0.588
	77% vs 71%	0.708	0.458
2.7 < ΔE < 3.6	95% vs 89%	0	1
	95% vs 82%	− 0.187	0.853
	95% vs 77%	1.714	0.098
	95% vs 71%*	2.711	0.011
	89% vs 82%	− 0.207	0.837
	89% vs 77%	1.791	0.084
	89% vs 71%**	2.823	0.009
	82% vs 77%	1.622	0.116
	82% vs 71%*	2.295	0.029
	77% vs 71%	1.409	0.170

To assess visual comfort levels by calculating the visual comfort (VICO) index, we measured the corneal-refractive power (KR), axial length (AL), ciliary accommodation (ACC), and high-order aberrations (HOAs): KR and AL values were measured using the NIDEK AL-Scan automatically. The NIDEK AR-1S instrument was used to collect the ACC automatically. For the HOA measurements, we used the NIDEK OPD Scan III to automatically collect the participants' data.

3. Results

3.1. CV Comparisons. We measured CVs in the color-deviation level of 0.9 < ΔE < 1.8, 1.8 < ΔE < 2.7, and 2.7 < ΔE < 3.6, and the results were 76.97%, 77.46%, and 77.15%, respectively (Figure 3). The CVs in the three color-deviation levels presented little differences, and the three corresponding spectrums were similar in their effects on CV. As the three spectrums were obtained by non-oxidative blue (455-475 nm) filtering, the non-oxidative blue light seemed to cause little damage to the retinal cells. Conversely, filtering the necessary blue light might induce color-deviation reduction.

3.2. ΔFVD Responses. We observed significant ΔFVD differences among the study participants (Table 3). Within the same color-deviation level, we did not identify any significant differences in ΔFVD values in different color-gamut coverages, implying that the variations of color-gamut coverage do not induce changes in ΔFVD. In contrast, we observed significant ΔFVD differences in different color-deviation levels (Table 4). In summary, differences in ΔFVD seemed to rely on the color-deviation level rather than the color-gamut coverage.

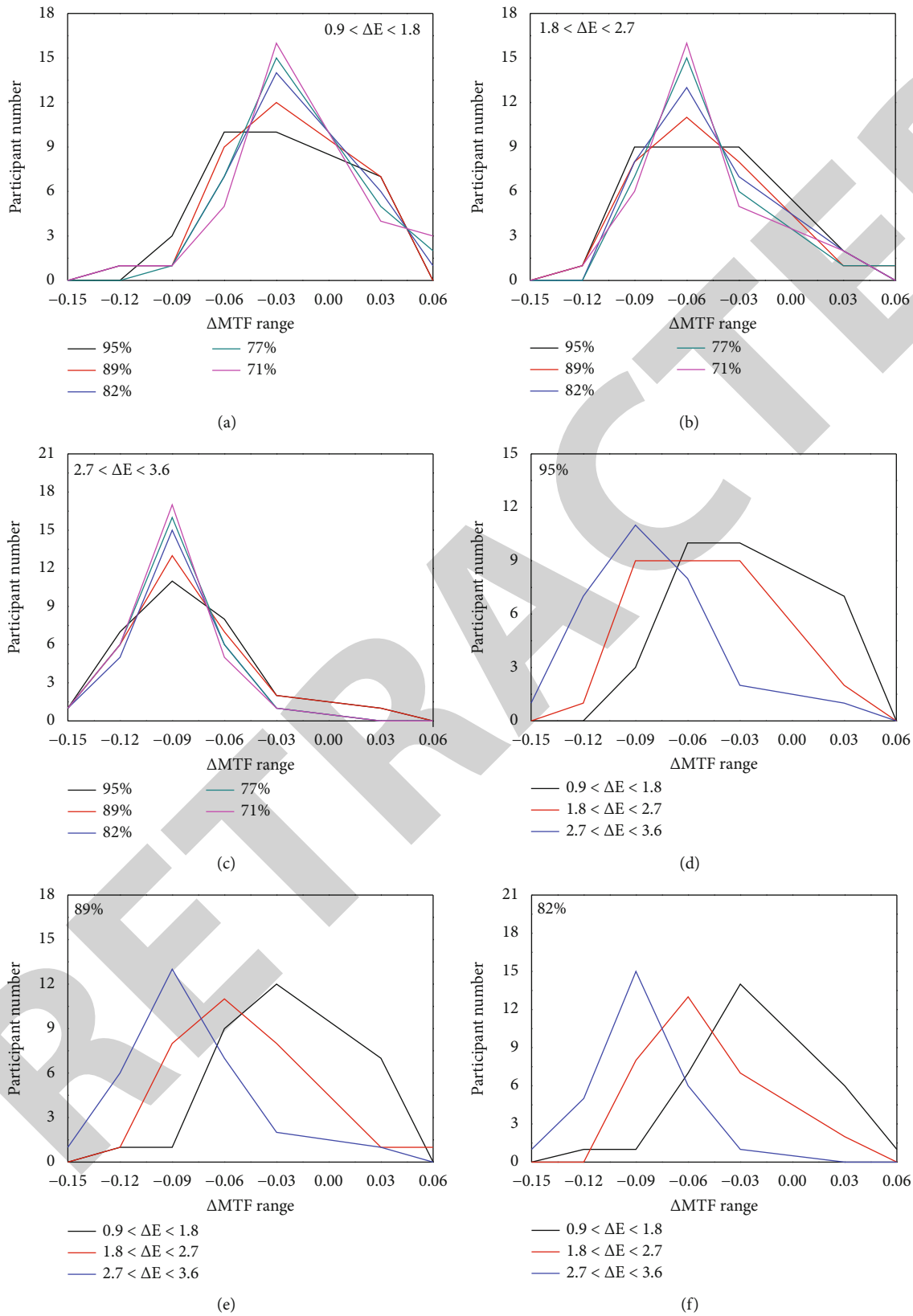

Figure 5: Continued.

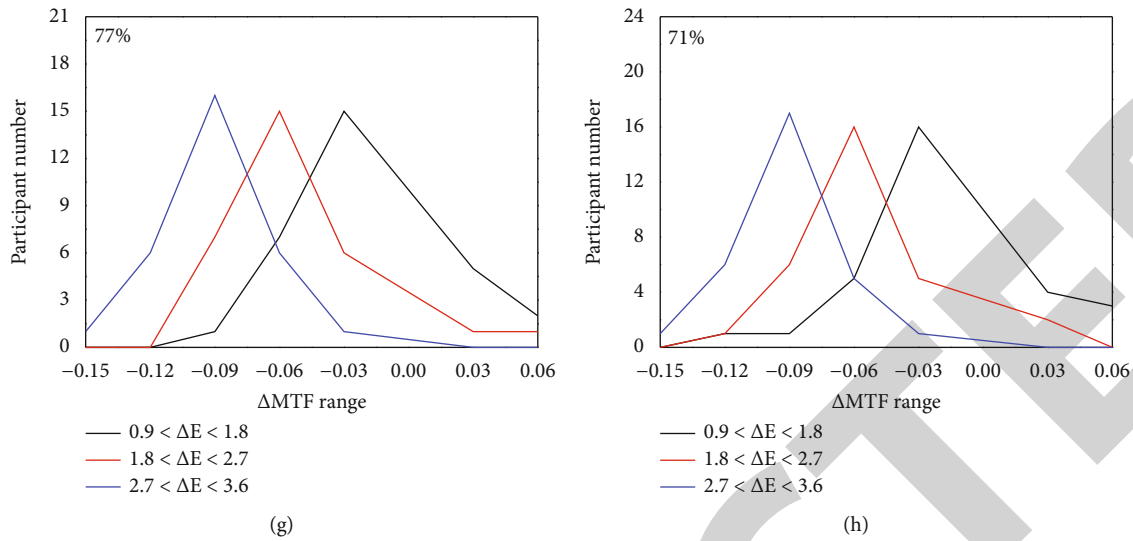

Figure 5: ΔMTF-distribution curves caused by various color-gamut coverages in the range of (a) 0.9 < E < 1.8, (b) 1.8 < E < 2.7, and (c) 2.7 < E < 3.6 and caused by different color-deviation levels in (d) 95%, (e) 89%, (f) 82%, (g) 77%, and (h) 71%.

Table 6: Comparing ΔFVD between the adjacent color-deviation-level pairs in multiple color-gamut coverages; t represents Student's t-test value, and P represents significance probability; $^{*}P < 0.05$ and $^{**}P < 0.01$.

Color-gamut Coverage	Color-deviation Levels	t	P
95%	1.5 vs 2.3**	6.453	0.001
	2.3 vs 3.3**	7.973	0.001
89%	1.5 vs 2.3**	4.667	0.001
	2.3 vs 3.3**	11.829	0.001
82%	1.5 vs 2.4**	10.029	0.001
	2.4 vs 3.3**	6.696	0.001
77%	1.6 vs 2.4**	8.865	0.001
	2.4 vs 3.3**	11.258	0.001
71%	1.6 vs 2.4**	12.339	0.001
	2.4 vs 3.4**	11.333	0.001

We observed bell-shaped distribution curves for ΔFVD values collected for various color-gamut coverages and color-deviation levels. Although changes in the color-gamut coverage hardly affected the locations of the bell-shaped curves, it caused their deformations. For each color-deviation level, the distribution curves grew more dispersive with the increase of the color-gamut coverage (Figures 4(a)–4(c)). The color-deviation level differed from the color-gamut coverage based on differential effects on FVD. With increased color-deviation levels, the bell-shaped distribution curves exhibited crests that were shifted toward higher values (Figures 4(d)–4(h)).

3.3. ΔMTF Responses. The ΔMTF data were similar to ΔFVD data in performance, as the color-gamut coverage variation altered the ΔMTF-distribution dispersity (Table 5, Figures 5(a)–5(c)) while the color-deviation-level variation caused the bell-shaped-curve's shift (Table 6, Figures 5(d)–5(h)). Compared to the color-gamut, the color-deviation level had a more significant effect on ΔMTF.

4. Discussion

4.1. ΔFVD-ΔMTF Correlation. During the screen-watching tasks, we found that the participants' ocular responses depended on both the color-deviation level and the color-gamut coverage. The ΔFVD and ΔMTF presented similar variation regularities, with their distribution curves deformed to be more dispersive with increases in color-gamut coverage and shifting toward higher values with a larger color-deviation level. The similar performances observed corresponded with their possible correlation, which was confirmed by correlation analysis using SPSS 20.0 software (Table 7). The correlation was significant for each color deviation and each type of color-gamut coverage. The MTF determines the spatial distribution of photos in photoreceptors, which attach to retinal vessels. The RVA describes blood circulation in retinal vessels. In our study, the ΔFVD-ΔMTF correlation indicated that retinal vessel circulation might vary with photoreceptor-activation distribution.

4.2. VICO Mapping. We used the VICO index to determine the effects of each color-deviation and color-gamut coverage on ocular fatigue. With a ΔE < 2.7, increased color-gamut coverage led to a decreased VICO. Furthermore, a color-gamut coverage of 82% NTSC was an inflection point that divided the VICO curve into different-slope parts (Figure 6). With an ΔE > 2.7, however, the VICO index did not change with the color-gamut coverage.

In this study, there were 15 combinations of color-deviation and color-gamut coverage (Table 2). By designating the color-gamut coverage as the horizontal coordinate

Table 7: Correlation between ΔFVD and ΔMTF with different color-gamut coverings and color-deviation levels; t represents Student's t-test value, and P represents significance probability; $^{*}P < 0.05$ and $^{**}P < 0.01$.

Color-deviation Level	Color-gamut Covering	Correlation coefficient	P
$0.9 < \Delta E < 1.8$	71%**	0.491	0.006
	77%**	0.521	0.003
	82%**	0.510	0.004
	89%**	0.486	0.006
	95%*	0.451	0.012
$1.8 < \Delta E < 2.7$	71%*	0.455	0.012
	77%**	0.469	0.009
	82%**	0.479	0.007
	89%**	0.464	0.010
	95%	0.420	0.021
$2.7 < \Delta E < 3.6$	71%**	0.483	0.007
	77%*	0.450	0.013
	82%*	0.448	0.013
	89%*	0.444	0.014
	95%**	0.536	0.002

and the color deviation as the vertical coordinate, we could graph all 15 combinations in a two-dimensional coordinate system as 15 dots, corresponding to 15 VICO values. Since the color-deviation and color-gamut coverage variations contributed to VICO values continuously, we simulated the VICO value for each dot in the two-dimensional coordinates (with a color-gamut range from 70% to 95% NTSC, and a color-deviation range from 1.5 to 5.5) using the Newton interpolation method (Figure 6). The VICO heat map showed that the color distribution contributed more significantly to VICO than the color-gamut coverage, and also showed that color-deviation modulated color-gamut coverage's effects on VICO. In the heat map, the yellow color is likely a boundary whose shape highlights the color-gamut coverage at 82% as the inflection point.

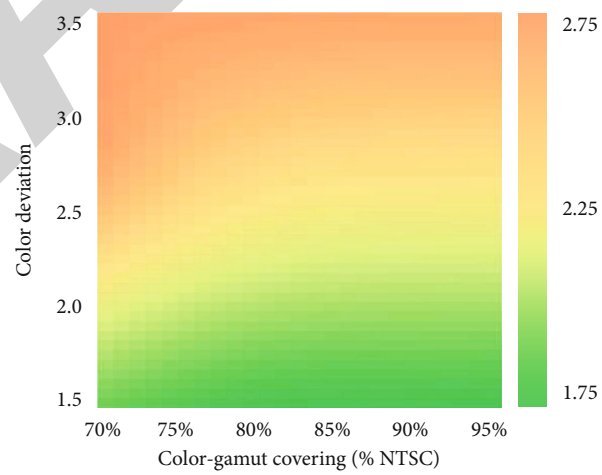

Figure 6: VICO heat map in the two-dimensional coordinates of color-deviation and color-gamut coverage.

5. Conclusion

In this study, we analyzed fundus-vascular responses to color-deviation reduction caused by non-oxidative blue filtering. Variations in FVD were used to indicate fundus-vascular responses. Our results showed that color-gamut coverage variations caused altered dispersions in the distribution curves for ΔFVD and ΔMTF, while color-deviation changes induced distribution's curve shifts. We also discovered that ocular comfort relied on color deviation more than color-gamut coverage by VICO heat map, since the color transition was more rapid along the color-deviation- coordinate axis. Specifically, a color deviation of 2.7 seemed to be a VICO heat map boundary. Increased color-gamut coverage caused a reduction in VICO when $\Delta E < 2.7$ and no longer induced VICO variation when $\Delta E > 2.7$. As ΔMTF and ΔFVD were significantly correlated, we inferred that retinal-photon distribution determined the fundus-vascular activities in certain paths. Our findings showed that non-oxidative blue light did not damage retina; instead, it was necessary for display to decrease the reduction of fundus-vascular function. In display technology research and development, the role of non-oxidative blue wavelength is indispensable to limit the color-deviation increase and benefit visual function.

Data Availability

The data that support the findings of this study are available from the corresponding authors upon reasonable request.

Conflicts of Interest

The authors declare that there is no conflict of interest regarding the publication of this paper.

Authors' Contributions

Jianqi Cai contributed to the project administration, funding acquisition, supervision, validation, and resources. Wentao Hao contributed to the writing-review and editing and formal analysis. Shanshan Zeng contributed to the methodology and data curation. Junkai Li contributed to the methodology and data curation. Ya Guo contributed to the methodology and data curation. Kai Tan contributed to the supervision, validation, and resources. Yongyin Kang contributed to the supervision, validation, and resources. Yitao Huang contributed to the supervision, validation, and resources. Yue Zhang contributed to the supervision, validation, and resources. Thebano Santos contributed to the writing-review and editing and formal analysis. Cheng Qian contributed to the writing-review and editing and formal analysis. Aiqin Luo contributed to the writing-review and editing and formal analysis.

Acknowledgments

The research was funded by the Research and Applications of Photo-biological Effects of Yellow Light on Human Body (512022Y-9447), the Running Insurance Program of Visual Health and Safety Protection Laboratory in 2022 (512022Z-9499), the Research and Development of the Optic-Fiber System for Human-Ocular Requirement (512022Z-9240), the China Association for Science and Technology (CAST) Program of International Collaboration Platform for Science and Technology Organizations in Belt and Road Countries (2021ZZGJB050616), the Research of Ocular Biological Characteristics based on Proteomics (512020Z-7422), and the Research of Thermal Damage and Protection Equipment for Head and Face of Human Body (512016Y-4497). We thank LetPub (http://www.letpub.com) for its linguistic assistance during the preparation of this manuscript.

References

[1] J. Q. Core, M. Pistilli, E. Daniel et al., "Predominantly persistent subretinal fluid in the comparison of age-related macular degeneration treatments trials," *Ophthalmology Retina*, vol. 5, no. 10, pp. 962–974, 2021.

[2] X. Li, H. Li, J. Cheng et al., "Causal associations of thyroid function and age-related macular degeneration: a two-sample Mendelian randomization study," *American Journal of Ophthalmology*, vol. 239, pp. 108–114, 2022.

[3] L. Fang and H. Qiao, "Diabetic retinopathy classification using a novel DAG network based on multi-feature of fundus images," *Biomedical Signal Processing and Control*, vol. 77, article 103810, 2022.

[4] J. M. Coney and A. W. Scott, "Racial disparities in the screening and treatment of diabetic retinopathy," *Journal of the National Medical Association*, vol. 114, no. 2, pp. 171–181, 2022.

[5] R. N. G. Vianna, G. Squeri, R. Turquetti, O. F. M. Brasil, and M. N. Burnier Jr., "Intravitreal pegaptanib reduces fluorescein leakage in idiopathic parafoveal telangiectasis," *Canadian Journal of Ophthalmology. Journal Canadien D'ophtalmologie*, vol. 43, no. 4, pp. 492-493, 2008.

[6] R. Windisch and V. Kozousek, "Intravitreal bevacizumab compared with photodynamic therapy with verteporfin for group 2a parafoveal retinal telangiectasis," *Canadian Journal of Ophthalmology. Journal Canadien D'ophtalmologie*, vol. 43, no. 4, pp. 489-490, 2008.

[7] D. R. Pur, L. L. Catherine Danielle Bursztyn, and Y. Iordanous, "Branch retinal vein occlusion in a healthy young man following mRNA COVID-19 vaccination," *American Journal of Ophthalmology*, vol. 26, article 101445, 2022.

[8] A. Naranjo, N. Rayess, E. Ryan, M. Iv, and V. B. Mahajan, "Retinal artery and vein occlusion in calciphylaxis," *American Journal of Ophthalmology*, vol. 26, article 101433, 2022.

[9] C. Zhao, D. Wei, X. Shi, and M. Zhao, "Unilateral isolated optic nerve infiltration combined with central retinal artery occlusion in a patient with acute myeloid leukemia," *American Journal of Ophthalmology*, vol. 26, article 101493, 2022.

[10] S. Hwang, S. W. Kang, K. J. Choi et al., "High-density lipoprotein cholesterol and the risk of future retinal artery occlusion development: a nationwide cohort study," *American Journal of Ophthalmology*, vol. 235, pp. 188–196, 2022.

[11] T. Tran, M. Okada, J. Goh, T. Gin, and C. A. Harper, "Choroidal effusion as a manifestation of central serous chorioretinopathy: a case report," *American Journal of Ophthalmology*, vol. 25, article 101311, 2022.

[12] S. Sawaguchi, N. Terao, N. Imanaga et al., "Scleral thickness in steroid-induced central serous chorioretinopathy," *Ophthalmology Science*, vol. 2, no. 2, article 100124, 2022.

[13] C. S. Tan, L. W. Lim, and P. Margaron, "Evolution of polypoidal lesions after treatment of polypoidal choroidal vasculopathy," *Ophthalmology Science*, vol. 2, no. 1, article 100082, 2022.

[14] B. J. Fenner, K. Y. C. Teo, Y. C. Tham, U. Chakravarthy, and C. M. G. Cheung, "Prevalence of polypoidal choroidal vasculopathy using non-indocyanine green angiography-based criteria," *Retina*, vol. 6, no. 2, pp. 179–181, 2022.

[15] H. Yu, T. Akita, T. Koga, and N. Sano, "Effect of character contrast ratio of tablet PC and ambient device luminance ratio on readability in low ambient illuminance," *Displays*, vol. 52, pp. 46–54, 2018.

[16] H. Yu and T. Akita, "Influence of ambient-tablet PC luminance ratio on legibility and visual fatigue during long-term reading in low lighting environment," *Displays*, vol. 62, article 101943, 2020.

[17] L. C. Ou, P. L. Sun, H. P. Huang, and M. Ronnier Luo, "Visual comfort as a function of lightness difference between text and background: a cross-age study using an LCD and a tablet computer," *Color Research and Application*, vol. 40, no. 2, pp. 125–134, 2015.

[18] L. L. A. Price, L. Udovičić, T. Behrens et al., "Linking the non-visual effects of light exposure with occupational health," *International Journal of Epidemiology*, vol. 48, no. 5, pp. 1393–1397, 2019.

[19] J. C. G. Ortega, B. R. S. Figueiredo, W. J. da Graça, A. A. Agostinho, and L. M. Bini, "Negative effect of turbidity on prey capture for both visual and non-visual aquatic predators," *The*

Hindawi
Oxidative Medicine and Cellular Longevity
Volume 2024, Article ID 9871986, 1 page
https://doi.org/10.1155/2024/9871986

Retraction

Retracted: Tumor Necrosis Factor-Alpha Disrupts Cx43-Mediated Corneal Endothelial Gap Junction Intercellular Communication

Oxidative Medicine and Cellular Longevity

Received 8 January 2024; Accepted 8 January 2024; Published 9 January 2024

This article has been retracted by Hindawi following an investigation undertaken by the publisher [1]. This investigation has uncovered evidence of one or more of the following indicators of systematic manipulation of the publication process:

(1) Discrepancies in scope
(2) Discrepancies in the description of the research reported
(3) Discrepancies between the availability of data and the research described
(4) Inappropriate citations
(5) Incoherent, meaningless and/or irrelevant content included in the article
(6) Manipulated or compromised peer review

The presence of these indicators undermines our confidence in the integrity of the article's content and we cannot, therefore, vouch for its reliability. Please note that this notice is intended solely to alert readers that the content of this article is unreliable. We have not investigated whether authors were aware of or involved in the systematic manipulation of the publication process.

Wiley and Hindawi regrets that the usual quality checks did not identify these issues before publication and have since put additional measures in place to safeguard research integrity.

We wish to credit our own Research Integrity and Research Publishing teams and anonymous and named external researchers and research integrity experts for contributing to this investigation.

The corresponding author, as the representative of all authors, has been given the opportunity to register their agreement or disagreement to this retraction. We have kept a record of any response received.

References

[1] J. Meng, K. Xu, Y. Qin et al., "Tumor Necrosis Factor-Alpha Disrupts Cx43-Mediated Corneal Endothelial Gap Junction Intercellular Communication," *Oxidative Medicine and Cellular Longevity*, vol. 2022, Article ID 4824699, 9 pages, 2022.

Hindawi
Oxidative Medicine and Cellular Longevity
Volume 2022, Article ID 4824699, 9 pages
https://doi.org/10.1155/2022/4824699

Research Article

Tumor Necrosis Factor-Alpha Disrupts Cx43-Mediated Corneal Endothelial Gap Junction Intercellular Communication

Jufeng Meng,[1] Ke Xu,[2] Yinyin Qin,[3] Ya Liu,[4] Lin Xu,[4] Shigang Qiao,[3] Jianzhong An,[3] Jianjun Liu,[4] and Zhenhao Zhang[3]

[1]*School of Life Science and Technology, ShanghaiTech University, Shanghai 201210, China*
[2]*Key Laboratory of Tropical Translational Medicine of Ministry of Education, NHC Key Laboratory of Control of Tropical Diseases, School of Tropical Medicine, Hainan Medical University, Haikou 571199, China*
[3]*Institute of Clinical Medicine Research, Suzhou Science & Technology Town Hospital, Suzhou 215153, China*
[4]*Department of Ophthalmology, Suzhou Science & Technology Town Hospital, Suzhou 215153, China*

Correspondence should be addressed to Zhenhao Zhang; zhang.687001@163.com

Jufeng Meng and Ke Xu contributed equally to this work.

Received 10 July 2022; Revised 23 August 2022; Accepted 27 August 2022; Published 19 September 2022

Academic Editor: Pei-Wen Zhu

Connexin43 (Cx43)-mediated gap junctions are vital in maintaining corneal endothelium homeostasis. Tumor necrosis factor-alpha (TNF-α) is among the most important inflammatory factors which cause corneal endothelial dysfunction in various eye diseases. However, the effect of TNF-α on Cx43-mediated gap junctions of the corneal endothelium remains undefined. In the current research, we determined the effect of TNF-α on gap junction intercellular communication (GJIC) in rabbit corneal endothelium. To evaluate alterations of GJIC, if any, we treated ex vivo cultured rabbit corneal endothelium with different concentrations of TNF-α (2-20 ng/ml). The localization of Cx43 was analyzed by immunostaining, while RT-qPCR and western blot were used to profile the expression of Cx43 and zonula occludens-1 (ZO-1). The association between ZO-1 and Cx43 was evaluated using immunoprecipitation and double staining. GJIC activity was determined by the scrap loading and dye transfer assay (SLDT). Our data demonstrated that a high concentration of TNF-α (10 ng/ml and 20 ng/ml) disrupts the Cx43 mediated gap junction distribution in rabbit corneal endothelium and suppresses the expression of Cx43 protein. Furthermore, rabbit corneal endothelial GJIC was inhibited due to the decreased association between the ZO-1 and Cx43 proteins. Current results demonstrate that TNF-α inhibits corneal endothelial GJIC via decreasing the association between ZO-1 and Cx43, disrupting the distribution of Cx43, and downregulating the expression of Cx43 protein. This study offers a new theoretical foundation for diagnosing and treating corneal endothelial cell decompensation induced by elevated TNF-α in various eye diseases.

1. Introduction

With the increase in age, the density of human corneal endothelial cells reduces by 0.6% annually [1]. Following insults such as intraocular surgical trauma, topical application of drugs, and corneal transplantation, the cell cycle is arrested at the G1 phase and fails to proliferate in vivo [2]. In endothelial cells of patients with decompensation, corneal endothelial transplantation is the best treatment option. However, the lack of donors and low survival rate after corneal endothelial transplantation severely limit the wide clinical development of corneal transplantation. To circumvent this challenge, there is a critical need to study the homeostasis of the corneal endothelium. Under normal physiological circumstances, gap junction channels made of 2 connexons that dock between corneal endothelial cells can allow small molecular nutrients, signal compounds, like inositol trisphosphate (IP3), nucleotides, and Ca^{2+}, as well as metabolites, to pass through and perform

intercellular communication, thus playing a key role in maintaining the internal environment and metabolism of the corneal endothelial cells [3, 4]. Connexon is composed of six connexin subunits [5], and 21 different types of connexins have been identified to date. Out of the various types of connexins, connexin43 (Cx43) has been the most studied and widely distributed gap junction protein. The Cx43 protein is the most common connexin subtype expressed in bovine [4], human [6], rabbit [7], and rat corneal endothelial cells [8]. Our previously published results also confirm that Cx43 plays an important role in maintaining the homeostasis of GJIC in rabbit corneal endothelial cells [9]. Gap junctions can influence cell death and survival responses to oxidative and metabolic stress [10]. However, dysfunction of Cx43-mediated gap junction intercellular communication (GJIC) induces many diseases, including cardiovascular diseases [11], neuropathy [12], cancer [13], and ocular diseases [14].

Connexin family members have a half-life of 2-5 h and undergo gap junction plaque organization to final degradation in this process [3]. However, the specific mechanisms that regulate the assembly and degradation of gap junctions remain poorly understood. It is reported that Cx43 binds to PDZ domain of ZO-1 through the C-terminal domain to maintain the dynamic balance of gap junction [15]. The ZO-1 protein not only helps organize gap junction plaques but also participates actively in Cx43 trafficking and internalization, and thereby exerts biological effects [16]. Meanwhile, phosphorylation of Cx43 regulates gap junction plaques organization and GJIC activity [17].

Inflammatory factors in aqueous humor induced by endophthalmitis, uveitis, ocular trauma, and other ocular surgeries lead to corneal endothelial dysfunction, thus affecting the metabolism of endothelial cells and maintenance of the internal homeostasis [18, 19]. TNF-α is one of the most important inflammatory factors which causes corneal endothelial impairment and is crucial in immune regulation [20]. Hao et al. and Kimura et al. showed that TNF-α inhibits Cx43-mediated GJIC activity by activating JNK signaling pathway in cultured human corneal fibroblasts, suggesting that the JNK pathway can regulate the functions of the gap junction [21, 22]. The study also showed that TNF-α can induce Cx43 degradation by the ubiquitin-proteasome pathway and can inhibit the GJIC activity of corneal fibroblasts [23]. Our previous study have found that TNF-α disrupts the corneal endothelial barrier function maintained by tight junction protein ZO-1 by promoting myosin light chain (MLC) phosphorylation [24]. Another study demonstrated that preservative benzalkonium chloride (BAK) inhibits GJIC by phosphorylating Cx43 and downregulating Cx43 expression [9]. Although several studies on TNF-α and corneal gap junction have been carried out, the effect of TNF-α on Cx43-mediated gap junctions of the corneal endothelium remains unclear. In this study, our data showed that in ex vivo cultured rabbit corneal endothelial tissue and primary cultured rabbit corneal endothelial cells, treatment with high concentration of TNF-α (10, 20 ng/ml), could disrupt GJIC via attenuating the association between ZO-1 and Cx43 proteins as well as disrupting the distribution of Cx43 and decreasing the expression of Cx43.

In summary, this study demonstrated how rabbit corneal endothelial cells respond to TNF-α stimuli and showed changes in the GJIC. The current results highlight a novel molecular mechanism underlying the damage to corneal endothelial functions caused by increased TNF-α in various eye diseases. Thus, targeting the gap junctions could be a novel strategy to protect the corneal endothelium.

2. Materials and Methods

2.1. Animals. The Shanghai SLAC Laboratory Animal Co., Ltd. (Shanghai, China) provided us with male New Zealand white rabbits weighing between 1.5 and 2 kg each (Shanghai, China). The animals were fed in a standard environment at 20 ± 1°C, and the lighting was simulated day and night. All experiments on animals have been performed in accordance with the guidelines of ARVO for Ophthalmic and Vision Research and were authorized by the Laboratory Animal Council of the Suzhou Science and Technology Town Hospital.

2.2. Reagents and Antibodies. DMSO and Triton X-100 were purchased from Abcone (Shanghai, China). Pentobarbital sodium, TNF-α, and Lucifer yellow dye were obtained from Sigma-Aldrich (St. Louis, MO). Primary ZO-1 antibody (mouse anti-rabbit), donkey anti-mouse IgG Alexa Fluor 488, and donkey anti-goat IgG Alexa Fluor 555 were purchased from Thermo Fisher Scientific (Carlsbad, CA). Santa Cruz (Santa Cruz, CA) provided goat-anti-rabbit Cx43 antibodies; HRP-conjugated donkey anti-goat IgG was from Bio-Rad (Hercules, CA). HUABIO (Hangzhou, China) supplied mouse anti-rabbit β-actin antibody, whereas Bio-Rad supplied HRP-conjugated goat anti-mouse IgG (Hercules, CA). Magnetic protein G beads and protein A/G beads were from Millipore (Billerica, MA) and Bimake (Houston, TA) ,repectively. PVDF membrane and 0.25% Trypsin-EDTAwere obtained from Thermo (Carlsbad, CA); ECL kit was provided by Shanghai Epizyme Biomedical Technology Co., Ltd (Shanghai, China); DAPI-mounting media were provided by Vector Laboratories (Burlingame, CA); BSA powders and collagenase I were acquired from Sangon Biotech (Shanghai, China) while DMEM, DMEM/F12, FBS, and Penicillin-Streptomycin (PS) were obtained from Thermo (Carlsbad, CA).

2.3. Ex Vivo Culture of Rabbit Corneal Endothelial Tissue Layers. After the rabbits were euthanized, the corneal epithelial cells were carefully scraped under a stereomicroscope (Olympus, Japan), and then venus scissors were employed to remove the remaining corneal tissue along the limbus. Isolated rabbit corneal endothelial tissue layers were grown in DMEM supplemented with 10% FBS and 1% PS as our previously reported study. The corneal endothelial tissue layers were then exposed to different concentrations of TNF-α (2-20 ng/ml) in a humid environment that included 5% CO_2 at 37°C for 24 h. On the other hand, ex vivo cultured rabbit corneal endothelial tissue layers without TNF-α treatment were used as normal controls.

2.4. Immunostaining. After TNF-α (0-20 ng/ml) treatment at 4°C, rabbit corneal endothelial tissue layers were promptly fixed with 4% paraformaldehyde for 15 minutes. Following

three washes cycles using TD buffer solution (PBS containing Triton 1% and DMSO 1%), a nonspecific interaction was inhibited by incubating tissues with BSA 2% at RT for 60 min. The rabbit corneal endothelial tissue layers were then incubated with goat anti-rabbit Cx43 polyclonal antibody (Santa Cruz) or polyclonal ZO-1 antibody (Thermo), then was diluted in BSA 1% and kept at 4°C overnight. Thereafter, the tissues were subject for 3 cycles of washing using PBS, and then it treated at RT for 60 minutes using different secondary antibodies (donkey anti-goat IgG Alexa Fluor 594 conjugated, goat anti-rabbit Alexa Fluor 488 conjugated, both diluted 1 : 300 in 1 percent BSA). Following a 3 washing cycle utilizing PBS, 4 incisions were performed in the cornea, and DAPI staining was performed on the endothelial tissues of the cornea. The slices were viewed under a confocal laser scanning microscope (CLSM, Zeiss 880) and then photographs were processed and investigated utilizing Zeiss Blue software.

2.5. Western Blot. The isolated rabbit corneal endothelial tissue layers were washed 3 times in a phosphate buffer saline before being lysed in RIPA buffer solution containing protease inhibitor 1% (Thermo). The concentration of the proteins was measured using a BCA protein kit (Beyotime Biotechnology, Shanghai, China) via centrifuging at 14000 g for a half-hour at 4°C. After SDS-PAGE separation, the proteins were transported to membranes of PVDF. At room temperature, the membranes were blocked with TBST that was supplemented with 2% BSA. After that, the membranes were incubated with primary anti-ZO-1, Cx43, or anti-actin antibodies at 4°C in TBST that contains 1% BSA. Thereafter, membranes were incubated with the secondary antibodies at room temperature for 1.5 hours. After washing 3 times with TBST, the blots were exposed to ECL reagents for visualization of immunocomplexes. An image analysis software package was used to analyze the band intensities with a gel imaging system (Bio-Rad, CA).

2.6. RT-qPCR Analysis. The rabbit corneal endothelial layers were isolated under a surgical microscope as previously described. Total RNA of the corneal endothelium was extracted with EasyPure RNA kit and then adjusted to the same concentration. Subsequently, the Reverse Transcriptase kit (Vazyme biotech, China) was used to synthesize cDNA from the extracted RNA, which was then amplified using an SYBR qPCR Mix kit (Vazyme biotech, China) in a QuantStudio 5 PCR instrument (Thermo, USA) using specific primers for Cx43, ZO-1, and GAPDH. Following are the PCR primer sequences: ZO-1 (forward, 5′-GTCTGCCATTACACGGTCCT-3′ reverse, 5′-GGTCTCTGCTGGCTTGTTTC-3′), Cx43 (forward, 5′-GCAAGCTCCTGGACAAAGTC-3′, reverse, 5′-CGTTGA CACCATCAGTTTGG-3′), and GAPDH (forward, 5′-ACCA CAGTCCACGCCATCAC-3′, reverse, 5′-TCCACCACCCT GTTGCTGTA-3′). The mRNA expression profiles were assessed utilizing the $\Delta\Delta$CT technique, then standardized to rabbit GAPDH.

2.7. Immunoprecipitation. Fresh isolated rabbit corneal endothelium were homogenized in immunoprecipitation buffer and lysed on ice for 2 h. Protein concentration was determined after centrifugation at 16000 g for 35 min at 4°C for cell lysates. Magnetic protein G beadswere used to remove nonspecific binding for 1 h at RT. After removing the magnetic beads, the supernatant was incubated overnight with primary Cx43 antibody and protein A/G beads. Thereafter, the beads were collected by centrifugation at 18000 g for 18 min at 4°C and washed 4 times with immunoprecipitation buffer. The proteins bound to the magnetic beads were denatured by heating at 100°C, followed by immediate WB analysis as described above.

2.8. Primary Rabbit Corneal Endothelial Cells Culture and SLDT Assay. GJIC activity can be analyzed using SLDT assay by measuring the distance, the dye permeates through gap junction, or calculating how many dye-containing cells there are. In order to effectively evaluate GJIC activity, primary cultured corneal endothelial cells were used in this study to analyze the effect of TNF-α on GJIC. Firstly, isolated rabbit corneal endothelial layers were digested overnight at 37°C by 10 mg/ml collagenase I, followed by treatment with 0.25% trypsin-EDTA for 5 minutes to break up into single cells. When primary rabbit corneal endothelial cells cultured in DMEM/F12 supplemented with 10% FBS and 1% PS reached to 70% confluence, 2-20 ng/ml TNF-α were added to the culture medium and incubated for 24 h, respectively. Cultured cells were washed three times with PBS and then 10 scratches were made in a 6-well plate using a sterile pipette tip in the presence of 1 mg/ml Lucifer yellow dye. Next, the cells were incubated in a 37°C incubator for 5 min. The Lucifer yellow was discarded and washed three times with PBS. Subsequently, cells were fixed with 4% PFA for 12 min and observed under a Leica confocal microscopy. GJIC activity was expressed as the number of cells labeled with Lucifer yellow.

2.9. Statistical Analysis. The quantitative data was evaluated using an unpaired t-test or a one-way analysis of variance ANOVA, and the results are displayed as a mean ± SEM. The statistical significance was assessed by a p value less than or equal to 0.05.

3. Results

3.1. TNF-α Disrupts the Structure of Cx43 Mediated Gap Junction in the Rabbit Corneal Endothelium. The impact of TNF-α on Cx43 structure in the rabbit corneal endothelium was analyzed by immunostaining. The isolated corneal endothelial tissues were initially treated with 2, 10, or 20 ng/ml TNF-α for 24 hours. In the normal control, there was a large gap junction complex mediated by Cx43 in the cornea endothelium (Figure 1(a)). Treatment with a lower concentration of TNF-α (2 ng/ml) did not affect the Cx43 mediated gap junction plaques (Figure 1(b)). However, after treatment with a higher concentration of TNF-α (10 ng/ml), large gap junction plaques were rarely observed in the corneal endothelium (Figure 1(c)). On the other hand, treatment with 20 ng/ml of TNF-α led to the disappearance of typical Cx43 plaques in the endothelial cell border

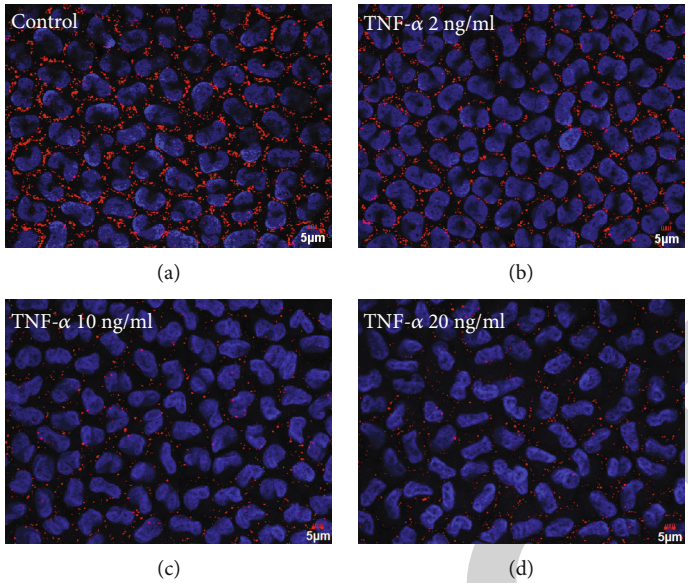

Figure 1: Impact of TNF-α on Cx43 distribution in rabbit corneal endothelium. (a) Cx43 distribution in normal rabbit corneal endothelium. (b) Cx43 distribution in rabbit corneal endothelium treated with 2 ng/ml TNF-α. (c) Cx43 distribution in 10 ng/ml TNF-α treated rabbit corneal endothelium. (d) Cx43 distribution in 20 ng/ml TNF-α treated rabbit corneal endothelium. DAPI: blue color; Cx43: red color; and scale bar: a – d = 5 μm ($n = 6$ rabbits per group).

(Figure 1(d)). These results demonstrated that treatment with TNF-α induces disruption of Cx43 mediated gap junction of cultured rabbit corneal endothelial tissues in a dose-dependent fashion.

3.2. TNF-α Attenuates Expression of Cx43 Protein in Rabbit Corneal Endothelium. We employed western blot evaluation to analyze the correlation of the disruption of Cx43 with the differential expression of gap junction proteins. The results showed significant suppression of the expression of Cx43 following exposure to 10 ng/ml (36.8%) and 20 ng/ml TNF-α (70%). In contrast, treatment with 2 ng/ml TNF-α did not alter the Cx43 expression (Figures 2(a) and 2(b)). These results demonstrated that high concentrations of TNF-α reduce the protein expression of Cx43. Since the tight junction marker ZO-1 is pivotal in regulating corneal endothelial barrier properties and gap junction intercellular communication [16, 25], we examined the impact of TNF-α on the ZO-1 expression. Western blot findings demonstrated a nonsignificant difference between the normal control group and the TNF- treated group in the amount of ZO-1 protein expression (Figure 2(a)).

3.3. Effect of TNF-α on Cx43 mRNA Levels in Rabbit Corneal Endothelium. To determine whether Cx43 mRNA expression corresponded with protein expression, the different TNF-α treatment concentration groups underwent RT-qPCR analyses. Our findings showed no marked differences in the mRNA expression between the Cx43 and ZO-1 after treatment with lower concentrations of TNF-α at 2 ng/ml. Besides, concentrations of TNF-α at 20 ng/ml did not also downregulate the expression of Cx43 mRNA (Figures 3(a) and 3(b)). These results suggest that Cx43 may undergo posttranslational modification after exposure to TNF-α.

3.4. TNF-α Reduces the Interaction between ZO-1 and Cx43 in Cultured Rabbit Corneal Endothelium. We previously reported that treatment with TNF-α disrupted the tight junction-mediated corneal endothelial barrier function in a dose-dependent manner [24]. The tight junction marker, ZO-1, is crucial in regulating corneal epithelial and endothelial barrier properties. In addition, the interaction within ZO-1 and Cx43 mainly maintains the functions of the gap junction and regulates GJIC activity [4, 24]. Thus, Cx43 and ZO-1 interaction decrease or increase may induce gap junction dysfunction. In order to determine the impact of TNF-α on the association between Cx43 and ZO-1, double staining of ZO-1 and Cx43 proteins and immunoprecipitation were used to assess the gap junction integrity. The double immunostaining results showed a marked decline in the binding of ZO-1 with Cx43; large gap junctional complexes were rarely observed in the 10 ng/ml and 20 ng/ml TNF-α treated groups (Figures 4(c) and 4(d)). On the other hand, tight binding among ZO-1 and Cx43 was observed in the normal rabbit corneal endothelium (Figure 4(a)). Similarly, a low concentration of TNF-α at 2 ng/ml did not destroy the interaction between ZO-1 and Cx43 (Figure 4(b)). Immunoprecipitation results showed that the interaction between ZO-1 and Cx43 was significantly decreased by 29% and 46.1% in the rabbit corneal endothelial cells treated with high concentrations of TNF-α compared with the control group (Figures 4(e) and 4(f)). Taken together, these results indicated that TNF-α disturbs the connection between ZO-1 and Cx43 in the rabbit corneal endothelium.

3.5. TNF-α Inhibits GJIC Activity of Primary Rabbit Corneal Endothelial Cells. The SLDT assay is a very important method for evaluating the GJIC activity. To investigate the effect of TNF-α on GJIC activity of rabbit corneal

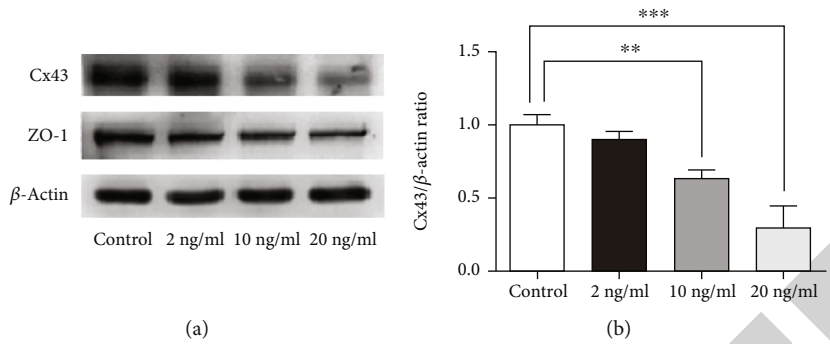

Figure 2: Impact of TNF-α on Cx43 and ZO-1 protein expression in rabbit corneal endothelium. (a) The expression of Cx43 and ZO-1 protein in different concentrations of TNF-α-treated rabbit corneal endothelium. (b) Quantification of the Cx43 protein expression in different TNF-α treatment groups. ($n = 6$ rabbits per group; mean ± SEM, $**$ represented $p < 0.01$ vs. control, and $***$ represented $p < 0.001$ vs. control).

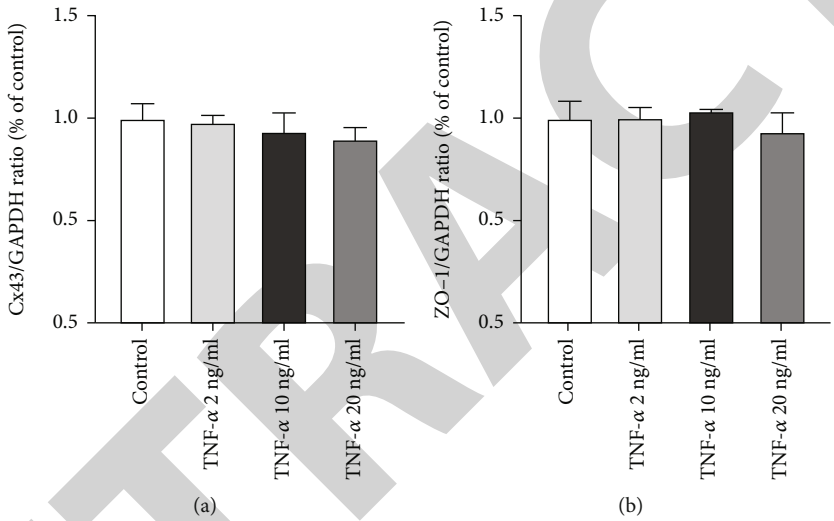

Figure 3: Impact of TNF-α on Cx43 and ZO-1 mRNA expression in rabbit corneal endothelium. (a) Quantifying Cx43 mRNA expression in normal rabbit corneal endothelium and TNF-α treatment groups. (b) Quantifying ZO-1 mRNA expression in normal rabbit corneal endothelium and TNF-α treatment groups. ($n = 6$ rabbits per group; mean ± SEM).

endothelial cells, primary cultured rabbit corneal endothelial cells were used in this study. Firstly, cells were treated with different concentrations of TNF-α (2-20 ng/ml) for 24 h before the detection of GJIC activity. The SLDT assay was then adopted to determine the number of cells labeled with Lucifer yellow (LY) through gap junctions. The results showed that low concentration of TNF-α (2 ng/ml) (Figure 5(b)) did not decrease the activity of GJIC compared with the control group (Figure 5(a)). However, high concentration of TNF-α (10, 20 ng/ml) significantly inhibited the activity of GJIC by 47.1% and 64%, respectively (Figures 5(c) and 5(d)). Taken together, we showed that TNF-α disrupts GJIC by reducing the association between Cx43 and ZO-1 and downregulating the expression of Cx43.

4. Discussion

Human corneal endothelial cells fail to proliferate because of restriction of the cell cycle in G1 phase. A variety of eye diseases such as surgical trauma, cataract surgery, glaucoma, or topically applied of eye preparations could damage corneal endothelial cells, which then induces corneal endothelial dysfunction. Elevated TNF-α in various chronic eye diseases contributes a major impact in the dysfunction of corneal endothelial homeostasis. Prior research has demonstrated that TNF-α can disrupt the localization and expression of tight junction proteins by phosphorylating myosin light chain kinase (MLCK), leading to corneal endothelial dysfunction in rabbits. We also confirmed that preservative BAK induces gap junction dysfunction by phosphorylating Cx43 and disrupting the association between Cx43 and ZO-1. Although the effect of BAK on the gap junctions has been well demonstrated, the impact of TNF-α on the GJIC of corneal endothelium remains unclear.

In this study, we demonstrated that TNF-α can damage the Cx43 mediated gap junction structure of the rabbit corneal endothelium and reduce the expression of Cx43 (Figures 1 and 2). Besides, the effect of TNF-α on gap junction dysfunction

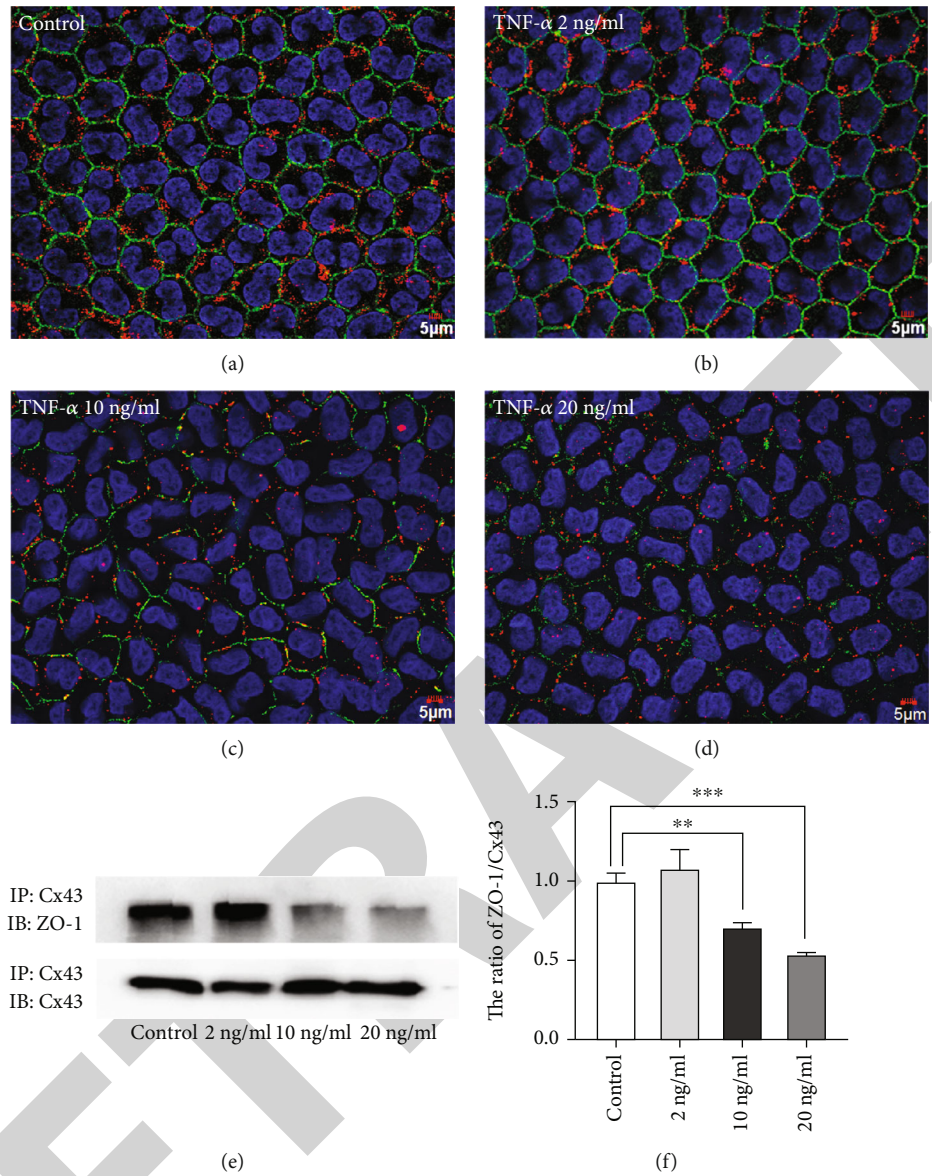

Figure 4: Reduced association between Cx43 and ZO-1 in the TNF-α-treated corneal endothelium. (a) Cx43 (red color) and ZO-1 (green color) double staining in normal rabbit corneal endothelium. (b) Cx43 (red color) and ZO-1 (green color) colocalization in 2 ng/ml TNF-α-treated rabbit corneal endothelium. (c) Cx43 (red color) and ZO-1 (green color) colocalization in 10 ng/ml TNF-α-treated rabbit corneal endothelium. (d) Cx43 (red color) and ZO-1 (green color) interaction in 20 ng/ml TNF-α-treated rabbit corneal endothelium. Scale bar: a – d = 5 μm ($n = 6$ rabbits per group). (e) Immunoprecipitation indicated changes in the interaction of Cx43 with ZO-1 in different TNF-α treatment groups. (f) Quantification of the ratio of ZO-1 to Cx43 in different TNF-α treatment groups. ($n = 6$ rabbits per group; mean ± SEM, ∗∗ represented $p < 0.01$ vs. control, and ∗∗∗ represented $p < 0.001$ vs. control).

was concentration-dependent (Figure 1). Further analysis showed that the dysfunction of GJIC activity of the rabbit corneal endothelial cells might be due to reduced interaction between the Cx43 and ZO-1 induced by high concentrations of TNF-α (Figures 4 and 5).

Although we have demonstrated the role of TNF-α in inducing gap junction dysfunction in rabbit corneal endothelium, some mechanisms still need to be explained. For instance, exposure to high concentrations of TNF-α downregulated Cx43 protein levels, there have been a nonsignificant variation in the mRNA levels between the different groups (Figure 3). This underlying mechanism is like the previously identified dysfunction of BAK in regulating the gap junctions [9]. We hypothesized that topical application of BAK on the ocular surface might fuel high expression of TNF-α in aqueous humor, thus accelerating the disruption of the function of the corneal endothelial gap junction. These common results suggest that posttranslational activities of Cx43 may modulate disruption of the gap junctions by TNF-α. Therfore, we speculated that this may be a common feature of TNF-α-related signaling induced corneal endothelial gap junction dysfunction. Consequently, the

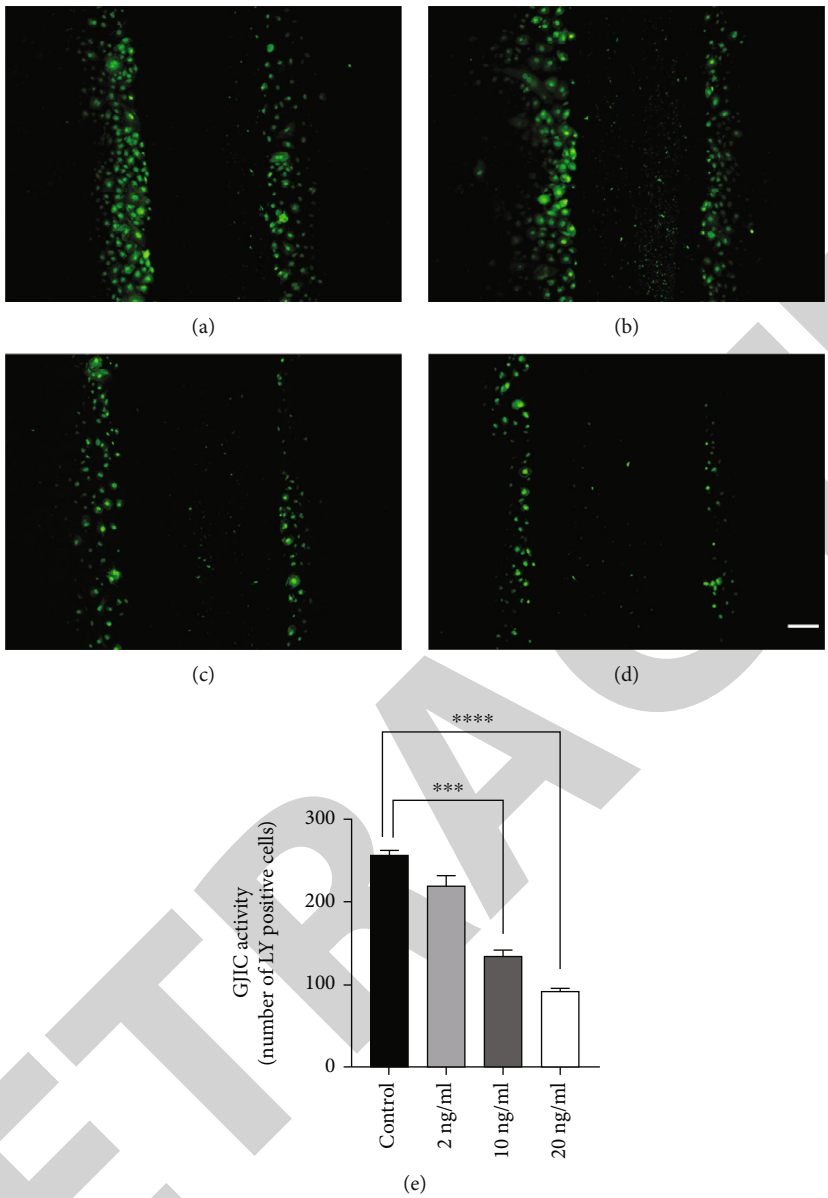

Figure 5: TNF-α treatment inhibited GJIC activity of primary cultured rabbit corneal endothelial cells. (a) LY-labeled cells in normal rabbit corneal endothelial cells. (b) LY-labeled cells in 2 ng/ml TNF-α-treated normal rabbit corneal endothelial cells. (c) LY-labeled cells in 10 ng/ml TNF-α-treated rabbit corneal endothelial cells. (d) LY-labeled cells in 20 ng/ml TNF-α-treated rabbit corneal endothelial cells. (e) Quantifying GJIC activity in normal rabbit corneal endothelial cells and TNF-α treatment groups. ($n = 6$ rabbits per group; mean ± SEM, scale bar = 10 μm, $***$ represented $p < 0.001$ vs. control, and $****$ represented $p < 0.0001$ vs. control).

downregulation of Cx43 and the disruption of the tight junction marker, ZO-1, contribute to the TNF-α-caused malfunction of GJIC in the corneal endothelium.

TNF-α plays a bidirectional role in regulating GJIC mediated by Cx43. Lin et al. revealed that TNF-α could upregulate the expression of Cx43 and promote the proliferation of aortic smooth muscle cells [26]. In addition, Lagos-Cabre et al. demonstrated increased Cx43 expression in astrocytes after TNF-α treatment [27]. On the other hand, Kabatkova et al. showed that TNF-α-treated rat hepatocytes caused downregulation of the Cx43 expression and inhibited GJIC of hepatocytes [28]. Our study revealed that TNF-α treatment reduces Cx43-mediated GJIC in rabbit corneal endothelium. Therefore, the effect of TNF-α on gap junction function may be different in different tissues or cells and thus needs further research to identify the underlying specific mechanism.

The regulation of gap junctions is significantly impacted by the cooperation between ZO-1 and Cx43. To exert its biological effect, the C-terminal of the Cx43 protein binds the PDZ2 structure of ZO-1 [29–31]. Previous studies reported that Cx43 interacts with ZO-1 to regulate cell migration in cerebral endothelial wound healing [30]. The structure and stability of the gap junction channel can be controlled by a complex that consists of Cx43 and ZO-1 [32]. In this study, we demonstrated that TNF-α inhibits rabbit corneal

endothelial GJIC by decreasing the interaction between ZO-1 and Cx43, downregulating the expression of Cx43 and disrupting the distribution of Cx43. However, this research still has some limatations. For example, how TNF-α downregulates the interaction between ZO-1 and Cx43 remains undertemined, a more detailed mechanism still needs to be elaborated in the future. In fact, we have detected TNF-α-related classical NF-κB, JNK, and AKT signaling pathways in previous experiments. Unfortunately, no significant activation of the related signaling pathways was detected. Due to the special anatomy of the cornea, the corneal endothelium is directly exposed to aqueous humor. However, Cx43-mediated gap junction and the barrier integrity of the endothelium are effective in maintenance of stromal deturgescence and corneal transparency. When patients with endophthalmitis, uveitis, and other ocular trauma, the level of TNF-α will rise sharply in aqueous humor. Due to the direct physical contact between aqueous humor and corneal endothelium, we hypothesized that high concentrations of TNF-α may act directly on Cx43 protein, disrupt the interaction between ZO-1 and Cx43, and downregulate the expression level of Cx43 to disrupt corneal endothelial gap junctional intercellular communication (GJIC). We are well aware of the limitations of this study and will continue to explore the specific mechanisms and potential drugs that protect GJIC of corneal endothelial cells in the future.

5. Conclusions

In conclusion, we examined the impact of TNF-α on the corneal endothelial gap junction. Our findings demonstrated that TNF-α could disrupt the gap junctional intercellular communication (GJIC) of rabbit corneal endothelium by disturbing the connection between Cx43 and ZO-1, downregulating the expression of Cx43, and destroying the distribution of Cx43. The gap junction plays a crucial part in regulating corneal endothelial cell homeostasis. Additionally, the current investigation elucidates the effect of stimulation of TNF-α on Cx43-mediated GJIC in the corneal endothelium. It offers a new basis for the therapy of the corneal endothelial malfunction induced by elevated TNF-α in various eye diseases.

Data Availability

All experimental data supporting this study are available from the corresponding author upon reasonable request.

Ethical Approval

This study was approved by the ethics committee of Suzhou Science & Technology Town Hospital. All experiments were treated in accordance with the guidelines and statements of the ARVO in Ophthalmic and Vision Research.

Conflicts of Interest

The authors declare that they have no conflict of interest.

Authors' Contributions

Zhenhao Zhang designed the experiment. Jufeng Meng and Ke Xu executed most of the experiments, statistical analysis, and data interpretation. Ya Liu and Lin Xu participated in conducting the experiments and performed data analysis. Yinyin Qin performed the primary rabbit corneal endothelial cell culture and SLDT assay in this study. Zhenhao Zhang wrote the manuscript, while Jianjun Liu, Shigang Qiao, and Jianzhong An participated in the major revision of the article. Jufeng Meng and Ke Xu contributed equally to this work.

Acknowledgments

This study was supported by grants (GSWS2021068) from the Gusu Health Talent Program (to Dr. Zhang), (2020Z007) (to Dr. Zhang) from the Suzhou New District Science and Technology Project, and (81600711) (to Dr. Zhang) from the National Natural Science Foundation of China. We give our thanks to the native English speaker from Home for Researches (http://www.home-for-researchers.com) for improving the grammar and readability.

References

[1] A. Bartakova, K. Alvarez-Delfin, A. D. Weisman et al., "Novel identity and functional markers for human corneal endothelial cells," *Investigative Ophthalmology & Visual Science*, vol. 57, no. 6, pp. 2749–2762, 2016.

[2] N. C. Joyce, S. E. Navon, S. Roy, and J. D. Zieske, "Expression of cell cycle-associated proteins in human and rabbit corneal endothelium in situ," *Investigative Ophthalmology & Visual Science*, vol. 37, no. 8, pp. 1566–1575, 1996.

[3] I. Epifantseva and R. M. Shaw, "Intracellular trafficking pathways of Cx43 gap junction channels," *Biochimica et Biophysica Acta - Biomembranes*, vol. 1860, no. 1, pp. 40–47, 2018.

[4] D. S. Roh and J. L. Funderburgh, "Rapid changes in connexin-43 in response to genotoxic stress stabilize cell-cell communication in corneal endothelium," *Investigative Ophthalmology & Visual Science*, vol. 52, no. 8, pp. 5174–5182, 2011.

[5] H. V. Danesh-Meyer, J. Zhang, M. L. Acosta, I. D. Rupenthal, and C. R. Green, "Connexin43 in retinal injury and disease," *Progress in Retinal and Eye Research*, vol. 51, pp. 41–68, 2016.

[6] K. Williams and M. Watsky, "Gap junctional communication in the human corneal endothelium and epithelium," *Current Eye Research*, vol. 25, no. 1, pp. 29–36, 2002.

[7] K. K. Williams and M. A. Watsky, "Bicarbonate promotes dye coupling in the epithelium and endothelium of the rabbit cornea," *Current Eye Research*, vol. 28, no. 2, pp. 109–120, 2004.

[8] Y. Nakano, M. Oyamada, P. Dai, T. Nakagami, S. Kinoshita, and T. Takamatsu, "Connexin43 knockdown accelerates wound healing but inhibits mesenchymal transition after corneal endothelial injury in vivo," *Investigative Ophthalmology & Visual Science*, vol. 49, no. 1, pp. 93–104, 2008.

[9] Z. Zhang, Y. Huang, H. Xie et al., "Benzalkonium chloride suppresses rabbit corneal endothelium intercellular gap junction communication," *PLoS One*, vol. 9, no. 10, article e109708, 2014.